D

Data Banks of Electrolytes

Richard Sass
DECHEMA e.V., Informationssysteme und Datenbanken, Frankfurt, Germany

Introduction

For the design and modeling of chemical plants, process calculations are carried out during the whole process life cycle. Especially in the case of the synthesis, simulation, and optimization of separation processes, the phase equilibrium of the system to be separated has to be known exactly. Chemical and process engineers are nowadays able to model or even predict a vapor-liquid equilibrium, the density or viscosity of a multicomponent mixture containing numerous different species with sufficient reliability. However, these calculations depend heavily on availability and reliability of thermophysical property data of the pure components and mixtures involved, especially when in a later status of a process design the accuracy of models (equations of state or group contribution methods) are no longer sufficient [1]. This is especially true when the mixtures contain salts. Even traces of salts have the consequence that nearly all models work with less accuracy or even tend to fail. Another area influenced greatly by electrolyte modeling is biochemical engineering. Until now, it is nearly impossible to predict quantitatively salting-out effect of proteins. Nevertheless, modeling results have a great impact on the design and construction of single chemical apparatus as well as whole plants or production lines. Another problem is that inaccurate data may lead to very expensive misjudgments, whether it is to proceed with a new process or modification of it or not to go ahead. So even today, where the usage of process simulation packages is a standard feature, many improvements can be done for the precision of the models in using experimental thermophysical properties. Therefore, chemical engineers developing new production processes are having a pressing need to access reliable thermophysical property data.

Important Properties of Electrolyte Solutions

Process as well as model development – either predicting or even only interpolating – requires multitudinous amounts of reliable thermophysical property data for electrolytes and electrolyte solutions. Among the most important property types are:

- Vapor-liquid equilibrium data
- Activity coefficients
- Osmotic coefficients
- Electrolyte and ionic conductivities
- Transference numbers
- Viscosities
- Densities
- Frequency-dependent permittivity data

How to get such data?

G. Kreysa et al. (eds.), *Encyclopedia of Applied Electrochemistry*, DOI 10.1007/978-1-4419-6996-5,
© Springer Science+Business Media New York 2014

Reliable Data Sources

Print Format

Compilations of data can be found in the classical papers, e.g., by Pitzer and coworkers [2] or Barthel and coworkers [3–7], in books [8] as well as in printed data collections as the DECHEMA Chemistry Data Series [9, 10], which contains a sound collection of electrolyte data, mainly transport properties (conductivity, viscosity, dielectric properties, and phase equilibria). Part of DECHEMA's Chemistry Data is the **Electrolyte Data Collection** published by Prof. J. Barthel and his coworkers from the University of Regensburg. The printed collection and the database ELDAR (described later) have complementary functions. The data books are giving a clear arrangement of selected recommended data for each property of an electrolyte solution. The electrolyte solutions are classified according to their solvents and solvent mixtures. All solution properties have been recalculated from the original measured data with the help of compatible property equations. A typical page of the books contains for the described system:

- General solute and solvent parameters
- Fitted model parameter values
- Measured data together with deviations against the fit
- A plot
- The literature references

The Electrolyte Data Collection has meanwhile 20 volumes and consists of 7,400 printed pages. Covered properties are:

- Specific conductivities
- Transference numbers
- Limiting ionic conductivities
- Dielectric properties of water, and aqueous and no aqueous electrolyte solutions
- Viscosities of aqueous and no aqueous electrolyte solutions

The preferred way for reliable data sources today is to search within an electronic database for the components, mixtures, and properties one needs. Printed data collections or databases are typically compiled and/or maintained from individuals or groups having a well-known reputation in that field. Therefore, they have an overview of the primary literature publishing physical property data and are able to continuously add new data to their collections. In many cases, these groups are able to check the consistency of the data published in literature. Efforts are even made today by publishers to avoid the publication of data with doubts about the repeatability and uncertainty of published data during the referee process (e.g., NIST data tools [11, 12]). In most cases, these groups also use their own collections and methods for model development [13].

In the following, a survey of currently maintained databases for electrolyte properties is given [14]:

Examples of Databases with Properties of Electrolyte Solutions

DETHERM/ELDAR Database

The **El**ectrolyte **Da**tabase **R**egensburg **ELDAR** [15] is a numerical property database for electrolytes and electrolyte solutions from the Institute of Physical and Theoretical Chemistry of the University of Regensburg. It started in 1976 and contains data on pure substances and aqueous as well as organic solutions. The database was designed as a literature reference, numerical data, and also model database for fundamental electrochemical research, applied research, and also the design of production processes.

ELDAR contains data for more than 2000 electrolytes in more than 750 different solvents with a total of 56,000 chemical systems, 15,000 literature references, 45,730 data tables, and 595,000 data points. ELDAR contains data on **physical properties** such as densities, dielectric coefficients, thermal expansion, compressibility, p-V-T data, state diagrams and critical data. The **thermodynamic properties** include solvation and dilution heats, phase transition values (enthalpies, entropies and Gibbs' free energies), phase equilibrium data, solubilities, vapor pressures, solvation data, standard and reference values, activities and activity coefficients, excess values, osmotic coefficients, specific heats, partial molar values and apparent partial molar values. **Transport properties** such as electrical conductivities, transference numbers, single ion conductivities, viscosities, thermal conductivities, and diffusion coefficients are also included.

ELDAR is distributed as part of DECHEMA's numerical database for thermophysical property data DETHERM [16, 17]. To access ELDAR, one can therefore use several options.

- In-house client-server installation as part of the DETHERM database
- Internet access using DETHERM ... *on the Web*

To get an overview of the data available, the Internet access option is recommended, because existence of data for a specific problem can be checked free of charge and even without registration.

Data Bank for Electrolyte Solutions at CERE DTU Chemical Engineering

The Center for Energy Resources Engineering (CERE) of the Technical University of Denmark (DTU) is operating a data bank for electrolyte solutions [18]. It is a compilation of experimental data for (mainly) aqueous solutions of electrolytes and/or nonelectrolytes. The database is a mixture between a literature reference database and a numerical database. Currently references to more than 3,000 papers are stored in the database together with around 150,000 experimental data. The main properties are activity and osmotic coefficients, enthalpies, heat capacities, gas solubilities, and phase equilibria like VLE, LLE, and SLE. The access to the literature reference database is free of charge. The numerical values must be ordered at CERE.

The Dortmund Database DDB

The Dortmund Database published by DDBST GmbH [19] of Prof. J. Gmehling from the University of Oldenburg is well known for its data collections in the areas of vapor-liquid equilibria and related properties [20]. While the major part of the data collections is dealing with nonelectrolyte systems, two collections contain exclusively electrolyte data. They are focused on:

- Vapor-liquid equilibria
- Gas solubilities

The two collections together currently contain around 11,000 data sets. Access to these collections is possible either online using the DETHERM ... *on the Web* service or in-house using special software from DDBST or DECHEMA.

JESS

A very useful tool is provided by the Joint Expert Speciation System (JESS), a joint project of two groups in Australia and South Africa [21, 22]. JESS has a large database for physicochemical properties of electrolytes in aqueous solution. This comprises about 300,000 property values for over 100 electrolytes. Data from the literature are available for activity coefficients, osmotic coefficients, heat capacities, and densities/volumes.

Springer Materials: The Landolt-Börnstein Database

Based on the Landolt-Börnstein (New Series) book collection [23], the Springer Materials database provides also data on electrochemical systems, for example, on electrochemical processes at the boundaries of electrodes and electrolytes or electrical conductivities and equilibrium data [24].

Closed Collections

In addition to the above-described publicly available and still maintained databases, old electrolyte data collections were built up in the past. One of these is the ELYS database, which was compiled by Professor Victor M.M. Lobo, Department of Chemistry, University of Coimbra, Portugal, with thermodynamic and transport property data, such as density, viscosity and diffusion coefficients. Other noteworthy examples include the DIPPR 811 and 861 Electrolyte Database Projects [25]. But these closed collections are typically not maintained anymore and also not publicly available. Likely the references and/or data published in these collections could be also found inside the before mentioned, living collections.

A Glance at the Future of the Properties Databases

Most of the engineers in chemical companies trust in the power of their evaluation of the equations of state for the calculation of the optimal point of work. Nevertheless, the opinion that databases have less importance these days is growing up, mainly when budgetary elements come into consideration. Unfortunately, the

production of many basic chemicals is today transferred into low cost countries, i.e., also not very relevant for research purposes. Many companies outsourced their measurements so that only a limited amount of experts in industry hold the knowledge for these activities.

When we look at the constraints to find new methods for the design of biologic or polymer solutions, we must be skeptical to find enough people to manage future visions for models with the knowledge what was in the past. In an age where China is replacing the United States as world's leading consumer of steel, there is the hope that the rapidly growing demand of energy increases also the interest in physical properties. Meanwhile it is a good sign that new projects are coming up in order to find a new approach to build evaluated databases.

Cross-References

- ▶ Activity Coefficients
- ▶ Conductivity of Electrolytes
- ▶ Electrolytes, Thermodynamics
- ▶ Ion Properties
- ▶ Thermodynamic Properties of Ionic Solutions - MSA and NRTL Models

References

1. Carlson EC (1996) Don't gamble with physical properties for simulations. Chem Eng Progr 92(10):35–46
2. Pitzer KS, Pelper JC, Busey RH (1984) Thermodynamic properties of aqueous sodium chloride solutions. J Phys Chem Ref Data 13(1):1–102
3. Barthel J, Lauermann G, Neueder R (1986) Vapor pressure measurements on non-aqueous electrolyte solutions. Part 2. Tetraalkylammonium salts in methanol. Activity coefficients of various 1-1 electrolytes at high concentrations. J Solution Chem 10:851–867
4. Barthel J, Neueder R, Poepke H, Wittmann H (1999) Osmotic coefficients and activity coefficients of nonaqueous electrolyte solutions. Part 2. Lithium perchlorate in the aprotic solvents acetone, acetonitrile, dimethoxyethane, and dimethylcarbonate. J Solution Chem 28:489–503
5. Nasirzadeh K, Neueder R, Kunz W (2005) Vapor pressures, osmotic and activity coefficients of electrolytes in protic solvents at different temperatures. 3. Lithium bromide in 2-propanol. J Solution Chem 34:9–24
6. Tsurko EN, Neueder R, Kunz W (2007) Water activity and osmotic coefficients in solutions of glycine, glutamic acid, histidine and their salts at 298.15 K and 310.15 K. J Solution Chem 36:651–672
7. Barthel J, Krienke H, Kunz W (1998) Physical chemistry of electrolyte solutions. Modern aspects. Springer, New York
8. Robinson RA, Stokes RH (2002) Electrolyte solutions, Second revised edition. Dover, Mineola
9. Barthel J et al (1992–2010) Electrolyte data collection, vol XII, Chemistry data series, Parts 1–5. DECHEMA, Frankfurt
10. Engels H (1990) Phase equilibria and phase diagrams of electrolytes, vol XI, Chemistry data series, Part 1. DECHEMA, Frankfurt
11. Frenkel M, Chirico RD, Diky V, Yan X, Dong Q, Muzny C (2005) ThermoData engine (TDE): software implementation of the dynamic data evaluation concept. J Chem Inf Model 45(4):816–838
12. Frenkel M, Chirico RD, Diky V, Muzny C, Dong Q, Marsh KN, Dymond JH, Wakeham WA, Stein SE, Königsberger E, Goodwin ARH, Magee JW, Thijssen M, Haynes WM, Watanasiri S, Satyro M, Schmidt M, Johns AI, Hardin GR (2006) New global communication process in thermodynamics: impact on quality of published experimental data. J Chem Inf Model 46(6):2487–2493
13. Barthel J, Popp H (1992) Methods of the knowledge based system ELDAR for the simulation of electrolyte solution properties. Anal Chim Acta 265: 259–266
14. Westhaus U, Sass R (2004) Reliable thermodynamic properties of electrolyte solutions – a survey of existing data sources. Z Phys Chem 218:1–8
15. http://www.uni-regensburg.de/Fakultaeten/nat_Fak_IV/Physikalische_Chemie/Kunz/eldar/eldhp.html
16. Westhaus U, Droege T, Sass R (1999) DETHERM – a thermophysical property database. Fluid Phase Equilib 158–160:429–435
17. http://www.dechema.de/en/detherm.html
18. http://www.cere.dtu.dk/Expertise/Data_Bank.aspx
19. http://www.ddbst.de
20. Onken U, Rarey-Nies J, Gmehling J (1989) The Dortmund data bank: a computerized system for retrieval, correlation, and prediction of thermodynamic properties of mixtures. J Int J Thermophys 10(3):739–747
21. http://jess.murdoch.edu.au/jess_home.htm
22. May PM, Rowland D, Königsberger E, Hefter G (2010) JESS, a joint expert speciation system – IV: a large database of aqueous solution physicochemical properties with an automatic means of achieving thermodynamic consistency. Talanta 81(1–2):142–148
23. http://www.springer.com/springermaterials
24. Holze R, Lechner MD (to be published in 2014) Electrochemistry, Subvolume B: Electrical conductivities and equilibria of electrochemical systems. Springer, Berlin, Heidelberg
25. Thomson GH, Larsen AH (1996) DIPPR: satisfying industry data needs. J Chem Eng Data 41:930–934

Defect Chemistry in Solid State Ionic Materials

H.-I. Yoo
Department of Materials Science and Engineering, Seoul National University, Seoul, Korea

Introduction

Solid state electrochemistry is concerned with all kinds of electrical phenomena associated with chemical changes, and vice versa, in solid state. These are induced by migration of charged mass particles or ions under the action of a variety of thermodynamic forces, gradients of component chemical potentials, electrical potential, temperature, stress, and the like. Naturally the solids composed of ions, viz., ionic solid compounds serve the main stages for solid state electrochemistry. In solid state, electrons may also be mobile, which makes solid state electrochemistry even more versatile and interesting.

An ionic compound, e.g., MO, consists of charged components, cations (M^{2+}), anions (O^{2-}) and electrons (e^-). These charged components are rendered mobile only via defects. It is thus a prerequisite in solid state electrochemistry to understand the defect structure of the system of interest, that is, types of defects and their concentrations against the thermodynamic variables of the system.

Defects are defined as whatsoever makes a crystalline solid deviate from its ideal crystal structure. An ideal crystal refers to an infinite crystal with component ions all sitting at their respective lattice sites in a periodic array as stipulated by its crystallographic structure, the interstitial sites all empty, electrons all at the valence band sites, and the conduction band sites all empty. For example, an "infinite" crystal $M^{2+}O^{2-}$ with M^{2+} on M^{2+} sites $\left(M^{2+}_{M^{2+}}\right)$; O^{2-} on O^{2-} sites $\left(O^{2-}_{O^{2-}}\right)$; electrons e^- on the filled valence-band e^- sites $\left(e^-_{e^-}\right)$; ionic emptiness or vacancy V^0 with actual charge 0 on interstitial sites where there should be no charge $\left(V^0_{I^0}\right)$; electronic emptiness or holes h^0 with actual charge 0 on the empty conduction band h^0 sites $\left(h^0_{h^0}\right)$.

We here denote the structure elements constructing the ideal structure MO as $S^m_{L^n}$, indicating the species S(=M, O, V, e, h), with an actual charge unit m(=···,−2, −1, 0, +1, +2,···), sitting at the site or locus L(=M, O, I, e, h) where there would have to be an actual charge unit n(=···,−2, −1, 0, +1, +2,···) if ideal. Defining the effective charge of a structure element as c = m–n and denoting it, instead of numerals, as the same number of dots (•) and primes (′) for $c > 0$ and $c < 0$, respectively and a cross (x) for $c = 0$, the structure elements constructing the ideal structure MO may be simplified in the form of S^c_L as suggested by Kröger and Vink [1] as

$$M^x_M,\ O^x_O,\ V^x_I,\ e^x_e,\ h^x_h$$

which are often called the regular structure elements.

Anything which makes the structure deviate from the ideal one or defects or irregular structure elements may then be immediately sorted out as:

Missing cation or cation vacancy V''_M; missing anion or anion vacancy $V^{\bullet\bullet}_O$; interstitial cation $M^{\bullet\bullet}_I$; interstitial anion O''_I; misplaced cation $M^{\bullet\bullet\bullet\bullet}_O$; misplaced anion $O''_M{}''$; electron in empty conduction-band e'_h; missing electron or hole in filled valance-band $h^\bullet_e$; impurity or alien ion substituting cation, A^c_M or substituting anion, A^c_O; interstitial impurity or alien ion A^c_I.

Each of these is confined to a site or point, thus, they are called point defects. There are more: dislocations disturbing the periodicity of lattice sites; grain boundaries and surfaces spatially confining the crystal which would have to be infinite if ideal; voids and inclusions that are three-dimensional aggregates of point defects of a kind. Depending on their geometries, they are often called line defects, planar defects and volume defects, respectively.

Formation of a defect always requires work exerted on the system, thus increasing the energy

of the system. Therefore all these defects can only be stabilized by configurational entropy gain as temperature goes up. In this sense, only point defects are thermodynamically stable in the normal temperature range of existence of ionic solids. It means that their concentrations are uniquely determined by the thermodynamic variables of the system in equilibrium state. For higher dimensional defects, the entropy gain can hardly compensate the energy increase, if not impossible.

In this chapter, we will discuss the generation modes of thermodynamically stable point defects and the defect-chemical logic to calculate the equilibrium defect structure of a given system. As a stereotype of systems, we will consider only a binary oxide MO, but the idea and logic can be readily extended to other binary, ternary and higher systems with minor modifications [2–6].

Intrinsic or Thermal Disorders

For a given system, the ratio of the M-sites to O-sites must remain fixed in any case, as required by its crystallographic structure. For the case of e.g., MO,

$$[\text{M-sites}]/[\text{O-sites}] \equiv 1$$

where [ ] stands for the concentration of the thing therein. Whenever whatsoever defects are generated, this site ratio or structure condition must be observed by necessity. Otherwise, the structure would be no longer the structure of the system itself.

For pure MO, possible ionic defects are exhaustively V''_M, $M^{\bullet\bullet}_I$, $V^{\bullet\bullet}_O$, O''_I, $M^{\bullet\bullet\bullet\bullet}_O$, $O''_M{}''$. These defects can only be generated in pair involving either M- or O-sublattice alone or both sublattices in order to maintain the structure as

$$0 = V''_M + V^{\bullet\bullet}_O \tag{1a}$$

$$M^x_M + O^x_O = M^{\bullet\bullet}_I + O''_I \tag{2a}$$

$$M^x_M + V^x_I = M^{\bullet\bullet}_I + V''_M \tag{3a}$$

$$O^x_O + V^x_I = O''_I + V^{\bullet\bullet}_O \tag{4a}$$

$$M^x_M + O^x_O = M^{\bullet\bullet\bullet\bullet}_O + O''_M{}'' \tag{5a}$$

In these generation reactions, one should recognize that in addition to the structure condition or site (L) conservation, charge (c) and mass (S) are conserved, as a Kröger-Vink symbol S^c_L suggests. These three must be conserved in any case.

If the defect concentrations are small enough compared to those of the regular structure elements as is normally the case, one may apply the mass action law to write for each case in order as:

$$\left[V''_M\right]\left[V^{\bullet\bullet}_O\right] = K_s \tag{1b}$$

$$\left[M^{\bullet\bullet}_I\right]\left[O''_I\right] = K_{aS} \tag{2b}$$

$$\left[M^{\bullet\bullet}_I\right]\left[V''_M\right] = K_F \tag{3b}$$

$$\left[O''_I\right]\left[V^{\bullet\bullet}_O\right] = K_{aF} \tag{4b}$$

$$\left[M^{\bullet\bullet\bullet\bullet}_O\right]\left[O''_M{}''\right] = K_a \tag{5b}$$

Here, the mass action law constant K_j(j = S, aS, F, aF, a) takes the form

$$K_j = K_{j,o}\exp\left(\frac{\Delta h_j}{kT}\right) \tag{6}$$

where $K_{j,0}$ and Δh_j are the pre-exponential factor and standard enthalpy change of the generation reaction of j-type and kT has the usual significance. These defect pairs are named, in order, the Schottky disorder (j = S), anti-Schottky disorder(j = aS), Frenkel disorder (j = F), anti-Frenkel disorder (j = aF), and anti-structure disorder (j = a). All these defects are only internally generated for the entropic reason and hence, called the intrinsic or thermal disorder. The defect pair which is energetically least costly in a given structure usually overwhelms the rest, thus making the majority disorder type. The anti-structure disorder, however, will be too costly in ionic solids, thus normally out of concern.

In a similar way, electronic disorders are generated internally or thermally as

$$e_e^x + h_h^x = h_e^\bullet + e_h' \tag{7a}$$

It is here noted that even in generating the electronic defects, the three $\left(S_L^c\right)$ should be conserved, viz., the densities of states in the valence and conduction band, charge and mass. By defining free holes and electrons as $h^\bullet \equiv h_e^\bullet - e_e^x$ and $e' \equiv e_h' - h_h^x$, respectively, this intrinsic electronic excitation reaction is often represented more succinctly as

$$0 = e' + h^\bullet \tag{7b}$$

Again applying the mass action law, one may write

$$\left[e_h'\right]\left[h_e^\bullet\right] = K_i \tag{7c}$$

where K_i is called the intrinsic electronic excitation equilibrium constant. In terms of semiconductor jargons, $\left[e_h'\right] = [e'] = n$ and $\left[h_e^\bullet\right] = [h^\bullet] = p$ in number concentration and then

$$np = K_i = N_v N_c \exp\left(-\frac{E_g}{kT}\right) \tag{7d}$$

where N_v and N_c are the effective density of states at the valence (e^- sites) and conduction band edge (h^0 sites), respectively, and E_g the band gap.

Impurity-Induced Disorders

Nothing is pure for the thermodynamic reason. An impurity can be incorporated into the host lattice either substitutionally or interstitially depending mostly on the relative size of the impurity to host ion. For simplicity sake, we here consider two types of cation impurities only: one with a lower valence and the other with a higher valence than the host ion M^{2+} in MO. It is noted that our system exchanges mass particles with the surrounding only in electrically neutral forms, because it would otherwise be electrically charged to energetically prevent further exchange. It is thus always easier to consider an impurity doping as incorporating the impurity in the form of an oxide when the host is MO.

Let us first consider the incorporation of A_2O in MO. There can be two possibilities, A_M' or $A_I^\bullet$, which are charge-compensated by generating oppositely charged native defects, either $V_O^{\bullet\bullet}$ or $M_I^{\bullet\bullet}$ and either V_M'' or O_I'', respectively, or by themselves if amphoteric. Incorporation reactions may thus be formulated exhaustively as:

$$A_2O = 2A_M' + V_O^{\bullet\bullet} + O_O^x \tag{8a}$$

$$A_2O = 2A'_M + M_I^{\bullet\bullet} + 2O_O^x \tag{8b}$$

$$A_2O = 2A_I^\bullet + V_M'' + O_O^x \tag{8c}$$

$$A_2O = 2A_I^\bullet + O_I'' \tag{8d}$$

$$A_2O = A_M' + A_I^\bullet + O_O^x \tag{8e}$$

It is informative to write down the lattice molecular formula for each case. For xA_2O added, they are in order: $M_{1-2x}A_{2x}O_{1-x}$; $M_{1-x}A_{2x}O$; $M_{1-x}A_{2x}O$; $MA_{2x}O_{1+x}$; $M_{1-x}A_{2x}O$. This means that the mechanisms, Eqs. 8b, 8c, and 8e cannot be distinguished chemically.

We will next consider the case where the impurity with higher valence E_2O_3 is incorporated. Following the same logic as before, we may write the incorporation equations exhaustively as

$$E_2O_3 = 2E_M^\bullet + V_M'' + 3O_O^x \tag{9a}$$

$$E_2O_3 = 2E_M^\bullet + O_I'' + 2O_O^x \tag{9b}$$

$$E_2O_3 = 2E_I^{\bullet\bullet\bullet} + 3V_M'' + 3O_O^x \tag{9c}$$

$$E_2O_3 = 2E_I^{\bullet\bullet\bullet} + 3O_I'' \tag{9d}$$

The lattice molecular formulae for xE_2O_3 added are in turn $M_{1-3x}E_{2x}O$; $M_{1-2x}E_{2x}O_{1+x}$; $M_{1-3x}E_{2x}O$; $ME_{2x}O_{1+3x}$. In this case, they are all chemically distinguished from each other.

Which of these multiple possibilities is really responsible in a given structure is again determined by which is the least costly. Rule of thumb is that the charge compensating native defect is determined by the majority type of thermal disorder for the given system.

Redox-Induced Disorders

No compound exists in one and only fixed composition again for the thermodynamic reason. For example, MO should exist over a range of composition or homogeneity range between the M-saturated and O-saturated composition. The compound should, thus, be represented more appropriately as $M_{1-\delta}O$ or $MO_{1+\delta}$. Its homogeneity range may then be divided, in general, into three regions: hypostoichiometric ($\delta < 0$), near-stoichiometric ($\delta \approx 0$), and hyperstoichiometric ($\delta > 0$). In this light, the stoichiometric composition MO is nothing but a special composition in the region $\delta \approx 0$ or a symbolic representation of the compound $M_{1-\delta}O$. An extreme example will be "FeO," which does not even exist within its homogeneity range ($Fe_{1-\delta}O$ with $\delta > 0$ always).

For the composition of a system to vary, component particles should be exchanged with its surrounding, and the exchange is driven by a difference in component chemical potentials across the boundary. Once component chemical potential distributions are rendered uniform, particle exchange ceases and then the system is said to be in external equilibrium. For the case of binary $MO_{1+\delta}$, the number of composition variables is only one (δ), and only one of the two component chemical potentials or activities a_M and a_{O2} can be varied independently at given temperature T and pressure P due to the Gibbs-Duhem equation:

$$\mathrm{d}\ln a_M + \frac{1}{2}(1+\delta)\mathrm{d}\ln a_{O2} = 0 \qquad (10)$$

When the external equilibrium condition is disturbed, the system MO may change its composition by exchange of both components M and O in principle, but normally by the exchange of the more volatile component which is O for the case of oxides.

When the oxygen chemical potential in the surrounding is higher than that in the solid oxide, component oxygen tends to be incorporated to raise the oxygen content by creating oxygen interstitials or metal vacancies depending on which are energetically cheaper. This process is called oxidation. In the opposite case, oxygen leaves the crystal to lower the oxygen content by leaving behind oxygen vacancies or metal interstitials depending on which are energetically cheaper. This is called reduction. What is eventually achieved is reduction or oxidation equilibrium, thus often dubbed as redox equilibrium.

It is noted that because only neutral oxygen is exchanged, what are left behind should also be electrically neutral. A neutral interstitial oxygen may be regarded as a normal oxygen ion interstitial O_I'' bearing two free holes $2h^\bullet$ within it and a neutral metal vacancy as a missing metal ion V_M'' bearing two free holes $2h^\bullet$ within it or

$$O_I^x = \left(O_I'', 2h^\bullet\right)^x;\ V_M^x = \left(V_M'', 2h^\bullet\right)^x \qquad (11)$$

Likewise,

$$M_I^x = \left(M_I^{\bullet\bullet}, 2e'\right)^x;\ V_O^x = \left(V_O^{\bullet\bullet}, 2e'\right)^x \qquad (12)$$

In this sense, the former two bearing holes (or missing electrons) are like electron acceptors and the latter two bearing extra electrons electron donors in elemental semiconductors. They are indeed so: $MO_{1+\delta}$ always tends to be of p-type when $\delta > 0$ and of n-type if $\delta < 0$. For the sake of simplicity, we here assume that once these are generated, they immediately donate all holes (or equivalently, accept electrons) or donate all electrons. This is termed "fully ionized" and actually happens at elevated temperatures.

Oxidation reactions and corresponding mass action laws may then be written as:

$$\frac{1}{2}O_{2(g)} = O_I^x = O_I'' + 2h^\bullet : \quad \left[O_I''\right]p^2 = K_{Ox,1}a_{O_2}^{1/2} \qquad (13a)$$

$$\frac{1}{2}O_{2(g)} = O_O^x + V_M^x = O_O^x + V_M'' + 2h^\bullet \; : \; \left[V_M''\right]p^2 = K_{Ox,2}a_{O_2}^{1/2} \tag{13b}$$

Reduction reaction equilibria as:

$$O_O^x = \frac{1}{2}O_{2(g)} + V_O^x = \frac{1}{2}O_{2(g)} + V_O^{\bullet\bullet} + 2e' \; : \; \left[V_O^{\bullet\bullet}\right]n^2 = K_{Re,1}a_{O_2}^{-1/2} \tag{13c}$$

$$M_M^x + O_O^x = \frac{1}{2}O_{2(g)} + M_I^x = \frac{1}{2}O_{2(g)} + M_I^{\bullet\bullet} + 2e' \; : \; \left[M_I^{\bullet\bullet}\right]n^2 = K_{Re,2}a_{O_2}^{-1/2} \tag{13d}$$

These four redox reaction equilibrium constants K_j (j = Ox,1; Ox,2; Re,1; Re,2) each take the shape as in Eq. 6. The reader, however, should note that these four K_j's are not all independent of each other owing to the internal equilibria, Eqs. 1 to 4 or $K_{Ox,1}K_{Re,1} = K_{aF}K_i^2$; $K_{Ox,1}K_{Re,2} = K_{aS}K_i^2$; $K_{Ox,2}K_{Re,1} = K_SK_i^2$; $K_{Ox,2}K_{Re,2} = K_FK_i^2$. It turns out that only one out of the four is independent and hence, only one out of the four is enough to describe the redox equilibrium of the binary system MO. If ternary, there would be two composition variables and hence, there would be two external equilibria.

Defect Structure of "Pure" Nonstoichiometric Compound, $MO_{1+\delta}$

Nothing can be absolutely pure. Here "pure" means that the majority type of intrinsic disorder overwhelms impurities in concentration. Such a compound is said to be in its "intrinsic regime."

In order to calculate the equilibrium defect structure of a compound whether intrinsic or extrinsic, one should first postulate the most likely defects on the basis of the structure of MO. Let us suppose that our system MO has the Schottky disorder as the majority type of ionic disorder. The defects of present interest may then be listed as

$$V_M'', V_O^{\bullet\bullet}; e', h^\bullet$$

We therefore need four equations to calculate these four concentrations as functions of the thermodynamic intensive variables of the system $MO_{1+\delta}$, T, P and a_{O_2}. These equations are formulated from the requirements that the system has to meet:

1. 2 internal equilibria; Eqs. 1b and 7c
2. 1 external equilibrium: Eq. 13a or 13c
3. 1 charge neutrality: $n + 2\left[V_M''\right] = p + 2\left[V_O^{\bullet\bullet}\right]$

One may solve, in principle, these four simultaneous equations for each defect concentration as a function of T, P (via K_j) and a_{O_2}, but analytic solution is impossible in many cases because of different algebraic character of the charge neutrality condition compared to the other constraints. If the latter, however, can be approximated in terms of only one pair of oppositely charged defects or majority disorder type depending on δ-ranges, the analytic solution will be rendered trivial in the form of

$$\left[S_L^c\right] = \prod_j K_j^{n_j}a_{O_2}^m \tag{14}$$

where n_j and m are the exponents. This trick was first proposed by Brouwer, thus called the Brouwer approximation [1–3]. It goes as follows:

The charge neutrality condition may be approximated to the 2 × 2 limiting charge neutrality conditions or majority disorder types:

(i) $n \approx 2\left[V_O^{\bullet\bullet}\right](\delta < 0)$;
(ii) $n \approx p(\delta \approx 0)$;
(iii) $\left[V_M''\right] \approx \left[V_O^{\bullet\bullet}\right](\delta \approx 0)$;
(iv) $2\left[V_M''\right] \approx p(\delta < 0)$

The problem is then how to allocate these majority disorder types along the axis of oxygen activity at a given temperature. It is reminded that the homogeneity range of $M_{1-\delta}O$ is generally divided into the three regions: $\delta < 0$; $\delta \approx 0$; $\delta > 0$. The nonstoichiometry as defined

here as oxygen excess or metal deficit is given in the present case as

$$\delta = \left[V''_M\right] - \left[V^{\bullet\bullet}_O\right] = \frac{1}{2}(p - n) \qquad (16)$$

due to the charge neutrality condition. By using this relationship, each majority disorder type can be assigned to one of the three δ-ranges, which is already done in Eq. 15. Now one can see there are two majority disorder types (ii) and (iii) simultaneously in the near-stoichiometry region causing a logical conflict in appearance, but it is a matter of whether $K_i >> K_S$ or $K_S >> K_i$ for the system given. If the former is the case, sequence of the majority disorder types will be (i) → (ii) → (iv) with increasing oxygen activity a_{O_2}; if the latter, (i) → (iii) → (iv). The defect structure of the system across its entire range of existence can finally be constructed by combining the piecewise solutions, Eq. 14 for each disorder regime, in accord with the sequence of majority disorder types. Figure 1 shows an example for $K_i >> K_S$.

Defect Structure of "Impure" Nonstoichiometric Compound, $M_{1-2x}A_{2x}O_{1-x+\delta}$

Let us next calculate the defect structure of a more general case, A_2O-doped MO. Here we assume that A substitutes M and MO has the anti-Frenkel disorder as the majority type of ionic disorder. Then we may list the defects of the most concern as

$$A'_M,\ V^{\bullet\bullet}_O,\ O''_I,\ e',\ h^{\bullet}$$

We thus need five constraints for these five unknowns, which comprise:

1. Two internal equilibria: Eqs. 4b and 7c
2. One external equilibrium, Eq. 13a or 13c
3. One mass conservation for the dopants, $[A'_M] = x$ (constant)
4. One charge neutrality condition, $n + [A'_M] + 2[O''_I] = p + 2[V^{\bullet\bullet}_O]$

These are all and exhaustive. The last charge neutrality condition may be approximated to 3 × 2 limiting conditions or majority disorder types as:

$$\begin{aligned}
&\text{(i)}\quad n \approx p(\delta \approx 0);\\
&\text{(ii)}\quad n \approx 2\left[V^{\bullet\bullet}_O\right](\delta < 0);\\
&\text{(iii)}\quad \left[A'_M\right] \approx p(\delta > 0);\\
&\text{(iv)}\quad \left[A'_M\right] \approx 2\left[V^{\bullet\bullet}_O\right](\delta \approx 0);\\
&\text{(v)}\quad 2\left[O''_I\right] \approx p(\delta > 0);\\
&\text{(vi)}\quad \left[O''_I\right] \approx \left[V^{\bullet\bullet}_O\right](\delta \approx 0)
\end{aligned} \qquad (17)$$

Defining oxygen nonstoichiometry of the present xA_2O-doped MO as $M_{1-2x}A_{2x}O_{1-x+\delta}$,

$$\delta = \left[O''_I\right] - \left[V^{\bullet\bullet}_O\right] + x = \frac{1}{2}(p - n) \qquad (18)$$

due to the charge neutrality condition. Each majority disorder type is now assigned to each of the three δ-regions as indicated in Eq. 17. It should first be noted that once "impure" or extrinsic, the intrinsic disorder types should not be in majority in the near-stoichiometry region ($\delta \approx 0$) by definition, thus, the possibilities (i) and (vi) are already ruled out. Then noting that any two contiguous disorder regimes should have one defect in common, which is termed the "continuity principle," [6] one may establish the sequence of majority disorder types with increasing a_{O_2} as (ii) → (iv) → (iii) → (v). By combining the piecewise solution, Eq. 14 in each region in this sequence, one finally ends up with the defect map for the present system as shown in Fig. 2.

Defect Structure of Impure "Stoichiometric" Compound MO

Finally, we consider a special case, a "stoichiometric" compound, which normally refers to a compound with negligible nonstoichiometry. We have seen that for a nonstoichiometry to be generated, electronic defects are always involved accompanying the component particle exchanges with the surrounding. As Eqs. 11 and 12 suggest, the range of

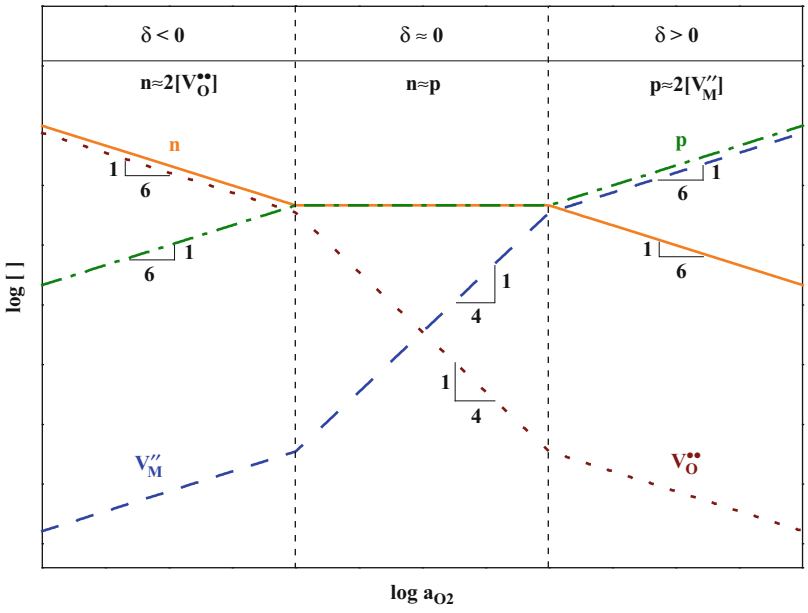

Defect Chemistry in Solid State Ionic Materials, Fig. 1 Defect structure of $M_{1-\delta}O$ versus oxygen activity at fixed temperature, as calculated assuming $K_i >> K_S$ (not to scale). The *triangles* represent the oxygen exponents "m" of the piecewise solutions

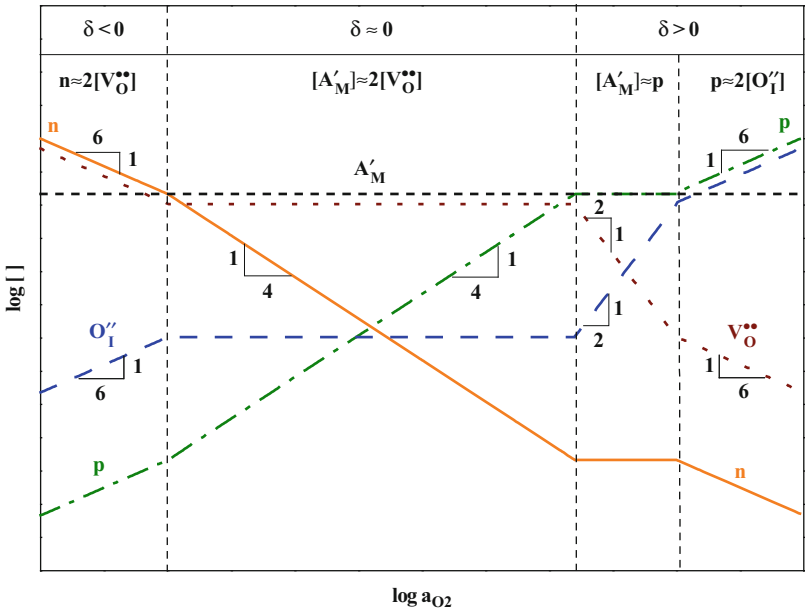

Defect Chemistry in Solid State Ionic Materials, Fig. 2 As-calculated defect structure of extrinsic $M_{1-2x}A_{2x}O_{1-x+\delta}$ versus oxygen activity at fixed temperature, not to scale. Note the continuity principle between nearest-neighboring disorder regimes. The *triangles* represent the oxygen exponents "m" of the piecewise solutions

nonstoichiometry is determined by the variability of the valences of the component ions from chemistry point of view. This is why transition metal compounds normally exhibit wider ranges of homogeneity. Therefore the compounds with almost fixed-valent ions, e.g., alkali halides, alkali earth oxides, and the like may be regarded "stoichiometric" and their electronic defects may also be neglected compared to the ionic defects. Once stoichiometric, the composition is fixed and hence, it is as if the system boundary were closed, therefore external equilibrium is no longer a concern. Then the defect structure will be determined only by the internal equilibria or

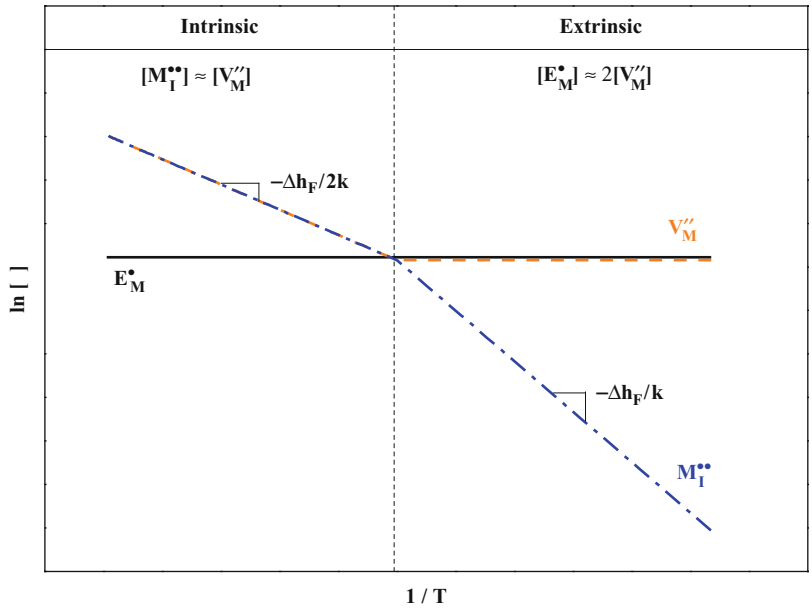

Defect Chemistry in Solid State Ionic Materials, Fig. 3 Defect structure of E_2O_3 doped, "stoichiometric" MO with the Frenkel disorder as the majority, not to scale. *Small triangles* denote the slopes. Note the intrinsic regime at the high temperatures and extrinsic regime at the low temperatures

temperature and impurity content no matter how many components there are.

Suppose that our "stoichiometric" MO has the Frenkel disorder as the majority and substitutional impurity E_2O_3 (see Eq. 9a). Then the defects of concern will be:

$$E_M^{\bullet},\ V_M'',\ M_I^{\bullet\bullet}$$

We have now

1. One internal equilibrium: Eq. 3b
2. One mass conservation: $[E_M^{\bullet}] = x(\text{constant})$
3. One charge neutrality: $[E_M^{\bullet}] + 2[M_I^{\bullet\bullet}] = 2[V_M'']$

By solving these three equations, one can get each defect concentration as a function of T and x independently of the component activities. The present situation can be solved even analytically, but for the consistency sake, we will employ the Brouwer approximations as: $[E_M^{\bullet}] \approx 2[V_M'']$; $[M_I^{\bullet\bullet}] \approx [V_M'']$. The former prevails at low temperatures such that $x >> K_S^{1/2}$ and the latter at high temperatures such that $x << K_S^{1/2}$. By combining the piecewise solutions for each temperature region, one obtains the defect structure as in Fig. 3. Note that in the high temperature intrinsic regime, the impurity concentration is overwhelmed by the intrinsic disorder and vice versa in the low temperature extrinsic regime.

Concluding Remarks

The very basic logical framework of defect chemistry has thus far been given to a binary system. This can be readily extended to ternary or higher systems simply by adding external equilibria each corresponding to additional composition variables in addition to the exhaustive internal equilibrium conditions, mass conservation condition, and charge neutrality condition. If the nonstoichiometry is negligible, thus, the composition practically remains fixed, however, one may disregard the external equilibria.

The defect structure gets more involved as defect concentrations increase so that the mass-action-laws are no longer applicable. This basic logical framework can also be extended by taking into account defect associates or long range interactions in terms of activity coefficients of defects.

For more extended treatments, the reader is referred to the general references [1–6].

Cross-References

- ▶ Defects in Solids
- ▶ Kröger-Vinks Notation of Point Defects

References

1. Kröger FA, Vink VJ (1956) Relations between the concentrations of imperfections in crystalline solids. In: Seitz F, Turnbull D (eds) Solid state physics, vol 3. Academic, New York
2. Kingery WD, Bowen HK, Uhlmann DR (1960) Introduction to ceramics. Wiley, New York (Chap. 4)
3. Kröger FA (1974) Imperfection chemistry of crystalline solids, vol 2, 2nd edn, The chemistry of imperfect crystals. North-Holland, Amsterdam
4. Schmalzried H (1964) Point defect in ternary ionic crystals. In: Reiss H (ed) Progress in solid state chemistry, vol 2. North-Holland, Amsterdam
5. Smyth DM (2000) The defect chemistry of metal oxides. Oxford University Press, New York
6. Yoo HI (2010) Defect structure, nonstoichiometry, and nonstoichiometry relaxation of complex oxides. In: Riedel R, Chen IW (eds) Ceramic science and technology, vol 2. Wiley-VCH, Weinheim

Defects in Solids

Ulrich Guth
Kurt-Schwabe-Institut für Mess- und Sensortechnik e.V. Meinsberg, Waldheim, Germany
FB Chemie und Lebensmittelchemie, Technische Universität Dresden, Dresden, Germany

Introduction

In a perfect solid, atoms, molecules, or ions are arranged in a three-dimensional lattice. The removal of any particle from that needs the overcome of the lattice force. Therefore, the perfect lattice of a solid is an ideal state. The real solid is imperfect respectively the arrangement of the particles (disorder in arrangement), the different orientation (orientation disorder), and not uniform in vibration and rotation (movement disorder). Most important for different properties like mechanical and electrical behavior is the nonideal arrangement of the lattice building blocks. According to the extension, it can be distinguished in three-, two-, one-, and zero-dimensional disorder, respectively. Most important for the understanding of electrical conductivity as well as for the diffusion in solids is the zero-dimensional disorder (point defects). From the view of thermodynamics, the generation of defects in solids is understandable. Only at temperature 0 K, the lattice is perfect; that means all particles take their normal positions and the entropy is zero. Due to the entropy effect, the amount of defects increases with increasing temperature and therefore the Gibbs energy is diminished. At a certain concentration of defects, the free energy increases because of the forming of defects has no influence on the entropy. Those defects which are formed without changing of stoichiometry and arise from the solid system itself according to the thermodynamic conditions are called as intrinsic defects or sometimes as stoichiometric defects. According to the place in the lattice, atoms, ions, or molecules move from their normal positions in the lattice into free spaces of the lattice between particles into the so-called interstitials (Frenkel defects) or to the surface (Schottky defects) [1].

Intrinsic Disorder

Besides the Frenkel and the Schottky disorders, also the anti-Frenkel and anti-Schottky disorders exist. But more important are the Frenkel and Schottky types. In the case of sodium sulfate, sodium ions on the normal lattice position Na_{Na}^{x} (the notation of Kröger-Vink is used; see entry "▶ Kröger-Vinks Notation of Point Defects") go into free space of ions (interstitials) and sodium vacancies remain (Frenkel defects):

$$Na_{Na}^{x} \rightleftharpoons Na_{Na}^{\bullet} + V_{Na}^{'}$$

Additional to the particles and mass balance as well as to the electroneutrality of chemical equation, the availability of free space has to be taken into account as well so that the equation has to be written in exact manner:

$$Na_{Na}^{x} + V_i \rightleftharpoons Na_{Na}^{\bullet} + V_{Na}^{'}$$

However, the number of interstitials is very high and does not change practically due to forming of defects of ions so that the V_i can be omitted from the equation.

According to the mass action law, the defect concentration is a function of temperature. Due to the same mole fraction x of vacancies and sodium ions on interstitials, the mass action constant can be expressed by

$$\sqrt{K_x} = x_{Na_{Na}^{\bullet}} = x_{V_{Na}^{'}}$$

With the Gibbs free energy of formation $\Delta_f G = -RT \ln K_x$, the mole fraction (concentration) of defects $x_{Na_{Na}^{\bullet}} = x_{V_{Na}^{'}}$ is given by

$$\begin{aligned} x_{Na_{Na}^{\bullet}} &= \sqrt{K_x} = \exp(-\Delta_f G/2RT) \\ &= \exp(-\Delta_f H/2RT)\exp(-\Delta_f S/2R) \propto \sigma \end{aligned}$$

where K_x is the mass action constant. The concentration of defects is proportional to the electric conductivity σ that can be measured in dependence on temperature where $\Delta_f H$ *and* $\Delta_f S$ are the enthalpy and the entropy of defect formation, respectively. The slope of the plot log σ vs. 1/T is equal to $\Delta_f H/2R$

On the other hand, the electrical conductivity depends on the electrical mobility of the mobile species u_{Na} as well:

$$\sigma \propto x_{V_{Na}^{'}} u_{Na}$$

The mobility u, in turn, depends exponentially from the temperature with the activation energy E_a which is necessary to overcome the potential barrier (diffusion by vacancy or interstitial mechanism) when the ion is moving from one site to the other one:

$$u = u_0 \exp(-E_a/RT)$$

For the temperature dependence of the electrical conductivity σ, the product of two exponential functions is obtained:

$$\sigma = const.\ \exp(-\Delta_f H/2RT)\exp(-E_a/RT)$$

The first exponential expression is thermodynamic origin and the second is the kinetic one.

In the Schottky types of disorder, a pair of ions moves from the normal sites to the surface of the solid [2–4]. For LiI the Schottky equilibrium can be expressed by

$$Null \rightleftharpoons V_{Li}^{'} + V_I^{\bullet}$$

For this equation the mass action law can be applied as well. The number of Schottky defects N_V depends exponentially from the temperature. A similar expression as for Frenkel defects is obtained (N is the total number of sites):

$$N_V = const.N\exp(-\Delta_f H/2RT)$$

Defects can be also generated due to the interaction of a gas with its ion formed from it in the solid. Oxides which are in close contact with oxygen-containing gas phase are able to release or to built in oxygen as oxide ion from or into the lattice.

The release of oxygen from the normal lattice position (O_O^x) is connected with the generation of excess electrons (e'). From the chemical point of view, these electrons can be located at the ion in a lower valence state. In the case of oxides like TiO_2, SnO_2, and ZrO_2, three valent ions Ti^{3+}, Sn^{3+}, and Zr^{3+} can be formed. This is in accordance with the gray or black color which is typical for lower-valent compound and for the electronic conductivity. Physically spoken the excess electrons are in the conductivity band:

$$O_O^x \rightleftharpoons \tfrac{1}{2}O_2(gas) + V_O^{\bullet\bullet} + e'$$

The incorporation of oxygen can occur on interstitials with forming of electronic holes, e.g.,

$$\tfrac{1}{2}O_2(gas) + V_O^{\bullet\bullet} \rightleftharpoons O_O^x + 2h^{\bullet}$$

The holes can be imagined as oxygen ion with one negative charge O^{-}. In the Kröger-Vink notation, it can be expressed as $O_O^{\bullet} = h^{\bullet}$. In both

cases the mass action law can be applied. This leads to a logarithmic expression for the oxygen partial pressure dependence on the electrical conductivity. In the double logarithmic plot of σ vs p_{O_2}, a slope of 1/4. . .1/6 is obtained. In the case of an excess of electrons, the sign of the slope is negative, whereas for the hole conductivity, a positive sign can be expected.

Extrinsic Disorder

Extrinsic disorder can be established by admixing of alio-valent ions to the basic substance without changing the phase (homogeneous doping). That can be done for cations as well as for anions. In such cases a built-in equation is used. For the system $(Na_2SO_4)_{0.95}(BaSO_4)_{0.05} = Na_{1.9}Ba_{0.05}SO_4$, the following equation is obtained:

$$BaSO_4 \xrightarrow{Na_2SO_4} Ba^{\bullet}_{Na} + V'_{Na}$$

The anion lattice is complete. Ba^{++} has two positive charges and can compensate double amount of Na^+ so that in the cation lattice 0.05 mol remains empty as a negatively charged sodium ion vacancy V'_{Na}. The electroneutrality is ensured.

Yttria-stabilized zirconia (YSZ), e.g., the Nernst mass $(ZrO_2)_{0.84}(Y_2O_3)_{0.08} = Zr_{0.84}Y_{0.16}O_{1.92}$, is an example for a complete cation lattice and an incomplete anion lattice:

$$Y_2O_3 \xrightarrow{ZrO_2} 2Y'_{Zr} + V^{\bullet\bullet}_O + 3O^x_O$$

That means the cation sites result 0.84 + 0.16 = 2. The cation lattice is complete because the Y^{3+} ions occupy Zr^{4+} sites ($Y^{3+}_{Zr^{4+}}$ and in the Kröger-Vink notation Y'_{Zr}). For two Y^{3+} ions, a double positively charged oxide ion vacancy $V^{\bullet\bullet}_O$ is formed, in this case 0.08. The extrinsic disorder is often called as chemical disorder, mixed phase, or nonstoichiometric disorder.

In the real solid, all kinds of defects occur and have to take into account in a defect balance so

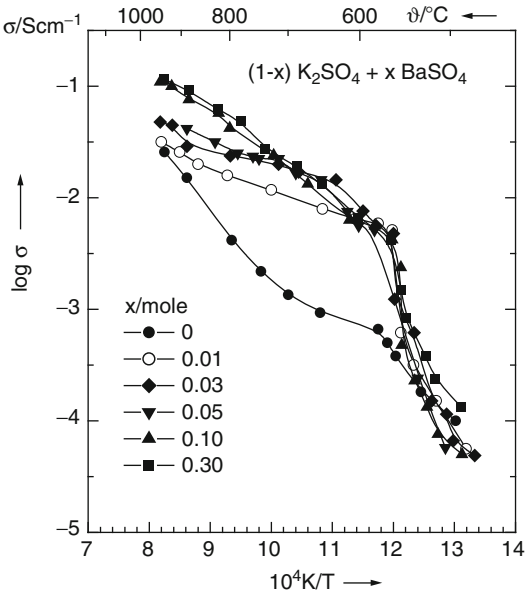

Defects in Solids, Fig. 1 Electrical conductivity in the system K_2SO_4-$BaSO_4$

that the concentrations of negatively and positively charged particles are equal. But mostly one type of defects is dominated. The role of intrinsic and extrinsic disorder can be illustrated in Fig. 1. In the range of 600–900 °C, the conductivity of pure and low-doped (up to 3 mol%) K_2SO_4 is determined by extrinsic disorder. The number of defects is nearly proportional to the concentration of dopant $BaSO_4$. At temperatures higher than 900 °C, all curves are merged by trend. In this range the conductivity is dominated by the intrinsic disorder. At higher amount of $BaSO_4$ (10–30 mol%), the system becomes heterogeneous and an increase of conductivity by heterogeneous doping (see below) can be observed.

Heterogeneous Doping

If an insulating material, e.g., γ-Al_2O_3, is mixed with an ionic conductor like LiI or Na_2SO_4, the electric conductivity increases due to the generation of defects on the surface of the ionic conductor. This effect is sometimes called as

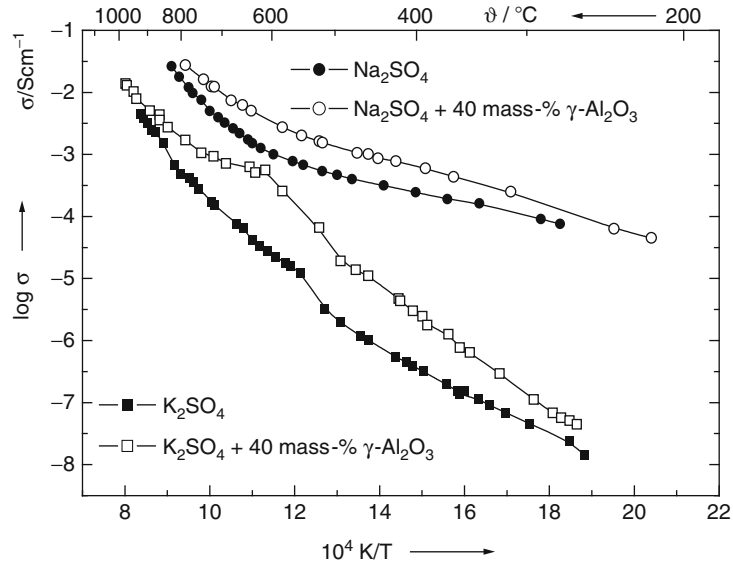

Defects in Solids, Fig. 2 Electrical conductivity of pure alkaline sulfates and composites consisting of salts with 40 mass% γ-Al_2O_3

"heterogeneous doping." That means in a two-phase system, Al^{3+} attracts counter ions in the ionic conductor so that ionic defects in the surface layer are formed [4]:

$$Na_{Na}^{x} + V_A \rightarrow Na_A^{\bullet} + V_{Na}^{'}$$
$$Na_A^{\bullet} + V' \rightarrow Na_i^{\bullet} + V_A$$

$Na_A^{\bullet}$ *and* $V_{Na}^{'}$ mean a sodium ion and vacancy at the grain boundary, respectively. This effect is caused by the interaction between the grains of electrolyte that disperse in fine grains of insulation material like γ-Al_2O_3 and depends on the volume fraction and the grain size of the dispersoid. This effect is illustrated in Fig. 2. The addition of 40 mass% γ-Al_2O_3 to sodium sulfate as well as to potassium sulfate provokes an increase in electrical conductivity.

Super Ionic Conductors

Besides the described disorder in some solids, there are more places than ions or the ions can occupy different sites. Such compounds like α-AgI or δ-Bi_2O_3 are called as super ionic conductors (see entry "▶ Solid Electrolytes"), and this disorder is described as structural disorder. Sometimes, it was distinguished between super ionic conductors of type I which show the conduction phenomenon over the whole temperature range like → β-alumina Na_2O*11 Al_2O_3, NASICON $Na_{1+x}Zr_2Si_xP_{3-x}O_{12}$ $(0 \leq x \leq 3)$ and such compounds which are super ionic conductors after the transition into the high-temperature phase like α-AgI or δ-Bi_2O_3 (type II).

Electronic Defects in Semiconductors

At 0 K the conduction band of semiconductors is completely empty (→ band theory). All electrons are in the valence band. With increasing temperature, electrons leave the valence band, overcome the band gap, and transfer into the conduction band. At given temperature an equilibrium between electrons and defect electrons is established:

$$e'\,(VB) = e'\,(CB) + V\,(VB)$$

Electron (valence band) $e'(VB)$ = electron (conduction band) $e'(CB)$ + electron vacancy (valence band) $V(VB)$

The electron vacancy is an electronic defect and can be regarded as a hole h°. This equilibrium can be expressed using the Kröger-Vink notation as

$$e' + h^{\circ} = Null = 0$$

Using the chemical potentials of electrons and holes with the concentrations of electrons and defect $[e']$ $[h^\circ]$ and the standard concentration $[e']^\circ$ *and* $[h^\circ]^\circ$, respectively

$\mu_e = \mu_e^\circ + RT \ln \frac{[e]}{[e]^\circ}$ and $\mu_h = \mu_h^\circ + RT \ln \frac{[h]}{[h^\circ]^\circ}$, the following expression is obtained:

$$[e'][h^\circ] = \text{const.}\ (p, T)$$

For a certain semiconductor, the product of the concentrations of electrons and holes is constant at defined partial pressure and temperature.

Experimental Methods for Defect Investigations

Defects can be discovered and determined by different experimental methods. By measurement of the electrical conductivity (see to ▶ Mixed Conductors, Determination of Electronic and Ionic Conductivity (Transport Numbers)) in dependence on partial pressure and temperature [5, 6] and the heat capacity in dependence on temperature [7], the defect formation could be detected. Hund investigated the defect structure in doped zirconia by measurement of specific density by means of XRD and pycnometric determination [8]. Transference measurements [9] and diffusion experiments with tracers [10–12] or colored ions [4] are suited for verifying defects.

Cross-References

- ▶ Defect Chemistry in Solid State Ionic Materials
- ▶ Kröger-Vinks Notation of Point Defects

References

1. Gellings PJ, Bouwmeester HJM (eds) (1997) Solid state chemistry. CRC Handbook, Boca Raton, New York, London, Tokyo
2. West AR (1984) Solid state chemistry and its applications. Wiley, Chichester/ New York/ Brisbane/ Toronto/Singapore
3. Rickert H (1982) Electrochemistry of solids. Springer, Berlin/Heidelberg/New York
4. Maier J (2004) Physical chemistry of ionic materials: ions and electrons in solids. Wiley, Chichester
5. Wagner C, (1936) Ionic conductivity in solid salts (in German) Die elektrische Leitfähigkeit in festen Salzen 42:635–654
6. Baumbach H-H-v V, Wagner C (1934) Electric conductivity of nickel oxide (in German) Die elektrische Leitfähigkeit von Nickeloxyd. Z Phys Chem B24:59–67
7. Nölting J (1970) Defect behavior of solids (Ionic crystals and metals) in Germ. Fehlordnungsverhalten von Festkörpern (Ionenkristallen und Metallen). Angew Chem 82:498
8. Hund F (1951) Abnormal mixed crystals in the system ZrO_2-Y_2O_3 Crystal structure of the Nernst glower (in Germany) Anomale Mischkristalle im System ZrO_2 Y_2O_3 Kristallbau der Nernst-Stifte. Z Elektrochem 55:363–366
9. Tubandt C (1932) Conductivity and transference number in solid electrolytes (in German) Leitfähigkeit und Überführungszahlen in festen Elektrolyten. In: Wien W, Harms F (eds), Handbuch der Experimantalphysik , Leipzig, pp 381–469
10. Jost W (1969) Diffusion in solids, liquids and gases. Academic, New York
11. Kingery WD, Bowen HK, Uhlmann DR (1976) An introduction to ceramic. Wiley, New York
12. Dieckmann R, Schmalzried H (1977) Defects and Cation Diffusion in Manganite (I). Ber Bunsen Phys Chem 81:344–347

Degradation of Organics, Use of Combined Electrochemical-Ultrasound

Jinren Ni
Peking University, Beijing, China

Introduction

Combined electrochemical–ultrasound systems are very efficient for organic degradation. Electrochemical oxidation processes are under mass-transport control at normal operating conditions [1, 2]. Therefore, enhancement of mass transport would be of primary importance to optimization of the processes. The ultrasound treatment, which is associated with acoustic cavitations in liquid media, is a rapid developing field in organic degradation [3, 4]. When

cavitation bubbles undergo asymmetrical implosion near a solid surface, it results in a strong microjet of liquid and violent shock wave towards the solid surface. Consequently, the solid–liquid mass transfer between the electrodes and the solution is strongly enhanced and the anode fouling is reduced [5, 6]. The combination of an ultrasonic field with an electrochemical oxidation can clean electrode surface and improve mass transport, resulting in a powerful alternative for efficient degradation of organic pollutants and particularly of biorefractory organics.

Functions of Combined Systems

Ultrasound-enhanced electrochemical systems with different electrodes have been widely reported for oxidation of variety of organics such as chlorinated organics [7, 8], dyes [9–11], phenolic substances [12–15], and other recalcitrant pollutants [16]. For example, the combined electrochemical–ultrasound process developed by Yasman et al. [7] was reported successfully at nickel anode for degradation of chlorinated aromatic compounds (2,4-dichlorophenoxyacetic acid and its derivative 2,4-dichlorophenol) in environmental water. Siddique et al. [9] investigated degradation of dye pollutants with a lead oxide anode enhanced by ultrasound under varying dye concentration, pH, ultrasonic frequency, and reaction time, followed by a full discussion of reaction kinetics, organic carbon, and mechanisms. The decomposition of reactive blue 19 dye and hence decolorization by ultrasound-assisted electrochemical process proved the higher efficiency and lower energy consumption of the combined system comparing with separated electrolysis or sonochemical system. Lima Leite et al. [14] used Pt electrode associated with ultrasound activation and totally oxidized the 2,4-dihydroxybenzoic acid at low concentrations, which was hardly completed by electrochemical process solely. Zhu et al. [17] investigated the effects of low-frequency (40 kHz) ultrasound on the electrochemical oxidation of several p-substituted phenols with BDD (boron-doped diamond) and PbO_2 anodes for a comparison, and considerable enhancement of organic degradation was achieved in different systems.

Influencing Factors

In the combined electrochemical–ultrasound systems, ultrasound frequency is one of the significant factors for degradation of organics. Under low-frequency ultrasound, cavitation leads to cleaning of the electrode surface thus increasing the active electrode surface and enhancing the mass transfer rates [14]. Then, the degradation of organics can be optimized with less intermediate compounds. At higher frequencies, hydroxyl radicals are generated acceleratedly as the lifetime of bubbles is shorter and collapse of cavitation bubbles occurs rather quickly. And then the oxidation between organics and hydroxyl radicals is increased. Siddique et al. [9] tested dyes pollutants on the lead oxide anode and found the degradation rate increased with the frequency in the scope of 0–80 kHz. However, no significant improvement was detected by increasing frequency from 80 to 100 kHz. There exists an optimal acoustic power as to a certain chemical reaction and a proper transfer condition of acoustic energy through the whole liquid as to a certain reaction system [18, 19].

Other influencing factors include initial pH, applied potentials, temperature, initial organic concentrations, and supporting electrolyte. [7]. It is indicated by Bringas et al. with 20–30 mg L^{-1} of diuron at BDD anode [16] that alkaline pH favors the mineralization rate and the total organic carbon removal was 92 % after 6 h of degradation, higher than that at neutral or acidic conditions (less than 80 %). Cañizares et al. obtained similar conclusions and the influence of pH depended on both the nature of organic compounds and its concentration [20, 21]. A faster degradation of organics could be achieved with increasing applied potentials; however, much more electric energy would be consumed. Optimal state could be established

for various kinds of electrochemical–ultrasound processes [7, 22]. No obvious impact of the temperature in the range between 10 °C and 40 °C was observed on the kinetics of the sonoelectrochemical mineralization of diuron [16].

Mechanism

The advantages of the combined ultrasound–electrochemical process over other techniques have been confirmed, and the mechanism of synergy has been fully investigated in the past years. Klima [23] emphasized the role of ultrasound and proposed four possible mechanisms such as electrochemistry-acoustic streaming, turbulent movement due to the cavitation, microjets resulting from the asymmetric collapse, and shock waves generated by spherical collapse of cavitating bubbles. Acoustic streaming optimizes the process of mass transfer, while other three mechanisms are helpful not only to transfer enhancement but also to electrode surface activation (depassivation). Compton et al. [24] pointed out that ultrasound can induce depassivation and erosion effects on electrode surfaces through cavitation events. They detected the huge effect of ultrasound on the mass transport by various voltammetric techniques and further described the effect using a model of an extremely thinned diffusion layer of uniform accessibility.

Some recent studies are focused on the mechanism of strong oxidation capacity dominated by hydroxyl radicals. Zhu et al. [17] made a significant contribution by revealing that anode materials determined the state of hydroxyl radicals and play an important part in electrochemical oxidation [12, 25]. In general, the hydroxyl radicals produced by water decomposition at active anodes (such as Pt, IrO_2, and RuO_2) can interact with the oxide anode and tend to form chemisorbed "active oxygen" (MO_{x+1}), leading to a weak oxidation ability [26], while at non-active anodes such as PbO_2, SnO_2, and BDD (boron-doped diamond), hydroxyl radicals do not react with anodes and thus they show a stronger degradation ability of organic compounds [27]. It is demonstrated [25, 28] that the hydroxyl radicals mainly exist as free state and react effectively with organic pollutants at BDD anodes, while adsorbed hydroxyl radicals dominate at PbO_2 anodes, and are not very effective for organics degradation. At SnO_2 anodes, the organic compounds reacted with both adsorbed hydroxyl radicals and free hydroxyl radicals. Furthermore, the effectiveness and mechanisms of combined electrochemical oxidation and ultrasound process was put forward with several p-substituted phenols as the model organics [17]. It is indicated that the enhancement of ultrasound on organic degradation was greater at the BDD anode (73–83 %) than at the PbO_2 anode (50–70 %) mainly due to the diverse effect of ultrasound on specialized existence of hydroxyl radicals at different electrodes.

Future Directions

Ultrasound plays a role in either the chemical degradation pathway or the electrochemical reaction at the electrode based on the frequency used. The increase extent is closely related with the electrode material. It seems that further investigation of the geometry of both electrodes and reactor is needed in order to optimize the ultrasound energy distribution, enhance the degradation efficiency, and reduce the energy consumption.

References

1. Polcaro AM, Mascia M, Palmas S, Vacca A (2004) Electrochemical degradation of diuron and dichloroaniline at BDD electrode. Electrochim Acta 49:649–656
2. Polcaro AM, Vacca A, Mascia M, Palmas S (2005) Oxidation at boron doped diamond electrodes: an effective method to mineralise triazines. Electrochim Acta 50:1841–1847
3. Pollet BG, Lorimer JP, Hihn JY, Phull SS, Mason TJ, Walton DJ (2002) The effect of ultrasound upon the oxidation of thiosulphate on stainless steel and platinum electrodes. Ultrason Sonochem 9:267–274
4. Del Campo FJ, Coles BA, Marken F, Compton RG, Cordemans E (1999) High-frequency sonoelectrochemical processes: mass transport, thermal and surface effects induced by cavitation in a 500 kHz reactor. Ultrason Sonochem 6:189–197

5. Kumbhat S (2000) Potentialities of power ultrasound in electrochemistry: an overview. Bull Electrochem 16:29–32
6. Bremner DH, Burgess AE, Li FB (2000) Coupling of chemical, electrochemical and ultrasonic energies for controlled generation of hydroxyl radicals: direct synthesis of phenol by benzene hydroxylation. Appl Catal A Gen 203:111–120
7. Yasman Y, Bulatov V, Gridin VV, Agur S, Galil N, Armon R, Schechter I (2004) A new sono-electrochemical method for enhanced detoxification of hydrophilic chloroorganic pollutants in water. Ultrason Sonochem 11:365–372
8. Esclapez MD, Sáez V, Milán-Yáñez D, Tudela I, Louisnard O, González-García J (2010) Sonoelectrochemical treatment of water polluted with trichloroacetic acid: from sonovoltammetry to pre-pilot plant scale. Ultrason Sonochem 17:1010–1020
9. Siddique M, Farooq R, Khan ZM, Khan Z, Shaukat SF (2011) Enhanced decomposition of reactive blue 19 dye in ultrasound assisted electrochemical reactor. Ultrason Sonochem 18:190–196
10. Rivera M, Pazos M, Sanromán MA (2009) Improvement of dye electrochemical treatment by combination with ultrasound technique. J Chem Technol Biotechnol 84:1118–1124
11. Cai M, Jin M, Weavers LK (2011) Analysis of sonolytic degradation products of azo dye Orange G using liquid chromatography-diode array detection-mass spectrometry. Ultrason Sonochem 18:1068–1076
12. Zhao G, Shen S, Li M, Wu M, Cao T, Li D (2008) The mechanism and kinetics of ultrasound-enhanced electrochemical oxidation of phenol on boron-doped diamond and Pt electrodes. Chemosphere 73:1407–1413
13. Zhao G, Gao J, Shen S, Liu M, Li D, Wu M, Lei Y (2009) Ultrasound enhanced electrochemical oxidation of phenol and phthalic acid on boron-doped diamond electrode. J Hazard Mater 172:1076–1081
14. Lima Leite RH, Cognet P, Wilhelm AM, Delmas H (2002) Anodic oxidation of 2, 4-dihydroxybenzoic acid for wastewater treatment: study of ultrasound activation. Chem Eng Sci 57:767–778
15. Trabelsi F, Aït Lyazidi H, Ratsimba B, Wilhelm AM, Delmas H, Fabre PL, Berlan J (1996) Oxidation of phenol in wastewater by sonoelectrochemistry. Chem Eng Sci 51:1857–1865
16. Bringas E, Saiz J, Ortiz I (2011) Kinetics of ultrasound-enhanced electrochemical oxidation of diuron on boron-doped diamond electrodes. Chem Eng J 172:1016–1022
17. Zhu XP, Ni JR, Li HN, Jiang Y, Xing X, Borthwick A (2010) Effects of ultrasound on electrochemical oxidation mechanisms of p-substituted phenols at BDD and PbO_2 anodes. Electrochim Acta 55: 5569–5575
18. Vajnhandl S, Marechal AML (2007) Case study of the sonochemical decolouration of textile azo dye Reactive Black 5. J Hazard Mater 141:329–355
19. Price JG (1992) Current trends in sonochemistry. The Royal Society of Chemistry, Cambridge, UK
20. Cañizares P, García-Gómez J, Sáez C, Rodrigo MA (2004) Electrochemical oxidation of several chlorophenols on diamond electrodes: part II. Influence of waste characteristics and operating conditions. J Appl Electrochem 34:87–94
21. Ai Z, Li J, Zhang L, Lee S (2010) Rapid decolorization of azo dyes in aqueous solution by an ultrasound-assisted electrocatalytic oxidation process. Ultrason Sonochem 17:370–375
22. Nagata Y, Nakagawa M, Okuno H, Mizukoshi Y, Yim B, Maeda Y (2000) Sonochemical degradation of chlorophenols in water. Ultrason Sonochem 7:115–120
23. Klima J (2011) Application of ultrasound in electrochemistry. An overview of mechanisms and design of experimental arrangement. Ultrasonics 51:202–209
24. Compton RG, Eklund JC, Marken F, Rebbitt T, Akkermans RP, Waller DN (1997) Dual activation: coupling ultrasound electrochemistry-an overview. Electrochim Acta 42:2919–2927
25. Zhu XP, Tong MP, Shi SY, Zhao HZ, Ni JR (2008) Essential explanation of the strong mineralization performance of boron-doped diamond electrodes. Environ Sci Technol 42:4914–4920
26. Johnson SK, Houk LL, Feng JR, Houk RS, Johnson DC (1999) Electrochemical incineration of 4-chlorophenol and the identification of products and intermediates by mass spectrometry, Environ Sci Technol 33:2638–2644
27. Panizza M, Michaud PA, Cerisola G, Comninellis C (2001) Anodic oxidation of 2-naphthol at boron-doped diamond electrodes. J Electroanal Chem 507:206–214
28. Zhu XP, Shi SY, Wei JJ, Lv FX, Zhao HZ, Kong JT, He Q, Ni JR (2007) Electrochemical oxidation characteristics of p-substituted phenols using a boron-doped diamond electrode. Environ Sci Technol 41:6541–6546

DFT Screening and Designing of Electrocatalysts

Ping Liu
Brookhaven National Laboratory, Upton, NY, USA

Introduction

One of the focuses in electrochemistry is to develop more active, more selective, and more stable electrocatalysts with low cost. To accomplish this task requires enough knowledge of how

a catalyst functions, such as the reaction mechanism and active sites. The ultimate goal is to have enough knowledge of important factors that determine the catalytic activity, which can be used to tailor catalysts atom by atom. However, it is extremely difficult to obtain all of the necessary details from current experimental techniques. Extensive theoretical and computational approaches have been employed to try to meet the goal of developing a fundamental understanding as a basis for catalyst design [1].

Development of DFT in Electrochemistry

Over the past few decades, density functional theory (DFT) starts to be recognized as an essential tool in describing electrocatalysts. Modeling the electrochemical systems using DFT presents a considerable challenge [2]. Quantum mechanical simulations are typically carried out within the canonical ensemble formalism, where the number of electrons is conserved. In order to model electrochemical systems, several factors have to be modeled simultaneously: the structure and chemistry that occurs at the anode and the cathode, the electron transfer between the two electrodes, and the local changes in the electrolytes. For the time being, this is impossible. Instead, various approximated approaches have been developed to simulate the electrochemistry, which describe the solid electrode surface, the liquid solution, the solvated ions, and the effect of changes in the chemical potential of the electrons in the solid.

Modeling the Solution

The presence of solution can dramatically alter the chemical reactions. This is clearly present in the electrochemical processes. Water has been considered critical to the performance of electrocatalysts [3–8], which may effectively stabilize both the protons and the reaction intermediates in various important electrochemical reactions (Fig. 1). Water/catalyst interfaces were described by optimizing a cluster or an ice-like solvent structure on the catalyst surfaces, partially or completely filling the volume between the upper and lower slab surfaces. In this way, the solvated proton can also be well described in the theoretical model.

Modeling the Potential

The solid–liquid interface is charge neutral as the electrolyte is conducting. The change on the solid surface will be counteracted by a countercharge built up by ions just outside the surface. The interface region, the Helmholtz layer, is approximated by a ca. 3Å thick electrical double-layer. The double-layer has a strong electrical field, which is central to the chemical activities of the interface. Although the quantum mechanical models have been developed to understand both qualitatively and quantitatively the effect of potential on the surface and intermolecular bindings [2], few ab initio efforts aimed at the potential dependence of a chemical reaction.

In order to include potential effects into considerations, Lozovio et al. developed a first-principles periodic DFT supercell approach [9], and Neurock et al. established a more advanced model [10]. In these methods, a potential across the interface is induced by tuning the charge on the electrode, where the countercharge is distributed homogeneously over the background of the cell. In this way, the water reorients according to the homogeneous background charge density and subsequently the reaction proceeds to form the well-known double-layer structure at the interface. By comparing the energies for different structures at a given potential, one is able to determine the free energy difference between these given states at a desired range of potentials. In the method of Otani and Sugino, an external dipole layer is introduced to create a charged surface, and the countercharge is therefore located approximately 10Å away from the electrode [11]. Both methods provide a large step forward towards a microscopic description of the electrochemical cell, but in the first case, the countercharge distributions are not localized, but arbitrary or broad. Anderson et al. recently have combined the DFT and a modified Poisson-Boltzmann theory, where the water molecules are not included directly but distributing the countercharge in a continuum dielectric medium.

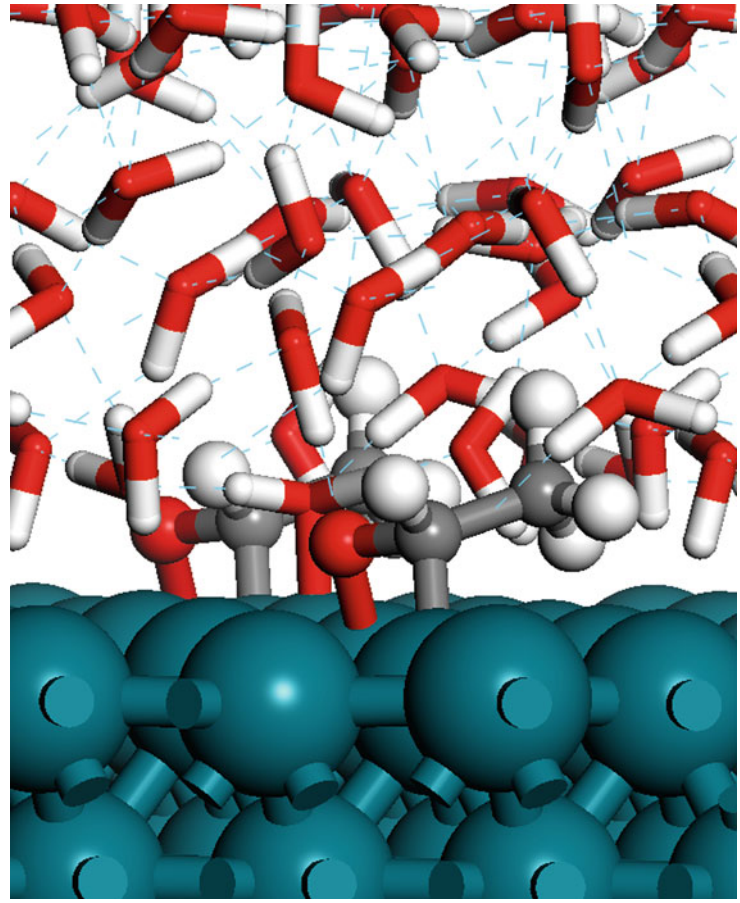

DFT Screening and Designing of Electrocatalysts, Fig. 1 Optimized CH_3CHO adsorption at the water/Rh(111) interface

It is able to predict with a useful accuracy the reversible potentials for electron transfer in acid and base aqueous solutions [12].

In order to avoid using these artificial treatments for counterchanges, Jonsson, Nørskov, and coworkers proposed to control the electrode potential by changing not only the charges of electrodes but also the number of protons to keep the system neutral [13]. However, the interactions from a long-ranged double-layer are not described. A more severe problem is that if a charge transfer reaction takes place and the unit cell is small, the potential changes significantly during the reaction. Therefore, it is very difficult to well control the electrode potential. However, these calculations are computationally expensive and limited to describe relatively simple reactions and electrocatalysts.

All the methods above cannot compare directly with experiments due to the difficulty in assigning the potential scale to the electrode. Rossmeisl et al. proposed a realistic atomic model for calculating reaction energies and activation energies for charge transfer reactions without finite-size errors [5]. It also provides a measure of the vacuum potential relative to the NHE and gives values for the interface capacitance in agreement with experiments. However, the calculations require several calculations for different unit cell sizes to extrapolate to the limit of an infinite surface unit cell. Therefore, it is computationally more expensive than the ordinary calculations for surface reactions.

Nørskov et al. developed a simple approach to describe the electrocatalytic reactions [14]. The thermochemistry of electrochemical reactions is

estimated by calculating the stability of the reaction intermediate using the DFT slab model. In this method, the chemical potential for $H^+ + e^-$ in solution is sent to that of $1/2H_2$ by setting the reference potential to that of the standard hydrogen electrode (SHE). The only two ways in which the potential enters the calculations are through the binding energy of ΔE_{ads}^{U} and the chemical potential of the electrons. An electrical field is introduced at the surface to simulate the double-layer. The potential dependence of adsorption energy was given largely by the first-order interaction between the adsorbate dipole moment μ_A and the field $F = U/d$ (U: potential, d: width of double-layer) with

$$\Delta E_{ads}^{U} = \Delta E_{ads}^{U-0} - \mu_A U/d$$

For all elementary reaction steps involving an electron, the enthalpy of the state is shifted by $-eU$. The free energy of the intermediates under a certain potential is expressed as a function of enthalpy, entropy, temperature, and pH value of the liquid phase. In this way, the artificial treatments for counterchanges can be avoided. The main downside is that this methodology only describes the thermodynamics. For estimating hydrogen binding with the surface intermediates by static methods and investigating the kinetics of surface process involving a charge transfer between the slab and the electrolyte, it will not be sufficient.

Application of DFT in Electrocatalysis

Developing a fundamental understanding of how catalyst function as a basis for design of improved catalysts has become one of the grand challenges in electrocatalysis. The electrochemical processes always involve multiple reaction pathways, active sites, and products and cannot be well characterized experimentally. The development of DFT in electrochemistry, as demonstrated above, makes it possible to understand the reaction mechanism at the atomic level. Such understanding allows the theoretical screening for better catalysts.

Description of the Electrochemical Reaction

Advances in DFT make it possible to describe electrocatalytic reactions at surfaces with the detail. The method developed by Neurock et al. [10] described qualitatively various electrochemical reactions, water activation, oxygen reduction reaction (ORR), as well as methanol decomposition on metal surfaces, being able to gain insights into the reaction mechanism under potential over aqueous-metal interfaces [3, 15, 16]. The method proposed by Nørskov et al. [14] is also extensively employed to describe the electrochemistry, which gives in some cases accuracy required for computational results to compare with experiment in a meaningful way. For instance, DFT calculations and a micro-kinetic modeling are combined to describe the H_2/CO electrooxidation on Pt and Pt alloy surfaces [17]. The model is very simple and is able to express the kinetics of a promoted anode surface relative to the activity of pure Pt directly from the calculated adsorption energy differences. As shown in Fig. 2, the calculated polarization curves on different surfaces agree well with the experimental measurements.

Understanding of Trend in Activity and Reaction Mechanism

DFT-based studies also provide the understanding of variations in catalytic activity from one catalyst to another, which is also qualitatively comparable to the experimental measurement [14, 17–20]. This allows more insight into the reaction mechanism. As shown in Fig. 2, both experiment and theory show that PtRu and Pt_3Sn are better electrocatalysts than Pt, being able to oxidize H_2 and CO at lower potential; in contract, higher potential should be applied to oxide CO on Ru. Within the model, the origin of the promoting effect of alloying can be analyzed. That is, the promoting effect of alloying on H_2/CO oxidation reaction can be attributed to the fact that alloyed metals modify Pt in the surface to bond CO weaker, thus decreasing the CO coverage under working conditions of the electrode. Such detailed understanding cannot be achieved merely using experimental techniques and is very important to the rational catalyst screening.

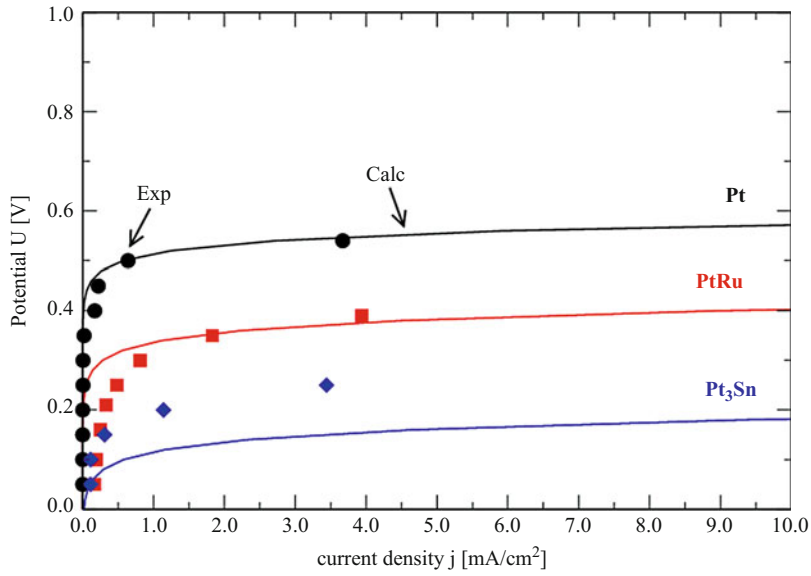

DFT Screening and Designing of Electrocatalysts, Fig. 2 Experimentally measured (*symbols*) and calculated (*curves*) overpotential as a function of current density for an anode half cell with 1 atm. of H_2 with 250 ppm of CO at 60°C (Adapted from Ref [17])

Screening of Catalysts Based on Single Descriptor

Such detailed understanding of mechanism based on DFT-based calculations leads to the theoretical screening for better catalysts using a single-scaling descriptor. A descriptor is a parameter, being able to capture the variation in overall activity or selectivity from one system to the next. One of representative examples is the study of the screening of anode catalysts for PEM fuel cell [21]. According to DFT-based kinetic studies [17], the experimentally measured activity of H_2/CO oxidation on Pt and Pt alloys is well correlated with a single descriptor including the DFT-calculated H_2 and CO binding energies. That is, the calculated descriptor is able to directly give a semiquantitative description of the experimentally measured difference in activity. The anode catalysts with better CO tolerance are the Pt alloys that bond CO more weakly than pure Pt while still dissociating H_2. Accordingly, tens of ternary catalysts, MPtRu, are screened at a theoretical level, where the activity trend predicted theoretically agrees well with the observations in the screening experiments [21]. In addition, the DFT-calculated O as well as CO and OH binding energies are considered as descriptors for ORR and methanol oxidation on metal or alloy surfaces, respectively [14, 22]. By using the single descriptor, the activity variation from one system to the next can be well explained, and more importantly new advanced catalysts are screened at a theoretical, which guides the experiment for catalyst development [23].

Future Directions

Even though some progress has been made towards understanding electrocatalytic process and screening electrocatalysts from DFT, the method has difficulty in providing quantitative numbers for detailed reaction steps. On one hand, methodological improvements are required to describe the electron transfer at solid–liquid interface, the band structure, and the excited states effectively, which is currently limitation of DFT. On another hand, the model systems in DFT studies are somewhat too simplified to model the real catalysts effectively. For instance, the real catalysts are powders, which may behave differently with size. Recently, efforts have been made to model the nanoparticles with the size of the real catalysts (<5 nm), showing indeed different behaviors from the extended surfaces even in term of trend (Fig. 3), a common model used in DFT studies [24, 25]. Thus, theoretical

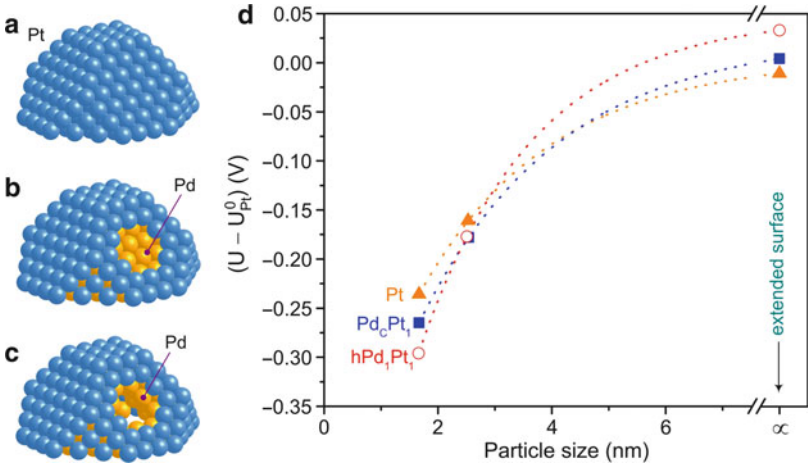

DFT Screening and Designing of Electrocatalysts, Fig. 3 Schematic illustration of surface models for the nanoparticles representing (**a**) pure Pt, (**b**) Pt shell-Pd core, (**c**) Pt shell-partially hollow Pd core, and (**d**) DFT-predicted dissolution potentials as a function of particle sizes (Adapted from Ref [24])

predictions based on the calculations of extended surfaces may not necessarily be able to describe the electrocatalysts with small size. In addition, the electrochemical processes may always be complex, including multiple reaction pathways, rate-limiting steps, and products. Given that, it will be difficult to capture the variation in overall activity or selectivity just using single descriptor. More sophisticated models are needed to capture knowledge needed to develop the rules for catalyst optimization. Finally, in contrast to the activity, the study of stability under potential and in solution is still at early stage [24, 26, 27]. Attention should be paid to ensure the stability of the screened electrocatalysts, which is of great importance for the practical application. With the further development of DFT method and models that can effectively treat more realistic catalysts and their environments, it can be envisioned that soon DFT modeling in electrochemistry will not only provide insight into the experimental measurements but also become the standard choice for designing a new catalyst for a catalytic process.

Cross-References

- ▶ Hydrogen Oxidation and Evolution on Platinum in Acids
- ▶ Oxygen Reduction Reaction in Acid Solution
- ▶ Platinum-Based Anode Catalysts for Polymer Electrolyte Fuel Cells
- ▶ Platinum-Based Cathode Catalysts for Polymer Electrolyte Fuel Cells

References

1. DOE-BES report (2007) Basic Research Needs: Catalysis for Energy: Department of Energy, http://science.energy.gov/~/media/bes/pdf/reports/files/cat_rpt.pdf.
2. Santan JA, Neurock M (2006) Molecular heterogeneous catalysis. Willey-VCH, Weinheim
3. Filhol J, Neurock M (2006) Elucidation of the electrochemical activation of water over Pd by first principles. Angew Chem Int Ed 45:402–406
4. Santan JA, Mateo JJ, Ishikawa Y (2010) Electrochemical hydrogen oxidation on Pt(110): a combined direct molecular dynamics/density functional theory study. J Phys Chem C 114:4995–5002
5. Rossmeisl J, Skulason E, Bjorketun ME, Tripkovic V, Norskov JK (2008) Modeling the electrified solid–liquid interface. Chem Phys Lett 466(1–3):68–71
6. Tian F, Jinnouchi R, Anderson AB (2009) How potential of zero charge and potentials for water oxidation to OH(ads) on Pt(111) electrodes vary with coverage. J Phys Chem C 113:17484–17492
7. Wang Y, Balbuena PB (2005) Ab initio molecular dynamics simulations of the oxygen reduction reaction on a Pt(111) surface in the presence of hydrated hydronium (H3O) + (H2O)2: direct or series pathways? J Phys Chem B 109:14896–14907
8. Hyman MP, Medlin JW (2006) Mechanistic study of the electrochemical oxygen reduction reaction on Pt (111) using density functional theory. J Phys Chem B 110:15338–15344

9. Lozovoi AY, Alavi A, Kohanoff J, Lynden-Bell RM (2001) Ab initio simulation of charged slabs at constant chemical potential. J Chem Phys 115(4): 1661–1669
10. Taylor CD, Wasileski SA, Filhol J, Neurock M (2006) First principles reaction modeling of the electrochemical interface: consideration and calculation of a tunable surface potential from atomic and electronic structure. Phys Rev B 73:165402
11. Otani M, Sugino O (2006) First-principles calculations of charged surfaces and interfaces: a plane-wave nonrepeated slab approach. Phys Rev B 73(11): 115407
12. Jinnouchi R, Anderson AB (2008) Electronic structure calculations of liquid–solid interfaces: combination of density functional theory and modified Poisson-Boltzmann theory. Phys Rev B 77: 245417
13. Skulason E, Karlberg GS, Rossmeisl J, Bligaard T, Greeley J, Jonsson H et al (2007) Density functional theory calculations for the hydrogen evolution reaction in an electrochemical double layer on the Pt(111) electrode. Phys Chem Chem Phys 9:3241–3250
14. Nørskov JK, Rossmeisl J, Logadottir A, Lindqvist L, Kitchin J, Bligaard T (2004) The origin of the overpotential for oxygen reduction at a fuel cell cathode. J Phys Chem B 108:17886–17892
15. Rossmeisl J, Nørskov JK, Taylor CD, Janik MJ, Neurock M (2006) Calculated phase diagrams for the electrochemical oxidation and reduction of water over Pt(111). J Phys Chem B 110(43):21833–21839
16. Janik MJ, Taylor CD, Neurock M (2009) First-principles analysis of the initial electroreduction steps of oxygen over Pt(111). J Electroanal Chem Soc 156(1):B126–B135
17. Liu P, Logadottir A, Nørskov JK (2003) Modeling the electro-oxidation of CO and H2/CO on Pt, Ru, PtRu and Pt3Sn. Electrochim Acta 48:3731–3742
18. Nørskov JK, Bligaard T, Logadottir A, Kitchin J, Chen JG (2005) Trends in the exchange current from hydrogen evolution. J Electrochem Soc 152(3): J23–J26
19. Kowal A, Li M, Shao M, Sasaki K, Vukmirovic MB, Zhang J et al (2009) Ternary Pt/Rh/SnO_2 electrocatalysts for oxidizing ethanol to CO_2. Nat Mater 8:325–330
20. Ingram DB, Linic S (2009) First-principles analysis of the activity of transition and noble metals in the direct utilization of hydrocarbon fuels at solid oxide fuel cell operating conditions. J Electrochem Soc 156(12): B1457–B1465
21. Strasser P, Fan Q, Devenney M, Weinberg WH, Liu P, Nørskov JK (2003) High throughput experimental and theoretical predictive screening of materials – a comparative study of search strategies for new fuel cell anode catalysts. J Phys Chem B 107(40): 11013–11021
22. Ferrin P, Nilekar AU, Greeley J, Mavrikakis M, Rossmeisl J (2008) Reactivity descriptors for direct methanol fuel cell anode catalysts. Surf Sci 602(21): 3424–3431
23. Greeley J, Stephens IEL, Bondarenko AS, Johansson TP, Hansen HA, Jaramillo TF et al (2009) Alloys of platinum and early transition metals as oxygen reduction electrocatalysts. Nat Chem 1(7):552–556
24. Sasaki K, Naohara H, Cai Y, Choi YM, Liu P, Vukmirovic MB et al (2010) Core-protected platinum monolayer shell high-stability electrocatalysts for fuel-cell cathodes. Angew Chem Int Ed 49(46): 8602–8607
25. Wang JX, Inada H, Wu L, Zhu Y, Choi Y, Liu P et al (2009) Oxygen reduction on well-defined core-shell nanocatalysts: particle size, facet, and Pt Shell thickness effects. J Am Chem Soc 131(47):17298–17302
26. Greeley J, Nøskov JK (2007) Electrochemical dissolution of surface alloys in acids: thermodynamic trends from first-principles calculations. Electrochim Acta 52(19):5829–5836
27. Tang L, Han B, Persson K, Friesen C, He T, Sieradzki K et al (2009) Electrochemical stability of nanometer-scale Pt particles in acidic environments. J Am Chem Soc 132(2):596–600

Dielectric Properties

Richard Buchner
Institute of Physical and Theoretical Chemistry, University of Regensburg, Regensburg, Germany

Static Relative Permittivity (Dielectric Constant)

Dielectric properties describe the polarization, $\boldsymbol{P}$, of a material as its response to an applied electric field $\boldsymbol{E}$ (bold symbols indicate vectors) [1–3]. In the field of solution chemistry, the discussion of dielectric behavior is often reduced to the equilibrium polarization, $\boldsymbol{P}_0 = \varepsilon_0(\varepsilon - 1)\,\boldsymbol{E}_0$ (ε_0 is the electric field constant), of the isotropic and nonconducting solvent in a static field, $\boldsymbol{E}_0$. Characteristic quantity here is the static relative permittivity (colloquially "dielectric constant"), ε, which is a measure for the efficiency of the solvent to screen Coulomb interactions between charges (i.e., ions) embedded in the medium. As such, ε enters into classical electrolyte theories, like Debye-Hückel theory or the Born model for solvation free energy [4, 5] and is used

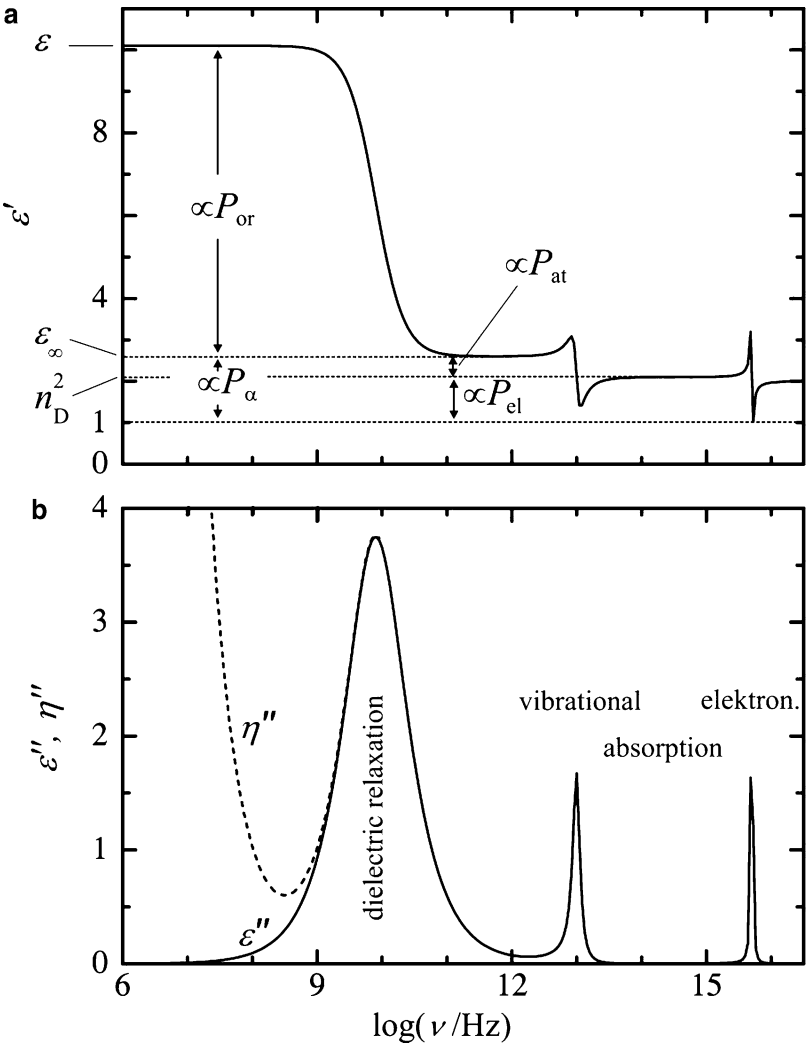

Dielectric Properties, Fig. 1 Schematic frequency dependence of (**a**) the relative permittivity, $\varepsilon'(\nu)$, and (**b**) the total loss, $\eta''(\nu)$ (*dashed line*), and the dielectric loss, $\varepsilon''(\nu)$ (*solid line*), of a sample with dc conductivity, κ_{dc}, static relative permittivity, ε, infinite-frequency permittivity, ε_∞, and optical refractive index, n_D. For simplicity, a single relaxation process and only one infrared-active vibration and one UV/vis absorption band are assumed. In (**a**), the dispersion steps associated with orientational ($\boldsymbol{P}_{or}\ \alpha\varepsilon - \varepsilon_\infty$), atomic ($\boldsymbol{P}_{at}\ \alpha\varepsilon_\infty - (n_D)^2$), and electronic ($\boldsymbol{P}_{el}\ \alpha(n_D)^2 - 1$) polarization are indicated

as a scale for solvent polarity. Note that ε also influences activation-barrier heights for chemical reactions in solution due to the necessary solvent reorganization along the reaction coordinate [6].

For molecular fluids, like most solvents, $\boldsymbol{P}$ can be split into induced polarization, $\boldsymbol{P}_\alpha$, associated with intramolecular polarizability, α, and orientational polarization, $\boldsymbol{P}_{or}$, arising from the partial alignment of the permanent dipole moments, μ, of the constituting molecules against thermal motions through $\boldsymbol{E}_0$. The induced polarization can be further subdivided into a generally small contribution $\boldsymbol{P}_{at}$ from the field-induced fluctuations of the molecular geometry (atomic polarizability) and the dominating electronic polarizability, $\boldsymbol{P}_{el}$, from the deformation of the electron cloud [1, 2]. Figure 1a schematically indicates the contributions of $\boldsymbol{P}_{or}$, $\boldsymbol{P}_{at}$, and $\boldsymbol{P}_{el}$ to the static permittivity and the frequency ranges up to which they are active. For atomic fluids, like liquid argon, only $\boldsymbol{P}_{el} \neq 0$ so that $\varepsilon \approx 2$. Since the electronic polarizability can follow changes of the electrical field without delay up to frequencies, ν, corresponding to visible light, we find $\varepsilon = (n_D)^2$ where n_D is the optical refractive index. Nonpolar liquids, like tetrachloromethane, also have $\mu = 0$ but intramolecular vibrations are possible, thus $\boldsymbol{P} = \boldsymbol{P}_{at} + \boldsymbol{P}_{el}$. As a result, the static permittivity, $\varepsilon = \varepsilon_\infty \approx 2...3$, is ~5–20 % higher than $(n_D)^2$. Larger values for the static

permittivity, $\varepsilon \approx 3\ldots200$ are only possible for polar fluids where the molecules possess a permanent dipole moment. Orientational polarization, $\boldsymbol{P}_{or}$, is essentially proportional to μ^2 and the molar concentration, c, of the dipoles. However, in a liquid, the molecular dipoles interact with each other and their resulting orientational correlations may significantly affect $\boldsymbol{P}_{or}$ and thus ε. Especially fluids composed of molecules forming hydrogen-bonded chains, like *N*-methylformamide, exhibit very large static permittivities due to a pronounced parallel alignment of the molecular dipoles. Such dipole-dipole correlations are conveniently expressed with the help of the Kirkwood factor, but they render the theoretical prediction of ε from α and μ difficult [1, 2]. Due to cross-correlations between the dipole moments of the component molecules, theoretical expressions for the static permittivity of liquid mixtures are rather elaborate [1, 2, 7].

Dielectric Response of Electrolytes

Even for pure liquids ε is not measured through the conceptually simple experiment of applying a static field, $\boldsymbol{E}_0$, to the sample-filled capacitor. Instead a harmonic ac field, $\boldsymbol{E} = \boldsymbol{E}_0 \cos(2\pi\nu t)$, with frequency $\nu \approx 1$ MHz is generally used and it is assumed that ν is sufficiently small to allow the molecular dipoles to follow changes of the electric field without delay, i.e., the equilibrium polarization is reached at any time t [8].

In the case of electrolyte solutions, composed of the solvent and a dissolved salt, with the latter more or less completely dissociated into free solvated ions, direct determination of ε is impossible due to the notable dc conductivity, κ_{dc}, of the solution. In this case, $\boldsymbol{E}$ not only aligns the permanent dipole moments of the solvent molecules and creates induced moments in all ions and molecules but additionally also drives an electric current. This *direct current* through ion transport dominates the sample response to a static field ($\nu = 0$, corresponding to observation times $t \rightarrow \infty$) whereas the *displacement current* associated with $\boldsymbol{P}_{or} + \boldsymbol{P}_{\alpha}$ vanishes as the time required for aligning the permanent and creating induced dipole moments is finite.

From this fact, it is sometimes erroneously concluded that ε is not defined or infinite for electrolyte solutions. However, the situation is more subtle and the time, respectively, frequency dependence of the sample response has to be considered: At low ν, the molecules bearing a permanent dipole moment can follow changes of the electric field acting on them without delay, i.e., the equilibrium value of $\boldsymbol{P}_{or} + \boldsymbol{P}_{\alpha}$ and thus the static permittivity, ε, is always reached. However, with increasing ν, the dipoles will more and more lag behind $\boldsymbol{E}(\nu)$ because of intermolecular friction and inertia. Consequence is an increasing phase shift between $\boldsymbol{E}(\nu)$ and $\boldsymbol{P}(\nu)$ which can be expressed by splitting polarization into a component in phase with $\boldsymbol{E}(\nu)$ and a component shifted by 180°. The first is characterized by the frequency-dependent relative permittivity, $\varepsilon'(\nu)$, which exhibits a decrease (dispersion) from ε at $\nu \rightarrow 0$ to ε_∞ at frequencies where orientational polarization is too slow to contribute (Fig. 1a). This dispersion of $\varepsilon'(\nu)$ is accompanied by energy dissipation in the sample, which is conveniently expressed by the dielectric loss, $\varepsilon''(\nu)$ (Fig. 1b), characterizing the out-of-phase component of $\boldsymbol{P}(\nu)$. In other words, because of intermolecular frictions, the ensemble of molecular dipoles requires a certain time to relax to the new equilibrium polarization after an instantaneous change of the electric field and this process dissipates heat. For most liquids around ambient temperature, characteristic relaxation times are in the order of picoseconds to nanoseconds, corresponding to dispersion frequencies in the microwave region (ca. 10 MHz–1 THz; Fig. 2); ε_∞ is reached in the far-infrared region. The response time for $\boldsymbol{P}_{at}$ and $\boldsymbol{P}_{el}$ is much shorter and governed by the quantum mechanics of intramolecular vibrations and electronic transitions. This leads to resonance features in $\varepsilon'(\nu)$ (Fig. 1b). The translational motions of the ions also depend on time so that in general, a frequency dependence of conductivity has to be assumed.

From Maxwell's equations, it follows that only the sum of direct and displacement currents

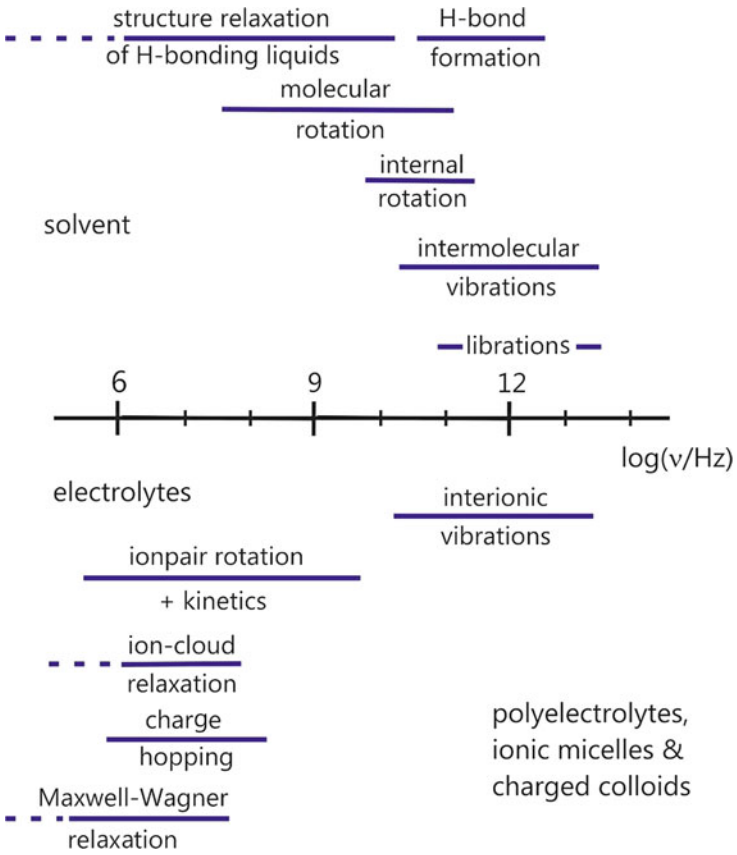

Dielectric Properties, Fig. 2 Frequency regions for typical processes contributing to the dielectric spectra of electrolyte solutions at room temperature

can be experimentally observed for a conducting sample in a time-dependent electric field [1–3]. This total dielectric response of the electrolyte solution is conveniently described by the total complex permittivity, $\eta^*(\nu) = \eta'(\nu) - i\eta''(\nu)$, where the real part, η', is in phase with $\boldsymbol{E}(\nu)$ and the total loss, η'', is shifted by 180° ($i^2 = -1$) [1, 2]. Alternatively, the total complex conductivity, $\kappa^*(\nu) = i2\pi\nu\varepsilon_0\eta^*(\nu)$, or the complex electric modulus, $M^*(\nu) = 1/\eta^*(\nu)$, can be used [3]. The causality principle requires that for $t \to \infty$ ($\nu = 0$), steady-state conditions (equilibrium values) are reached. Therefore, $\kappa^*(0) = \kappa'(0) = \kappa_{dc}$ and $\eta'(0) = \varepsilon$, so that $\eta''(0) = \lim_{\nu\to 0}\kappa_{dc}/(2\pi\nu\varepsilon_0) = \infty$ [1, 2]. Thus, despite diverging total loss for $\nu \to 0$, the static permittivity is a well-defined quantity for electrolyte solutions and its magnitude is essentially determined by orientational and induced polarization. Even more, for $\nu \to 0$, the slope of total relative permittivity vanishes, i.e., $d\eta'/d\nu = 0$, so that the required extrapolation $\varepsilon = \lim_{\nu\to 0}\eta'(\nu)$ of the experimental permittivity spectra is facilitated.

It is convenient to subtract the contribution arising from dc conductivity from the total complex permittivity, $\eta^*(\nu)$, yielding $\varepsilon^*(\nu) = \varepsilon'(\nu) - i\varepsilon''(\nu)$ where $\varepsilon'(\nu) = \eta'(\nu)$ and $\varepsilon''(\nu) = \eta''(\nu) - \kappa_{dc}/(2\pi\nu\varepsilon_0)$. In the following, we call $\varepsilon^*(\nu)$ the complex dielectric permittivity of the material (Fig. 1). Note that according to this pragmatic definition, which differs from Böttcher [1, 2], $\varepsilon^*(\nu)$ subsumes **all** processes contributing to $\boldsymbol{P}$ that explicitly depend on time/frequency, irrespective of their origin. In other words, no formal distinction is made between relaxations caused by dipole reorientation and modes originating from hindered ion translation or other possible mechanisms. This is reasonable as the origin of the features observed in the dielectric spectrum is not immediately obvious and additional information is required for their assignment to molecular-level motions. Figure 2

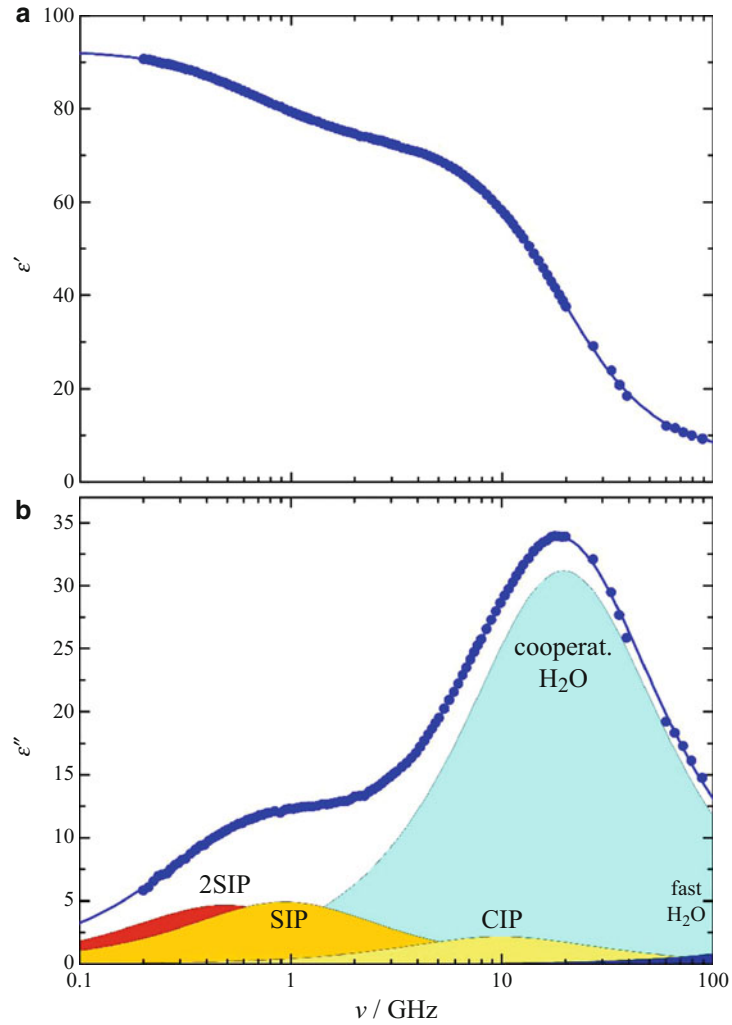

Dielectric Properties, Fig. 3 Spectra of (**a**) relative permittivity, $\varepsilon'(\nu)$, and (**b**) dielectric loss, $\varepsilon''(\nu)$, of 0.086 M $Al_2(SO_4)_3$ in water at 25 °C. Symbols represent experimental data, lines are calculated from a superposition of the five relaxation processes indicated by the *shaded areas* in (**b**)

provides an overview of dynamical processes relevant for electrolyte systems and their typical frequency ranges. Most of these modes, arising from the solvent and the solute, are relaxation processes but librations (hindered rotations), as well as intermolecular and interionic vibrations, are damped resonances.

Dielectric relaxation spectroscopy, i.e., the determination of ε*(ν) in the appropriate frequency range, provides a wealth of information on the dynamics of liquids and solutions at a molecular to mesoscopic (micelles, colloids) level (Fig. 2) [9, 10]. However, to get this, ε*(ν) has to be decomposed into individual modes (Fig. 3) which subsequently have to be assigned to physical processes. This is not always an easy task [10], especially as direct computer simulations of ε*(ν) reach only qualitative agreement so far [11]. For electrolyte solutions, a typical aim of dielectric studies is ion solvation. Since the solvent contribution to ε*(ν) (e.g., the bulk and fast water relaxations of Fig. 3) is characteristically affected, the determination of effective solvation numbers and inference on the relative strength of ion-solvent versus solvent-solvent interactions is possible [9, 10]. Ion association is a further focus as it manifests in relaxation processes specific to the ion pair species present (Fig. 3: 2SIP, SIP, CIP). In contrast to molecular spectroscopies, like NMR or

Raman, which only detect contact ion pairs (CIPs), dielectric spectroscopy is able to monitor all species with permanent dipole moment, including solvent-shared (SIP) and solvent-separated (2SIP) ion pairs [9, 10].

Note that in practice, experimental spectra – especially at low frequencies – may also contain contributions originating from the electrode/electrolyte interface. A typical example is electrode polarization arising from the formation of a diffuse double layer of ions close to a charged surface. Partly, such features depend on the dielectric properties of the electrolyte solution (our focus), but in essence, they are specific to the interface and thus are not topic of this contribution. However, such electrode processes are intensively studied in electrochemistry using, e.g., impedance spectroscopy.

Future Directions

The full potential of dielectric relaxation spectroscopy in electrolyte studies is just emerging. This is due to important progress in instrumentation during the last 5–10 years, which now allows access of the relevant frequency region of ~10 MHz–1 THz and beyond with relative ease. Also, quantitative computer simulation of $\eta^*(\nu)$ is coming into reach. This will provide a major step forward in the interpretation of dielectric spectra.

Cross-References

- ▶ Activity Coefficients
- ▶ Charged Colloids
- ▶ Electrochemical Impedance Spectroscopy (EIS) Applications to Sensors and Diagnostics

References

1. Böttcher CFJ (1973) Theory of electric polarization, vol 1. Elsevier, Amsterdam
2. Böttcher CFJ, Bordewijk P (1978) Theory of polarization, vol 2. Elsevier, Amsterdam
3. Kremer F, Schönhals A (2003) Broadband dielectric spectroscopy. Springer, Berlin
4. Bockris JO'M, Reddy AKN (1998) Modern electrochemistry 1: ionics, 2nd edn. Plenum, New York/London
5. Barthel J, Krienke H, Kunz W (1998) Physical chemistry of electrolyte solutions. Modern aspects. Springer, New York
6. Rainieri FO, Friedman HL (1999) Solvent control of electron transfer reactions. Adv Chem Phys 107: 81–189
7. Reis JCR, Iglesias TP (2011) Kirkwood correlation factors in liquid mixtures from an extended Onsager-Kirkwood-Fröhlich equation. Phys Chem Chem Phys 13:10670–10680
8. Moldover MR, Marsh KN, Barthel J, Buchner R (2003) Relative permittivity and refractive index. In: Goodwin ARH, Marsh KN, Wakeham WA (eds) Measurement of the thermodynamic properties of single phases, vol VI, Experimental thermodynamics. Elsevier, Amsterdam
9. Buchner R (2008) What can be learnt from dielectric relaxation spectroscopy about ion solvation and association? Pure Appl Chem 80:1239–1252
10. Buchner R, Hefter G (2009) Interactions and dynamics in electrolyte solutions by dielectric spectroscopy. Phys Chem Chem Phys 11:8984–8999
11. Schröder C, Steinhauser O (2010) Computational dielectric spectroscopy of charged, dipolar systems. In: Grünberg J (ed) Computational spectroscopy: methods, experiments and applications. Wiley-VCH, Weinheim

Direct Alcohol Fuel Cells (DAFCs)

Claude Lamy
Institut Européen des Membranes, Université Montpellier 2, UMR CNRS n° 5635, Montpellier, France

Introduction

In several applications, fuel cells are widely recognized as very attractive devices for producing directly electric energy from the combustion of a chemical product into oxygen, i.e., air. Low-temperature fuel cells, generally built around a proton exchange membrane, are aimed to be used for a large range of power sources. However, the final choice of the fuel is still difficult and depends greatly on the field of

application. If hydrogen or hydrogen-rich gas obtained by hydrocarbon reforming (e.g. methane steam reforming) is clearly the best choice for stationary applications, the difficulty of hydrogen distribution and on board storage for mobile applications leads to the necessity to look for alternative liquid fuels suitable for a direct oxidation fuel cell (DOFC) [1–3]. Several organic fuels have been often considered despite of their rather low electrochemical reactivity in comparison to hydrogen.

In this context, hydrogen carriers like alcohols feeding a direct alcohol fuel cell (DAFC) appear advantageous for two main reasons: they are liquid (which simplifies the problems of storage and distribution) and their theoretical mass energy density is rather high, close to that of gasoline (6.1 and 8.0 kWh/kg for methanol and ethanol, respectively [4]). The most studied alcohols are methanol [5], which is the simplest mono-alcohol, and ethanol [6].

One of the main advantages of methanol is its availability, its low price and the easiness of its storage as a liquid. But methanol is a toxic compound and a pollutant, so that extensive use is inconceivable because of environmental hazards (methanol is entirely miscible with water, which can lead to water contamination). On the other hand, ethanol appears to be an interesting alternative fuel for a wide range of utilization, even if its price is actually too high. Its low toxicity and its availability (from biomass, which will not change the natural balance of carbon dioxide in the atmosphere in contrast to the use of fossil fuels [1]) are important positive points for its use as an alternative fuel to methanol even if its reactivity is slightly lower [7].

The oxidation of ethanol is more difficult than that of methanol with the necessity to break the C–C bond to obtain its complete oxidation to CO_2. It was observed by "in situ" IR reflectance spectroscopy that the dissociation of ethanol leads also to the formation of adsorbed CO [8]. This is the proof that the C–C bond can be, at least to some extent, broken at room temperature and that carbon dioxide can be obtained. However, the main oxidation products are acetaldehyde and acetic acid, as observed after long term electrolyses of ethanol solution [9]. Conversely to methanol, Pt–Ru-based electrocatalysts lead to poor performances in ethanol electroxidation. Several works have indicated that the modification of Pt by tin gives very encouraging results leading to the oxidation of ethanol at lower potentials than on pure platinum.

Thermodynamics and Kinetics of Alcohol Oxidation in a DAFC

In a DAFC the total electro-oxidation to CO_2 of an aliphatic mono-alcohol, C_xH_yO, involves the participation of water (H_2O) or of its adsorbed residue (OH_{ads}) provided by the cathodic reaction (electro-reduction of dioxygen).

The overall electro-oxidation reaction in acid medium to reject the carbon dioxide produced can thus be written as follows:

$$C_xH_yO + (2x - 1)H_2O \rightarrow xCO_2 + nH^+ + ne^- \quad (1)$$

with $n = 4x + y - 2$. Such an anodic reaction is very complicated from a kinetics point of view since it involves multi-electron transfers and the presence of different adsorbed intermediates and several reaction products and by-products. However from thermodynamic data it is easy to calculate the reversible anode potential, the cell voltage under standard conditions, the theoretical efficiency and the energy density.

Thermodynamic Data

According to reaction (1) the standard Gibbs energy change $-\Delta G_1^o$, allowing calculating the standard anode potential $E_1^o = \frac{-\Delta G_1^o}{nF}$ can be evaluated from the standard energy of formation ΔG_i^f of reactant (i):

$$-\Delta G_1^o = x\Delta G_{CO_2}^f - \Delta G_{C_xH_yO}^f - (2x - 1)\Delta G_{H_2O}^f \quad (2)$$

In the cathodic compartment the electroreduction of oxygen does occur, as follows:

$$\frac{1}{2}O_2 + 2H^+ + 2e^- \rightarrow H_2O \quad (3)$$

with $\Delta G_2^o = \Delta G_{H_2O}^f = -237.1\,\text{kJ mol}^{-1}$, leading to a standard cathodic potential E_2^o:

$$E_2^o = -\frac{\Delta G_2^o}{2F} = \frac{237.1 \times 10^3}{2 \times 96485} = 1.229\ \text{V vs. SHE} \quad (4)$$

where SHE is the standard hydrogen electrode, acting as a reference electrode.

In the fuel cell the electrical balance corresponds to the complete combustion of the organic compound in the presence of oxygen, as follows:

$$C_xH_yO + \left(x + \frac{y}{4} - \frac{1}{2}\right)O_2 \rightarrow xCO_2 + \frac{y}{2}H_2O \quad (5)$$

with

$$\Delta G_r^o = \left(2x + \frac{y}{2} - 1\right)\Delta G_2^o - \Delta G_1^o = x\Delta G_{CO_2}^f + \frac{y}{2}\Delta G_{H_2O}^f - \Delta G_{C_xH_yO}^f, \quad (6)$$

leading to the equilibrium standard cell voltage:

$$E_{eq}^o = -\frac{\Delta G_r^o}{nF} = -\frac{\Delta G_2^o}{2F} + \frac{\Delta G_1^o}{nF} = E_2^o - E_1^o \quad (7)$$

Then it is possible to evaluate the specific energy W_e in kWh kg^{-1}:

$$W_e = \frac{(-\Delta G_r^o)}{3,600\,M} \quad (8)$$

with M the molecular mass of the compound, and knowing the enthalpy change ΔH_r^0 from thermodynamic data:

$$\Delta H_r^o = \left(2x + \frac{y}{2} - 1\right)\Delta H_2^o - \Delta H_1^o = x\Delta H_{CO_2}^f + \frac{y}{2}\Delta H_{H_2O}^f - \Delta H_{C_xH_yO}^f \quad (9)$$

one may calculate the reversible energy efficiency under standard conditions:

$$\varepsilon_{rev} = \frac{\Delta G_r^o}{\Delta H_r^o} \quad (10)$$

For methanol and ethanol, the electrochemical oxidation reaction and the standard anode potentials are:

$$CH_3OH + H_2O \rightarrow CO_2 + 6H^+ + 6e^-$$
$$E_{MeOH}^o = 0.016\,\text{V vs. SHE} \quad (11)$$

$$CH_3CH_2OH + 3H_2O \rightarrow 2CO_2 + 12H^+ + 12e^-$$
$$E_{EtOH}^o = 0.085\,\text{V vs. SHE} \quad (12)$$

This corresponds to the overall combustion reaction of these alcohols in oxygen:

$$CH_3OH + 3/2O_2 \rightarrow CO_2 + 2H_2O \quad (13)$$

$$CH_3CH_2OH + 3O_2 \rightarrow 2CO_2 + 3H_2O \quad (14)$$

with the thermodynamic data under standard conditions.

For higher alcohols, such as n-propanol, taken as an example, the following calculations can be made:

$$C_3H_7OH + 5H_2O \rightarrow 3CO_2 + 18H^+ + 18e^- \quad (15)$$

$$-\Delta G_1^o = 3\Delta G_{CO_2}^f - \Delta G_{C_3H_7OH}^f - 5\Delta G_{H_2O}^f = -3x394.4 + 168.4 + 5x237.1 = 171\,\text{kJ mol}^{-1} \quad (16)$$

so that $E_1^o = -\frac{\Delta G_1^o}{18F} = \frac{171.1 \times 10^3}{18 \times 96,485} = 0.098$ V vs. SHE and

$$C_3H_7OH + 9/2O_2 \rightarrow 3CO_2 + 4H_2O \quad (17)$$

with: $\Delta G_r^o = 9\Delta G_2^o - \Delta G_1^o = 3\Delta G_{CO_2}^f + 4\Delta G_{H_2O}^f - \Delta G_{C_3H_7OH}^f = -3x394.4 - 4x237.1 + 168.4 = -1,963\ \text{kJ mol}^{-1}$

Direct Alcohol Fuel Cells (DAFCs), Table 1 Thermodynamic data associated with the electrochemical oxidation of some alcohols (under standard conditions)

Alcohol	ΔG_l^o/kJ mol^{-1}	E_l^o/V vs. SHE	ΔG_r^o/kJ mol^{-1}	E_{cell}^o/V	W_e / kWh kg^{-1}	ΔH_r^o/kJ mol^{-1}	ε_{rev}
CH_3OH	–9.3	0.016	–702	1.213	6.09	–726	0.967
C_2H_5OH	–97.3	0.085	–1,325	1.145	8.00	–1,367	0.969
C_3H_7OH	–171	0.098	–1,963	1.131	9.09	–2,027	0.968
1-C_4H_9OH	–409	0.177	–2,436	1.052	9.14	–2,676	0.910
CH_2OH-CH_2OH	–25.5	0.026	–1,160	1.203	5.20	–1,189	0.976
CH_2OH-$CHOH$-CH_2OH	1	–0.001	–1,661	1.230	5.02	–1,650	1.01

The standard cell voltage is thus:

$$E_{eq}^o = -\frac{\Delta G_r^o}{18F} = \frac{1,963 \times 10^3}{18 \times 96,485} = \frac{237.1 \times 10^3}{2 \times 96,485} - \frac{171 \times 10^3}{18 \times 96,485} = 1.229 - 0.098 = 1.131 \text{ V}$$

and the specific energy is:

$$W_e = \frac{1,963 \times 10^3}{3,600 \times 0.060} = 9.09 \text{ kWh kg}^{-1} \quad (18)$$

The enthalpy change of reaction (17) is:

$$\Delta H_r^o = -3 \times 395.5 - 4 \times 285.8 + 302.6 = -2,027 \text{ kJmol}^{-1} \quad (19)$$

so that the reversible energy efficiency is:

$$\varepsilon_{rev} = \frac{\Delta G_r^o}{\Delta H_r^o} = \frac{1,963}{2,027} = 0.968 \quad (20)$$

Table 1 summarizes the results obtained with some mono-alcohols and polyols under standard conditions (25 °C, 1 bar, liquid phase).

For all the alcohols listed in Table 1, the cell voltage varies from 1.23 V to 1.05 V, which is very similar to that of a hydrogen/oxygen fuel cell (E°_{eq} = 1.23 V). The energy density varies between half to one that of gasoline (10–11 kWh kg^{-1}) so that these compounds are good alternative fuels to hydrocarbons. Furthermore the reversible energy efficiency ε_{rev} is close to 1, while that of the H_2/O_2 fuel cell is 0.83 at 25 °C (standard conditions).

However, the practical electric efficiency of a fuel cell is depending on the current which is delivered by the cell and is lower than that of the reversible efficiency. This is due to the irreversibility of the electrochemical reactions involved on the electrodes. The practical efficiency of a fuel cell can be expressed as follows:

$$\varepsilon_{cell} = \frac{n_{exp} \times F \times E(j)}{-\Delta H_r^o} = \frac{nFE_{eq}^o}{\left(-\Delta H_r^o\right)} \times \frac{E(j)}{E_{eq}^o} \times \frac{n_{exp}}{n} = \varepsilon_{rev} \times \varepsilon_E \times \varepsilon_F \quad (21)$$

with $E(j) = E_{eq}^o - (|\eta_a| + |\eta_c| + R_e j)$.

In most cases the anodic overpotential, η_a, is at least 0.5 V for a reasonable current density (100 mA cm^{-2}) so that the cell voltage, including an overpotential $\eta_c = -0.3$ V for the cathodic reaction, will be of the order of 0.4 V and the voltage efficiency will be $\varepsilon_E = 0.4/1.2 = 0.33$, under operating conditions. Such a drawback of the direct alcohol fuel cell can only be removed by improving the kinetics of the electro-oxidation of the fuel. This needs to have a relative good knowledge of the reaction mechanisms, particularly of the rate determining step, and to search for electrode materials (Pt–X binary and Pt–X–Y ternary electrocatalysts) with improved catalytic properties.

From equation (21), it follows that the increase of the practical fuel cell efficiency can be

achieved by increasing the voltage efficiency ($\varepsilon_E = E(j)/E^o_{eq}$) and the faradic efficiency ($\varepsilon_F = n_{exp}/n$), the reversible yield, ε_{rev}, being fixed by the thermodynamic data and the working conditions (temperature and pressure).

For a given electrochemical system, the increase of the voltage efficiency is directly related to the decrease of the overpotentials of the oxygen reduction reaction, η_c, and alcohol oxidation reaction, η_a, which needs to enhance the activity of the catalysts at low potentials and low temperature, whereas the increase of the faradic efficiency is related to the ability of the catalyst to oxidize completely or not the fuel into carbon dioxide, i.e. it is related to the selectivity of the catalyst. Indeed, in the case of ethanol, taken as an example, acetic acid and acetaldehyde are formed at the anode [10], which corresponds to a number of electrons involved of 4 and 2, respectively, against 12 for the complete oxidation of ethanol to carbon dioxide. The enhancement of both these efficiencies is a challenge in electrocatalysis.

Kinetics and Reaction Mechanism

The electro-oxidation of alcohols, even the simplest one, i.e. methanol, is a complex reaction, involving multi-electron transfer and several intermediate steps. The complete oxidation to CO_2, except for methanol, is never observed at room temperature. This is due to the difficulty of breaking the C–C bond, and of finding multifunctional electrocatalysts, in order to simultaneously activate one of the following main reaction steps : cleavage of C–H bonds with hydrogen adsorption and oxidation, breaking of the C–C bond, removal from the electrode active surface sites of strongly adsorbed intermediates (C_1 and/or C_n poisoning species) at low potentials, activation of the water molecule at low potentials to further oxidize the adsorbed residues, completion of the oxidation reaction to CO_2 by providing extra oxygen atoms, etc.

In order to improve the fuel utilization in a direct alcohol fuel cell (DAFC) it is important to investigate the reaction mechanism and to develop active electrocatalysts able to activate each reaction path. The elucidation of the reaction mechanism, thus, needs to combine pure electrochemical methods (cyclic voltammetry, rotating disc electrodes, etc.) with other physicochemical methods, such as "in situ" spectroscopic methods (infrared [11] and UV–VIS [12] reflectance spectroscopy), or mass spectroscopy such as DEMS [13], or radiochemical methods [14] to monitor the adsorbed intermediates and "on line" chromatographic techniques [15] to analyze quantitatively the reaction products and by-products.

The electrocatalytic oxidation of ethanol has been investigated for many years on several platinum-based electrodes, including Pt-X alloys (with X = Ru, Sn, Mo, etc.), and dispersed nanocatalysts. Pure platinum smooth electrodes are rapidly poisoned by some strongly adsorbed intermediates, such as carbon monoxide, resulting from the dissociative chemisorption of the molecule, as shown by the first experiments in infrared reflectance spectroscopy [8]. Both kinds of adsorbed CO, either linearly-bonded or bridge-bonded to the platinum surface, are observed. Besides, other adsorbed species have been identified by IR reflectance spectroscopy, including reaction intermediates, such as acetaldehyde and acetic acid, and other by-products [9].

Voltammetric results, completed by the different spectroscopic and chromatographic results, allowed us to propose a detailed reaction mechanism of ethanol oxidation, involving parallel and consecutive oxidation reactions, on Pt-based electrodes (such as Pt–Sn catalysts), where the key role of the adsorption steps was underlined.

$$Pt + CH_3 - CH_2OH \rightarrow Pt - (CHOH - CH_3)_{ads} + H^+ + e^- \quad (22)$$

$$Pt - (CHOH - CH_3)_{ads} \rightarrow Pt + CHO - CH_3 + H^+ + e^- \quad (23)$$

As soon as acetaldehyde (AAL) is formed, it can adsorb on platinum sites leading to a -$(CO–CH_3)_{ads}$ species (adsorbed acetyl):

$$Pt + CHO - CH_3 \rightarrow Pt - (CO - CH_3)_{ads} + H^+ + e^- \quad (24)$$

Then, because Sn is known to activate water at lower potentials than platinum, some OH species can be formed at low potentials on Sn sites according to reaction:

$$Sn + H_2O \rightarrow Sn - (OH)_{ads} + H^+ + e^- \quad (25)$$

and adsorbed acetaldehyde species can react with adsorbed OH species to give acetic acid (AA) according to:

$$Pt - (CO - CH_3)_{ads} + Sn - (OH)_{ads} \rightarrow Pt + Sn + CH_3 - COOH \quad (26)$$

Further oxidation to carbon dioxide is usually difficult on pure Pt electrodes at room temperature. However, carbon monoxide acting as a poisoning species, and CO_2, were clearly observed by infrared reflectance spectroscopy [8] or by DEMS [16], and CO_2 was detected by gas chromatography, whereas some traces of methane were observed at low potential ($E < 0.4$ V/RHE) by DEMS [16]. This may be explained by the following mechanism involving the dissociation of -$(CO–CH_3)_{ads}$ by breaking the C–C bond:

$$Pt + Pt - (CO - CH_3)_{ads} \rightarrow Pt - (CO)_{ads} + Pt - (CH_3)_{ads} \quad (27)$$

$$2Pt + H_2O \rightarrow Pt - H_{ads} + Pt - OH_{ads} \quad (28)$$

$$Pt - (CH_3)_{ads} + Pt - H_{ads} \rightarrow CH_4 + 2Pt \quad (29)$$

$$Pt - (CO)_{ads} + Sn - OH_{ads} \rightarrow CO_2 + H^+ + e^- + Pt + Sn \quad (30)$$

This mechanism can explain the higher efficiency of PtSn in forming AA compared to Pt at low potentials ($E < 0.35$ V vs. RHE), as was shown by electrolysis experiments. Moreover adsorbed OH species on Sn atoms can oxidize adsorbed -$(CO–CH_3)_{ads}$ species to CH_3–COOH or CO species to CO_2, according to the bifunctional mechanism [17].

This reaction mechanism of ethanol oxidation on a Pt-based electrode can be summarized by the following scheme [4] (Scheme 1).

In this mechanism the adsorbed acetyl plays a key role and its further oxidation is favored by the addition to platinum of metal atoms more easily oxidizable at low potentials, such as Ru, Sn, Mo, etc. Other electrocatalysts were considered for the electro-oxidation of ethanol, such as rhodium, iridium [18] or gold [19], leading to similar results in acid medium. The oxidation of ethanol on rhodium proceeds mainly through the formation of acetic acid and carbon monoxide, which is further oxidized to carbon dioxide when the rhodium surface begins to oxidize, at 0.5–0.7 V/RHE [18]. On gold in acid medium the oxidation reaction leads mainly to the formation of acetaldehyde [19].

Fuel Cell Results

The direct ethanol fuel cell is based on a proton exchange membrane fuel cell (PEMFC), in which the anodic compartment is fed with an ethanol-water mixture (Fig. 1).

Typical results were obtained with a membrane-electrode assembly (MEA) consisting of a Nafion®117 membrane on which are pressed the anodic electrocatalysts (Pt or Pt-based catalysts dispersed on a high surface area carbon support) and the cathodic catalyst (usually Pt/C with metal loading from 40 % to 60 %). An example of the electrical characteristics of a DEFC with Pt/C, PtSn/C or PtSnRu/C anode catalysts is given in Fig. 2.

Comparison between these three catalysts in terms of selectivity is difficult to perform for different reasons. As it can be seen in Fig. 2, the $E(j)$ polarization curves obtained with a DEFC mounted with a Pt/C anode does not achieve cell voltages high enough to be compared with the other catalysts. Thus data were recorded at

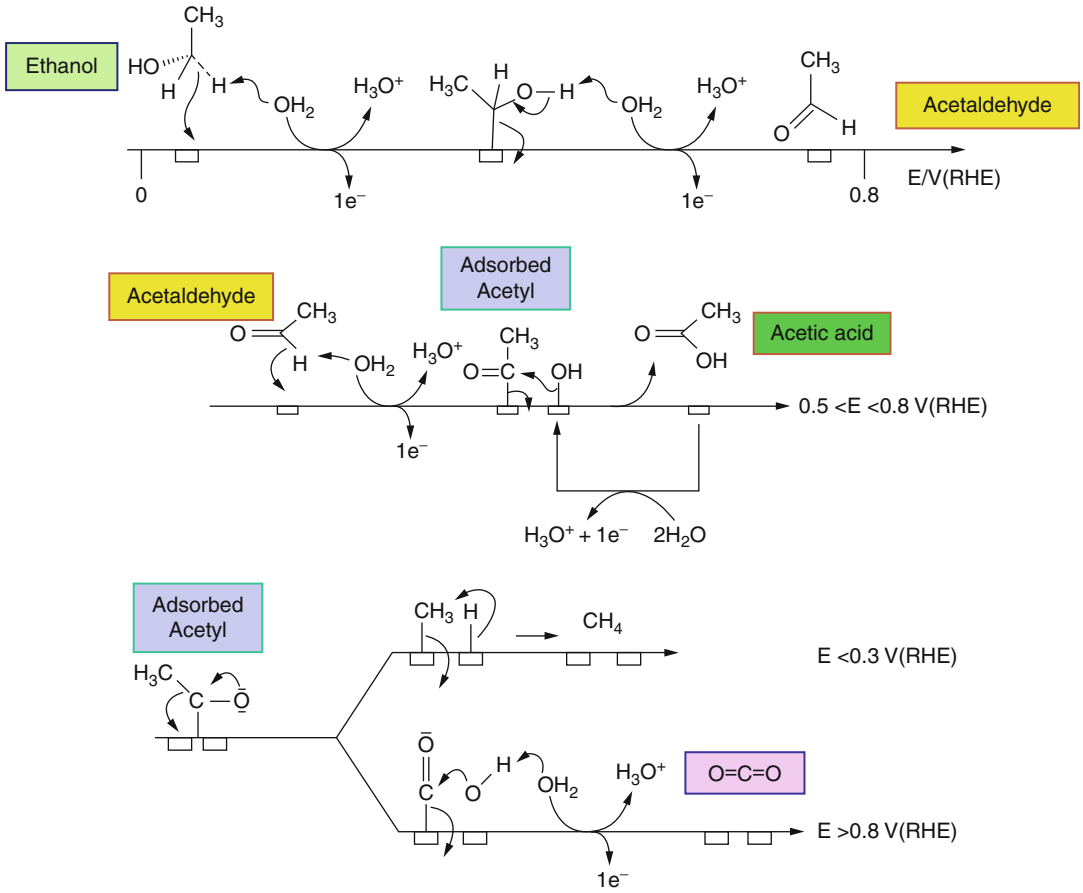

Direct Alcohol Fuel Cells (DAFCs), Scheme 1 Proposed mechanism for the electrocatalytic oxidation of ethanol on a Pt-based elecrode in acidic medium (all the species with color filling were detected either by *IR* reflectance spectroscopy or by chromatographic analysis)

cell voltages close to 0.2 V at a current density $j = 8$ mA cm^{-2} for the Pt/C anode and close to 0.48–0.58 V at $j = 32$ mA cm^{-2} for the PtSn/C and PtSnRu/C anodes.

The analysis of the reaction products at the exhaust from the anodic compartment can be made by HPLC. The analytical results are given in Table 2.

From these results it appears that the addition of tin to platinum greatly favors the formation of acetic acid comparatively to acetaldehyde. This can be explained by the bifunctional mechanism [17] where ethanol is adsorbed dissociatively at platinum sites, either via an O-adsorption or a C-adsorption process [9], followed by the oxidation of these adsorbed residues by oxygenated species formed on Sn at lower potentials giving AA.

On the other hand, the yield in CO_2 is twice higher with a Pt/C catalyst than with a Pt–Sn/C catalyst. This can be explained by the need to have several adjacent platinum sites to adsorb dissociatively the ethanol molecule and to break the C-C bond. As soon as some tin atoms are introduced between platinum atoms, this latter reaction is disadvantaged.

Future Directions

DEFC systems are claimed to be commercialized soon by some companies (e.g. Acta S.p.A. in

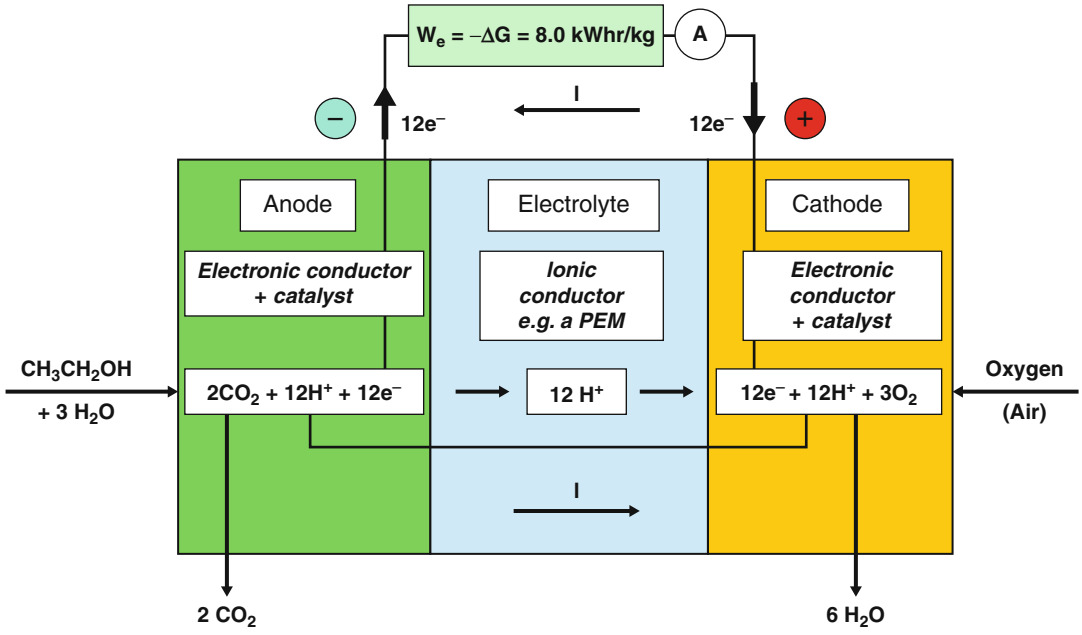

Direct Alcohol Fuel Cells (DAFCs), Fig. 1 Schematic diagram of a DEFC based on a proton exchange membrane

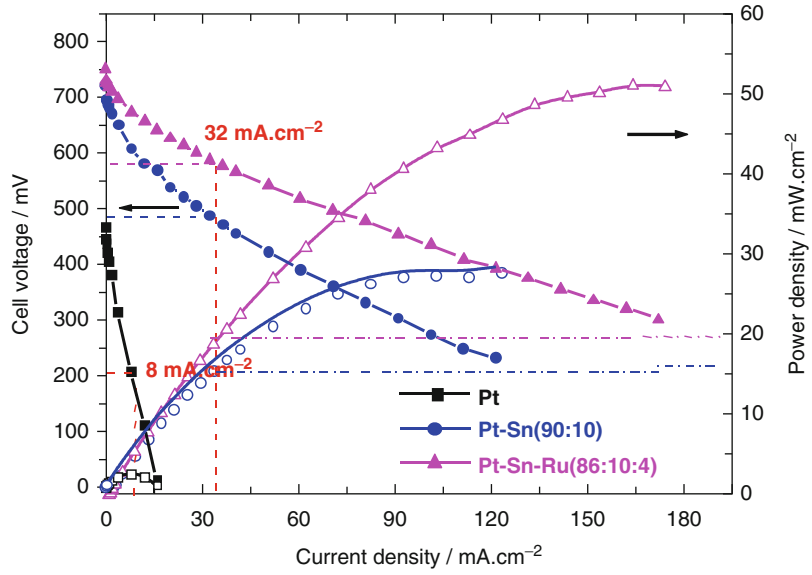

Direct Alcohol Fuel Cells (DAFCs), Fig. 2 Fuel cell characteristics of a DEFC with a 25 cm^2 surface area electrode recorded at 80 °C with different catalysts (2 M C_2H_5OH, N117)

Italy), but the technology is still immature for large-scale commercialization.

Indeed, the presence of both poisoning species (mainly CO) and intermediate reaction products (AAL, AA) decreases correspondingly the useful energy density of the fuel, and also the power density, since the oxidation current densities are lower than those obtained with the oxidation of

Direct Alcohol Fuel Cells (DAFCs), Table 2 Distribution of the reaction products resulting from the oxidation of 2 M ethanol at 80 °C after 4 h working at a current density of 32 $mA.cm^{-2}$ for PtSn and PtSnRu catalysts or of 8 $mA.cm^{-2}$ for Pt

Anode	Acetic acid	Acetaldehyde	CO_2
60 % Pt/XC72	13 mM	19 mM	8 mM
60 % Pt–Sn(90:10)/XC72	50 mM	10 mM	5 mM
60 % Pt–Sn–Ru (86:10:4)/XC72	44 mM	9 mM	6 mM

methanol and above all with that of hydrogen. To improve the kinetics of ethanol oxidation would require the development of new electrocatalysts able to break the C-C bond at low temperatures and to oxidize adsorbed CO at lower potentials, i.e. to reduce the oxidation overpotential.

In addition improvements in the sulfonated perfluorinated membranes, or development of new protonic membranes with reduced alcohol cross-over and better conductivity and stability at higher temperatures (up to 200 °C) are still challenging topics before any commercialization of DAFC systems.

Alternatively anion exchange membranes (AEM), conducting by OH^- anions, with good properties (stability, conductivity, etc.) will allow using non noble metal catalysts (transition metals) which are good electrocatalysts in alkaline medium for alcohol oxidation [20]. However the actually available AEMs are not stable above 60–70 °C and their ionic conductivity is one order of magnitude lower than that of Nafion®. Thus AEMFC needs the investigation of new OH^- conducting polymers with higher conductivity and stability at higher temperatures (above 100 °C).

Cross-References

- ▶ Alkaline Membrane Fuel Cells
- ▶ Electrocatalysis of Anodic Reactions
- ▶ Polymer Electrolyte Fuel Cells (PEFCs), Introduction

References

1. Gosselink JW (2002) Pathways to a more sustainable production of energy: sustainable hydrogen – a research objective for Shell. Int J Hydrogen Energy 27:1125
2. Takeichi N, Senoh H, Yokota T, Tsuruta H, Hamada K, Takeshita HT, Tanaka H, Kiyobayashi T, Takano T, Kuriyama N (2003) "Hybrid hydrogen storage vessel", a novel high-pressure hydrogen storage vessel combined with hydrogen storage material. Int J Hydrogen Energy 28:1121
3. Ströbel R, Oszcipok M, Fasil M, Rohland B, Jörissen L, Garche J (2002) The compression of hydrogen in an electrochemical cell based on a PE fuel cell design. J Power Sources 105:208
4. Lamy C, Belgsir EM (2003) Other direct alcohol fuel cells: fundamentals and survey of systems. In: Vielstich W, Lamm A, Gasteiger H (eds) Handbook of fuel cells, vol. 1. Wiley, Chichester, pp 323–334, Chap. 19
5. Zhang H, Liu H (eds) (2009) Electrocatalysis of direct methanol fuel cells. Wiley, Weinheim
6. Lamy C, Coutanceau C, Léger J-M (2009) The direct ethanol fuel cell: a challenge to convert bioethanol cleanly into electric energy. In: Barbaro P, Bianchini C (eds) Catalysis for sustainable energy production. Wiley, Weinheim, pp 3–46, Chap. 1
7. Lamy C, Lima A, Le Rhun V, Delime F, Coutanceau C, Léger J-M (2002) Recent advances in the development of direct alcohol fuel cells (DAFC). J Power Sources 105:283–296
8. Perez J-M, Beden B, Hahn F, Aldaz A, Lamy C (1989) "In situ" infrared reflectance spectroscopic study of the early stages of ethanol adsorption at a platinum electrode in acid medium. J Electroanal Chem 262:251–261
9. Hitmi H, Belgsir EM, Léger J-M, Lamy C, Lezna RO (1994) A kinetic analysis of the electro-oxidation of ethanol at a platinum electrode in acid medium. Electrochim Acta 39:407–415
10. Rousseau S, Coutanceau C, Lamy C, Léger J-M (2006) Direct ethanol fuel cell (DEFC): Electrical performances and reaction products distribution under operating conditions with different platinum-based anodes. J Power Sources 158: 18–24
11. Beden B, Lamy C (1988) Infrared reflectance spectroscopy. In: Gale RJ (ed) Spectroelectrochemistry – theory and practice. Plenum Press, New York, pp 189–261, Chapter 5
12. Kolb DM (1988) UV–VIS reflectance spectroscopy. In: Gale RJ (ed) Spectroelectrochemistry– theory and practice. Plenum Press, New York, pp 87–188, Chapter 4
13. Jusys Z, Massong H, Baltruschat H (1999) A new approach for simultaneous DEMS and EQCM: Electro-oxidation of adsorbed CO on Pt and Pt-Ru. J Electrochem Soc 146:1093

14. Horányi G (1999) In: Wieckowski A (ed) Interfacial electrochemistry: theory, experiment and applications. Marcel Dekker, New York, p 477
15. Belgsir EM, Bouhier E, Essis-Yei H, Kokoh KB, Beden B, Huser H, Léger J-M, Lamy C (1991) Electrosynthesis in aqueous medium: a kinetic study of the electrocatalytic oxidation of oxygenated organic molecules. Electrochim Acta 36: 1157–1164
16. Iwasita T, Pastor E (1994) A dems and FTir spectroscopic investigation of adsorbed ethanol on polycrystalline platinum. Electrochim Acta 39: 531–537
17. Watanabe M, Motoo S (1975) Electrocatalysis by adatoms: Part III. Enhancement of the oxidation of carbon monoxide on platinum by ruthenium adatoms. J Electroanal Chem 60:275–283
18. De Tacconi NR, Lezna RO, Beden B, Hahn F, Lamy C (1994) In-situ FTIR study of the electrocatalytic oxidation of ethanol at iridium and rhodium electrodes. J Electroanal Chem 379:329–337
19. Tremiliosi-Filho G, Gonzalez ER, Motheo AJ, Belgsir EM, Léger J-M, Lamy C (1998) Electrooxidation of ethanol on gold: analysis of the reaction products and mechanism. J Electroanal Chem 444:31–39
20. Varcoe JR, Slade RCT, Lam How Yee E, Poynton SD, Driscoll DJ (2007) Investigations into the ex situ methanol, ethanol and ethylene glycol permeabilities of alkaline polymer electrolyte membranes. J Power Sources 173:194–199

Direct Electrochemistry

► Direct Electron Transfer to Enzymes

Direct Electron Transfer to Enzymes

Roland Ludwig
Department of Food Science and Technology, Vienna Institute of Biotechnology
BOKU-University of Natural Resources and Life Sciences, Vienna, Austria

Synonyms

Direct electrochemistry

Definition

Direct electron transfer (DET) means an exchange of electrons between the cofactor of a redox-active enzyme (oxidoreductase) or a redox protein and an electrode (transducer) in the absence of redox mediators. DET is rarely observed and reported for only few redox proteins and redox enzymes. DET is of interest for fundamental studies on electron transfer in proteins and enzymes and for the development of sensitive and specific biosensors, robust biofuel cells and heterogeneous bioelectrosynthesis.

Background

Redox enzymes catalyze many biological processes, examples can be found in the bioenergetic cell metabolism which heavily depends on redox proteins and redox enzymes in the respiratory or photosynthetic chains. The importance of electron transfer reactions to sustain life is obvious. Many of these reactions occur in membranes (e.g., the mitochondrial inner membrane) where redox proteins and redox enzymes form electron transfer chains. Some of them exhibit DET when placed on electrodes. The reason is that electron transfer between proteins needs the ability of the involved proteins and enzymes to take-up or pass-on electrons from other constituents of the electron transfer chain along a potential gradient. Another group of redox-active enzymes capable of DET are extracellular enzymes involved in ligninolysis like laccase, lignin peroxidase and manganese peroxidase or cellulolysis like cellobiose dehydrogenase [1]. Obviously, an electrode surface of a suitable material or a properly modified electrode can replace redox proteins and redox enzymes, which are the natural electron transfer partners. Having redox enzymes directly connected to electrodes should allow the exploitation of their naturally high catalytic efficiency and selectivity in biosensors, biofuel cells and bioelectrosynthesis.

Research on the direct electron exchange between electrodes and proteins started in the late 1970s. In 1977 two groups independently

reported the observation of DET for cytochrome *c* on the surface of a tin doped indium oxide electrode [2] and a 4,4′-bipyridyl modified gold electrode [3]. The first enzymes shown to exhibit direct electrochemistry were a laccase [4] and a peroxidase [5]. Since then a growing number of redox proteins and redox enzymes have been shown to directly exchange electrons with electrodes. Many new electrode materials and surface modifications as well as new electrochemical techniques were developed to investigate the interaction of redox proteins and redox enzymes with the electrode surfaces in detail. Simultaneously, materials and techniques were improved and used to optimize DET to achieve high current densities and to develop reliable biosensors and biofuel cells.

Scientific Fundamentals

The redox enzymes that are most promising to exhibit DET have usually natural redox partners, e.g., cytochromes, ferredoxins or quinones. The electron transfer event between two nonbonded redox proteins or redox enzymes occur at, or close to, the surface of the protein (outer-sphere electron transfer). The electron transfer kinetics can be analyzed in various ways; the most commonly applied are the Butler-Volmer model and the Marcus theory [6]. According to the Marcus theory, the electron transfer kinetics between two redox species are determined by the driving force (potential difference), the reorganization energy (reflecting the structural rigidity of the redox species) and the distance between two redox centers. A greater distance between two redox-active prosthetic groups or a prosthetic group and the electrode surface reduces the electron transfer rate. It is often stated that at a distance greater than 15 Å the electron transfer rate becomes too low for physiological reactions or useful technical applications. Therefore, the design of optimized electrodes and redox proteins and enzymes pursues a high DET rate by reducing the electron transfer distance. Examples are the deglycosylation of proteins or the use of nanoparticles to achieve a more intimate contact

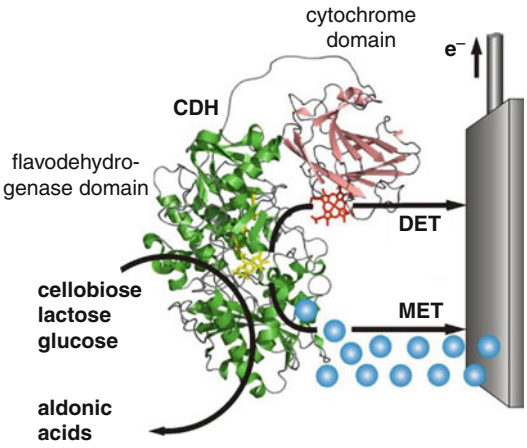

Direct Electron Transfer to Enzymes, Fig. 1 A schematic representation of a redox enzyme in vicinity to an electrode surface exemplifies two ways of electrical communication between the biorecognition element and the electrode. The shown flavocytochrome cellobiose dehydrogenase consist of two domains. The flavodehydrogenase domain (*green*) carries an FAD cofactor (*yellow*) in the catalytic site to oxidize aldoses at the anomeric carbon into aldonic acids. Connected to this catalytic domain via a short, flexible linker is the cytochrome domain (*pink*) carrying a *b*-type heme (*red*). The cytochrome domain is catalytically inactive, but can transfer electrons. Direct electron transfer (*DET*) can occur via the surface exposed heme. In this case the electrons from the reduced cofactor $FADH_2$ are transferred subsequently in one-electron steps to the electrode surface. Alternatively, electrons can be taken up directly from the $FADH_2$ by redox mediators (*blue spheres*) and transported to the electrode. Redox mediators for cellobiose dehydrogenase are one- or two-electron acceptors and can be soluble, diffusible redox mediators like redox dyes, metal complexes and quinones or Os-complex carrying redox polymers [9]

of redox center and conducting surface. If no direct electrochemistry between the enzyme's redox center and the electrode can be established, mediated electron transfer (MET) which uses diffusible redox mediators or redox polymers is the method of choice for contacting. An example of both approaches is given in Fig. 1. Two experimental approaches can be used to elucidate whether DET occurs between a redox protein or redox enzyme. Direct evidence comes from the observation of an electrochemical response of the redox-active cofactor. Indirect evidence can be obtained by observing a catalytic current in presence of an enzyme's substrate.

Active-Sites, Redox Proteins, and Redox Enzymes Exhibiting DET

DET has been observed for the following active sites of redox proteins or redox enzymes: iron-sulfur clusters (2Fe-2S, 3Fe-4S, 4Fe-4S, 4Fe-4S), flavins (FAD and FMN), hemes (*b*-type, *c*-type, etc. and subtypes) and quinones (PQQ). The best known and studied redox proteins exhibiting DET are cytochromes (cytochrome *c*, cytochrome c_3, cytochrome c_{552}, cytochrome b_5), globins (myoglobin, hemoglobin), ferredoxins, flavodoxins, plastocyanins, and cupredoxins. Redox enzymes are certainly proteins, but in contrast to redox proteins they do not store and transfer electrons, but catalyze reactions. The combination of DET and catalytic activity renders redox enzymes into valuable recognition elements for biosensors and biocatalysts for biofuel cells. Among others DET was reported for the following redox enzymes: Heme enzymes, e.g., nitrite reductase, cytochrome *c* oxidase, horseradish peroxidase, lignin peroxidase, manganese peroxidase, catalase; flavoenzymes, e.g., flavocytochrome b_2, cellobiose dehydrogenase, glucose oxidase, fumarate reductase, dimethyl sulfoxide reductase; copper-containing enzymes, e.g., laccase, tyrosinase, ascorbate oxidase, ceruloplasmin, galactose oxidase, nitrite reductase; molybdoenzymes, e.g., arsenit reductase, nitrate reductase, sulfite reductase and quinoheme alcohol dehydrogenase.

Techniques Used to Characterize Electron Exchange Processes

Bioelectrochemistry has benefited from the development of several new electroanalytic techniques like cyclic voltammetry or pulse voltammetry in the second half of the twentieth century. These technologies allowed solid macro- and microelectrodes of various materials to be used for the elucidation of electron transfer processes on various electrode materials. To overcome mass-transfer limitation rotating disc electrodes or flowcells for stationary electrodes have been developed. Cyclic voltammetry is the most widely used method but suffers sometimes from a lack of sensitivity or ill-defined redox waves. The familiar peak-like voltammograms appear for some species only at very low scan rates down to 1 mV s^{-1}. Square-wave voltammetry is a method that can be useful to overcome particular problems by being inherently more sensitive than cyclic voltammetry.

The success of protein voltammetry for DET measurements depends critically on the electrode material – how it is prepared and modified. The current response may come from (1) free diffusing molecules in solution or (2) tightly bound protein molecules. Diffusion-controlled electrochemistry (case 1) requires a transient interaction of the protein with the electrode so that the electrode is not blocked by reacted species. Nowadays the interest has turned more to electrode-bound protein molecules, allowing the study of redox proteins or redox enzymes as a stable monolayer or layer-by-layer assembly. Proteins can be immobilized by adsorption, electrostatic interaction, hydrophobic interaction or covalent bonds.

Electrode materials and surfaces that have successfully been used to study DET include: (1) metal electrodes made of gold, silver or platinum which can also be modified. (2) Metal oxide electrodes (tin(II) oxide, indium(III) oxide, zirconium(IV) oxide, ruthenium(IV) dioxide, FeO_3 nanoparticles, etc.) with or without modification. Gold and silver electrodes have been modified with alkanethiols, which form self-assembled monolayers (SAM). The head group (−SH) forms a covalent bond to the gold surface whereas the terminal group provides binding sites for the redox protein or redox enzyme. The terminal group can also be used to modulate hydrophobicity or surface charges of the SAM and therefore influence DET. The development of mixed SAM consisting of several species of head groups can be used to fine-tune the SAM properties to maximize binding and DET. Further modifications are ultrathin conductive polyion films and conductive polymer films. (3) Carbon (pyrolytic graphite, "edge" plane-oriented pyrolytic graphite, glassy carbon, or boron-doped diamond) is a suitable electrode

material for many redox proteins and redox enzymes. Especially the surface roughness of pyrolytic and "edge" plane graphite provides a high specific area for protein binding. Further carbon-based materials are carbon black, single-walled carbon nanotubes (SWCNT) and multiwalled carbon nanotubes (MWCNT), carbon nanoparticles or graphene sheets. The observed enhancement of the DET current comes from an increased specific surface area available for protein binding or from the closer contact of the nanostructures (spheres, edges, tubes) with the redox enzyme's active site.

Targeted Applications

Biosensors Based on DET

A biosensor is an analytical device consisting of a biological recognition element (bioelement) and an electrode. In the particular case of an amperometric biosensor the biorecognition element is oxidized or reduced by the analyte and generates a current that is proportional to the analyte concentration. The development of amperometric biosensors or enzyme electrodes was historically started by detecting an electroactive substrate, co-substrate or reaction product of the enzyme. Later, a second approach introduced uses nonphysiological redox mediators to shuttle electrons between the enzyme's active site and the biosensor's electrode. The third approach is to directly couple redox enzymes and electrodes by DET. These three sensor designs have been classified as first-, second- and third-generation biosensors [7].

An interesting feature of DET biosensors is a simple and robust electrode architecture (e.g., no leaking of soluble redox mediators). Additionally, many interfering substances affecting the detection in first- and second-generation biosensors do not interfere with biosensors based on DET. The number of possible analytes is of course restricted to the number of available enzymes, but by use of modern protein engineering techniques the spectrum of analytes will be broadened in future. An example is the modification of the substrate specificity of cellobiose dehydrogenase, which has a natural preference for cellobiose and cello-oligosaccharides. By rational engineering the enzyme's glucose turnover rate was improved and the enzyme can now serve as biocomponent for glucose detection.

DET Based Enzymatic Fuel Cells

In an enzymatic biofuel cell (BFC) the anode, cathode, or both are modified with enzymes to achieve bioelectrocatalysis. At the bioanode the fuel is oxidized and the biocathode reduces the oxidant. The catalytic process depends on the substrate specificity of the used enzymes. By cleverly selecting from the available DET enzymes, a variety of substrates and oxidants can be combined to achieve a high power output of the BFC. Substrates for DET-based BFCs are hydrogen, carbohydrates (glucose, fructose, lactose, maltose), alcohols (ethanol), amino acids, catecholamines, or ascorbic acid, which can be oxidized. The electrons are transferred from the enzyme to the anode and after passing the resistor/load electrons are transferred from the cathode to the biocatalyst where they reduce the oxidant. Protons are transferred through the electrolyte. Suitable oxidants are molecular oxygen (O_2), hydrogen peroxide (H_2O_2) or organic peroxides (ROOR') [8]. The main target of a BFC is to achieve a high power density – the ability to generate even in a small compartment a high current at a high cell voltage. A high specific current is pursued by three-dimensional, porous or nanostructured electrodes with a high specific surface area (m^2/m^3). A high cell voltage can only be achieved by careful selection of anode and cathode biocatalysts. A high equilibrium cell voltage (open circuit potential) is desired and requires an anode biocatalyst with an as low as possible and a cathode biocatalyst with an as high as possible redox potential of the cofactor. The thermodynamic border of the anode potential is −0.4 V versus SHE at pH 7.0 when using glucose as fuel and the border of the thermodynamic cathode potential is 0.8 V versus SHE when using oxygen as an oxidant. This sums up to a theoretical cell voltage of 1.2 V. The achieved cell voltages deviate from the

Direct Electron Transfer to Enzymes, Table 1 Fuels and biocatalysts tested in DET-based enzymatic BFCs

Fuel/oxidant	Anode biocatalysts/ cathode biocatalyst
Fuels	*Anode*
Cellobiose, lactose, glucose; maltose	Cellobiose dehydrogenase (CDH, EC 1.1.99.18)
Fructose	Fructose dehydrogenase (FDH, EC 1.1.99.11)
Ethanol	Alcohol dehydrogenase (ADH, EC 1.1.1.1)
Oxidants	*Cathode*
Oxygen (O_2)	Bilirubin oxidase (BOx, EC 1.3.3.5)
Oxygen (O_2)	Laccase (EC 1.10.3.2)
Hydrogen peroxide (H_2O_2)	Peroxidase (EC 1.11.1.7)

equilibrium voltage and decrease with increasing current. Reported cell voltages for enzymatic glucose/oxygen BFCs are between 0.2 and 0.8 V at power densities up to 1 mW/cm^2.

From the great number of oxidoreductases used to modify enzymatic BFC electrodes only a minority is capable of DET, which reduces the number of fuels and oxidants (Table 1). The substrate specificity of enzymes redners half-cell separation by e.g., membranes unnecessary. DET between enzyme and electrode also stops the need for soluble redox mediators to shuttle electrons between enzyme and electrode. This results in the possibility to design membraneless, non-compartmentalized enzymatic BFCs with a simple architecture. However, so far achieved DET currents are lower than MET currents, because usually only enzyme monolayers can be contacted. Strategies to improve the current density aim at the use of high surface area electrode materials like CNTs, AuNPs etc. or the layer-by-layer approach

Bioelectrosynthesis Employing DET

The application of enzymes as biocatalysts for the synthesis of organic molecules is a rapidly growing field. The most influential features of enzymes driving their application are their high chemo-, regio- and enantioselectivity as well as their substrate specificity. The high specificity of enzymes relieves the need for protecting groups and allows the transformation of complex molecules. Additionally, the advance of genetic engineering by rational design or directed evolution has a marked impact on the availability of stable and substrate specificity optimized enzymes. Redox enzymes catalyze a very wide range of reactions of interest in organic synthesis, but especially oxidoreductases with their need for cofactor- or coenzyme regeneration are difficult to employ and control. Clearly, these cofactors and coenzymes can be regenerated (oxidized or reduced) on electrodes. This is, in principle, the reverse approach of a biofuel cell which converts chemical energy into electricity. In bioelectrosynthesis the cheapest reduction equivalents (electrons) can be used for biochemical transformations. The application of DET-based enzyme electrodes for this purpose has, however, been hampered by the often poor electron transfer kinetics between electrode and interesting catalytic enzymes.

Future Directions

Basic research will further develop techniques for studies on electron transfer phenomena in biological macromolecules. In applied research, the optimization of the direct electron transfer between bioelements and electrodes is dominant. Improvement of DET is anticipated by a better orientation and binding of redox proteins and redox enzymes and the stabilization of the bioelement. Simultaneously an increased stability is pursued. The employed genetic methods for protein engineering are based on rational design and directed evolution. With the advance of analytical methods and a better knowledge of the structure/functional relationship of DET in redox proteins and redox enzymes the engineering of electron transfer pathways within proteins will become feasible.

Cross-References

▶ Biosensors, Electrochemical
▶ Cofactor Substitution, Mediated Electron Transfer to Enzymes

References

1. Christenson A, Dimcheva N, Ferapontova EE, Gorton L, Ruzgas T, Stoica L, Shleev S, Yaropolov AI, Haltrich D, Thornley RNF, Aust SD (2004) Direct electron transfer between ligninolytic redox enzymes and electrodes. Eletroanalysis 16:1074–1092
2. Yeh P, Kuwana T (1977) Reversible electrode reaction of cytochrome c. Chem Lett 10:1145–1148
3. Eddowes MJ, Hill HAOJ (1977) Novel method for the investigation of the electrochemistry of metal proteins: cytochrome c. Chem Soc Chem Commun:771b–772
4. Berezin IV, Bogdanovskaya VA, Varfolomeev SD, Tarasevich MR, Yaropolov AI (1978) Bioelectrocatalysis. Equilibrium oxygen potential in the presence of laccase. Dokl Akad Nauk SSSR 240:615–618
5. Yaropolov AI, Malovik V, Varfolomeev SD, Berezin IV (1979) Electroreduction of hadrogen peroxide on an electrode with immobilized peroxidase. Dokl Akad Nauk SSSR 249:1399–1401
6. Leger C, Bertrand P (2008) Direct electrochemistry of redox enzymes as a tool for mechanistic studies. Chem Rev 108:2379–2438
7. Habermüller K, Mosbach M, Schuhmann W (2000) Electron-transfer mechanisms in amperometric biosensors. Fresenius J Anal Chem 366:560–568
8. Falk M, Blum Z, Shleev S (2012) Direct electron transfer based enzymatic fuel cells. Electrochim Acta 82:191–202
9. Ludwig R, Harreither W, Tasca F, Gorton L (2010) Cellobiose dehydrogenase: a versatile catalyst for electrochemical applications. Chem Phys Phys Chem 11:2774–2697

Disinfection of Water, Electrochemical

Henry Bergman
Anhalt University, Anhalt, Germany

Introduction

Disinfection is the killing of vegetative microorganisms. Accepted methods must be able to reduce microorganisms by at least five orders of magnitude. Electrochemical water disinfection (ECD) is one of these methods [1]. ECD acts by means of electrochemical disinfectant generation onsite or inline (Fig. 1). Besides the disinfection effect, benefit of ECD arises from relatively simple cell construction and easy automation.

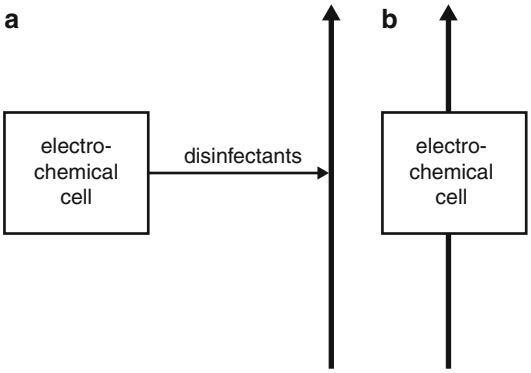

Disinfection of Water, Electrochemical, Fig. 1 Onsite (**a**) and inline addition (**b**) of disinfectants to water

The method must be distinguished from the killing or inactivation of microorganisms previously adhered to a surface (biofilm at different stages) by applying electrochemical surface polarization and from electroporation technologies working with field strength up to 10 MV m^{-1}. Whereas direct electron transfer seems to exist for adhered microorganisms [2], oxidant production is the most probable mechanism in electrochemical disinfection [3]. There were many speculations on the killing mechanisms in the past, including electrical field and pH effects. In flow-through treatment disinfection, however, immediate killing of all cells is not possible. The chemical reaction of disinfectants with microorganisms may proceed within a timescale from seconds to hours as well as outside the treatment unit.

Typical disinfectants that can be electrochemically produced are free active chlorine/free available chlorine (FAC) species as the sum of dissolved Cl_2, HOCl, and OCl^-. If these components react with selected water constituents, by-product formation occurs. In some cases, these by-products may also act as disinfectants (chloramines [4]). Other possible disinfectants obtained, depending on the electrolysis conditions, are ozone, hydrogen peroxide, chlorine dioxide, heavy metal ions, and bromine active species.

The participation of radicals, such as singlet and triplet oxygen radicals, hydroxyl radicals,

or radicals resulting from consecutive reactions of radicals with water constituents, is discussed very controversially. Radical lifetimes in the range of nanoseconds in a µm-reaction zone near the anode let one conclude that direct reactions with microorganisms are not decisive for their killing. Obviously, under these conditions, the majority of microorganisms are killed in reaction with more stable products (H_2O_2, O_3, FAC). Oxidant generation is mostly related to anodic reactions. However, cathodic reactions such as the reduction of dissolved oxygen to H_2O_2 may also contribute to generation of an oxidant:

$$O_2 + 2H_2O + 4e^- \rightarrow 2H_2O_2 \qquad (1)$$

A large variety of cell constructions, often using gas diffusion electrodes, have been developed or tested [5–7]. Widespread technologies using natural salt matrices for oxidant production in a flow-through regime (Fig. 1b) are known as *inline electrolysis, tube electrolysis, anodic oxidation, low-amperic electrolysis, electrochemical water activation*, or by brand names. In addition, immersion constructions have been reported. Fixed installations and mobile systems are in use (Fig. 2).

Inline methods are mostly related to the treatment of relatively low amounts of water per unit of time. Typical applications include the disinfection of pool and drinking water, for example, in hospitals, submarines, airplanes, senior residences, and other facilities. Potential nondrinking water applications include urban wastewater treatment, cooling water disinfection, saline wastewater disinfection, fish farming, vegetable washing, cleaning of pipe systems and containers, algae removal, tumor research, lens washing, dental implants, medical equipment, and cleaning of filters and permeates, often combined with odor abatement.

Disinfectants, if generated continuously in an electrochemical cell, may be added to a side or a mainstream of water. In special applications (i.e., drinking water), lower and upper limiting concentrations for FAC exist for the resulting concentration (often between 0.1 and 6 mg dm^{-3}).

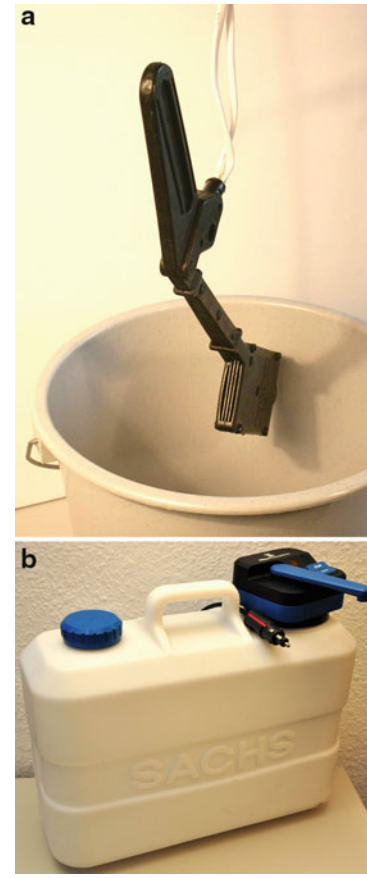

Disinfection of Water, Electrochemical, Fig. 2 (**a**) Immersion stack cell and (**b**) transportable disinfection cell with water container pump and electrolysis unit, both for discontinuous outdoor ECD; voltage sources are not shown

In comparison with ozone and chlorine dioxide, the main advantage of chlorine species as disinfectants is their reservoir effect in a system over increased time. The main disadvantage is the formation of halogenated by-products. Because of this, and to avoid microorganism adaptation effects, continuous use of disinfection cells without periodic interruption is not recommended.

Inline flow-through cells dominate the market. Divided and undivided cells are known. Cells have been commercialized to a remarkable extent since the 1970s, especially in Eastern Europe and Germany. Selected schematic constructions and technologies are shown in Figs. 3 and 4.

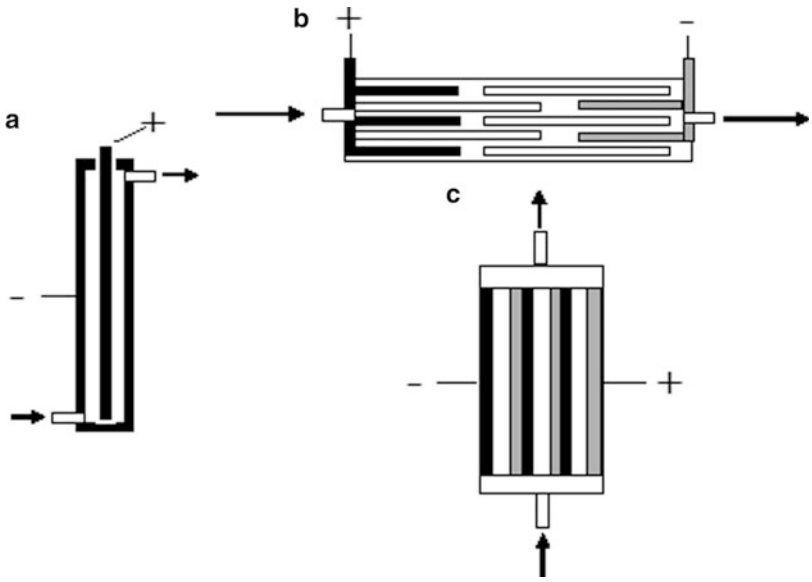

Disinfection of Water, Electrochemical, Fig. 3 Typical undivided flow-through constructions for ECD: tube electrolyzer (**a**), bipolar cell with nonoptimal current distribution (**b**), and bipolar parallel plate reactor (**c**)

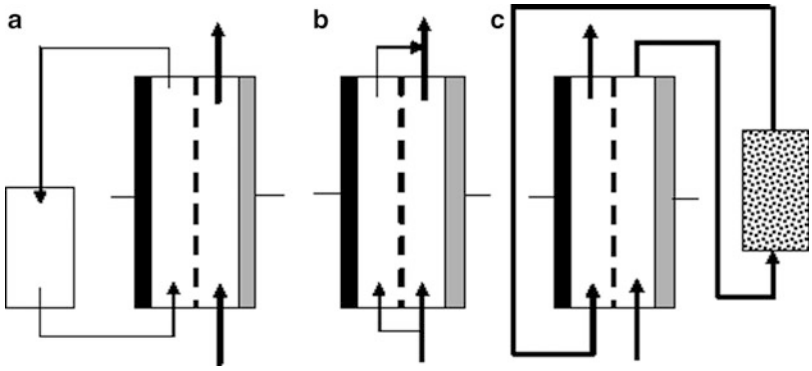

Disinfection of Water, Electrochemical, Fig. 4 Typical technologies using divided flow-through cells for ECD: with special catholyte recirculation (**a**), with addition of catholyte to the main water stream (**b**), and removal of by-products in a final fixed bed reactor (**c**)

Mostly, so-called mixed oxide (MIO) electrodes (typically TiO_2 doped with IrO_2, RuO_2, or VaO_x on Ti carrier material) are used in practical cases. TaO_x may be part of the oxide layers. Many researchers have studied other surface modifications. RuO_2-based electrodes seem to have better chlorine production compared with IrO_2 or Pt layers, but specific composition and methods of producing the activated layers are decisive for chlorine production efficiency [8, 9]. Untreated titanium, graphite, carbon cloth and glassy carbon, carbides, and nitrides were also studied. A relatively new, but sometimes problematic, material is boron-doped diamond (BDD, [10]). Applications of BDD anodes are accepted as so-called advanced oxidation methods. Summaries and disinfection-related papers can be found [8, 11–14]. Most applications and studies use direct current for disinfectant production. A few papers deal with alternating and pulsating current.

A large variety of technological schemes, electrode constructions, electrode materials, and water matrices have often resulted in confusion of health administrations in assessing applicability. There are big differences worldwide in practice

and legislation with respect to the usability of several disinfectants in special water systems. For example, contrary to North America or Australia, chloramine- or bromine-based disinfection is not widely used in Europe. In Germany, H_2O_2 may be used for pipe cleaning but not for drinking water disinfection, etc. Because in most cases (ECD) chlorine species are responsible for disinfection effects, the treated water must be classified as chloride containing or as water free of chloride.

Electrochemical onsite ClO_2 generation at ppm levels is a challenging new technology. Technologies dealing with the targeted electrochemical evolution of oxygen or the cathodic generation of H_2O_2, ferrates [15], chloramines, percarbonate, peroxodisulfate [16], or bromine for disinfecting waters are not included in the scope of this paper.

Main Systems and Reactions

Electrolytes Free of Chloride

In chloride-free water, the generation of ozone is the reaction of choice. Buffer or supporting electrolyte components must be added to the anolyte. Only anode materials with high oxygen overvoltage (Pt, glassy carbon, PbO_2, BDD) are able to generate ozone in water electrolysis. An overall reaction is shown in Eq. 2:

$$3H_2O \rightarrow O_3 + 6H^+ + 6e^- \quad (2)$$

Splitting of water is the main parasitic reaction (Eq. 3):

$$2H_2O \rightarrow O_2 + 4H^+ + 4e^- \quad (3)$$

To avoid side reactions and to isolate hydrogen evolution (Eq. 4 for acidic conditions), the anolyte and catholyte must be separated each from other:

$$2H^+ + 2e^- \rightarrow H_2 \quad (4)$$

Reaction mechanisms vary with different electrode materials. Ozone formation was first shown for Pt anodes [17, 18]. Initial commercial cells were equipped with PbO_2 layers on porous Ti carriers (*Membrel* technology). BDD is a promising commercial material despite its high price. The formation of hydroxyl radicals is accepted for many electrode materials in a more or less adsorbed state and in connection with more or less density of active sites. It is also accepted that on BDD, ozone is formed as the result of stepwise radical formation in a µm reaction zone (Eqs. 5, 6, 7, and 8):

$$H_2O \rightarrow {}^{\cdot}OH + H^+ + e^- \quad (5)$$

$${}^{\cdot}OH \rightarrow O^{\cdot} + H^+ + e^- \quad (6)$$

$$2O^{\cdot} \rightarrow O_2 \quad (7)$$

$$O_2 + O^{\cdot} \rightarrow O_3 \quad (8)$$

Hydroxyl radicals may quickly form H_2O_2: [19]

$$2\,{}^{\cdot}OH \rightarrow H_2O_2 \quad (9)$$

Other radical reactions are possible. In most cases, the reaction scheme is not well understood.

Current efficiency calculated from the concentration of dissolved ozone is a function of current density [20]. Technical cells are equipped with expanded mesh anodes to increase current densities. Ozone is added onsite or inline. Immersion constructions were also reported. As compared with silent discharge, electrochemical ozone generation is characterized by the high specific energy demand of about 2 kWh per kg ozone. Much higher ozone concentrations can be adjusted, however.

In electrolytes that are extremely poor in chloride ions, formation of ozone must be considered as a side reaction. Often, the standard DPD test for chlorine analysis shows higher values than expected [21]. Further research is still necessary. Application of MIO anodes under these conditions is highly risky because the obtained by-product spectrum can be contrary to rules for drinking water. Some researchers have studied the disinfection effect

in waters without chloride ions, mostly using sulfate electrolytes and Pt, stainless steel, and other electrode materials [22–25]. Discussions are sometimes questionable due to difficulties in relating the disinfection effect with species clearly responsible for it.

Electrolytes with Chloride Concentrations in the Range of Grams per Liter

MIO anodes are in widespread use for this technology. The anodic product is chlorine, with current efficiencies higher than 90 % (Eq. 10):

$$2Cl^- \rightarrow Cl_2 + 2e^- \quad (10)$$

The electrochemical reactor must be divided because hydrogen evolution is the main cathodic reaction (Eq. 4, avoiding explosive mixtures). As in industrial chlorine-alkaline electrolysis, chlorine can be directly contacted with the water to be disinfected, or it can be used for preparation of sodium hypochlorite by reacting with NaOH (Eq. 11) for subsequent addition:

$$Cl_2 + NaOH \rightarrow NaOCl + H^+ + Cl^- \quad (11)$$

Because this technology does not resolve problems with chlorine dosage from gas balloons (uncontrolled setting free of chlorine gas), it is not widely used in practice.

Electrochemical cells with MIO anodes for hypochlorite solution production as stock solutions for onsite addition of $HOCl/OCl^-$ mixtures have found increasing application worldwide (cell units producing more than 100 kg FAC per day). Divided cells and NaCl concentrations in the range of seawater (3.5 %) are typical, but undivided cells are also offered by some manufacturers. Chlorate formation inside the stock solution at longer storage times is a problem with this technology:

$$OCl^- + 2HOCl \rightarrow ClO_3^- + 2H^+ + 2Cl^- \quad (12)$$

Some plant manufacturers prefer the use of water with a chloride concentration close to that of drinking water with optional addition of NaCl salt. The production of anolyte solution for disinfection has the advantage that the resulting pH is relatively low, and HOCl may be the predominant species. Its disinfection ability is much higher than that of OCl^-.

Electrolytes with Chloride Concentrations Typical for Drinking Water

This technology for direct drinking water electrolysis has been the focus of interest for 60 years [26], but detailed kinetic studies began only at the end of 1990s. Many drinking water regulations recommend a maximum concentration of 250 mg dm^{-3} for chloride ions. This is sufficient to produce FAC with typical current efficiency amounts of 5–15 % on MIO anodes and in undivided cells. Nearly linear curve behavior for FAC production and current efficiency versus chloride concentration (Fig. 5) exist [8, 9]. Often, current efficiency maxima are observed between 100 and 200 A m^{-2} due to the competing oxygen evolution reaction. Specific electroenergy demands (for electrolysis current) of 50 kWh per kg FAC can be measured.

At very low chloride concentrations (normally lower than 10 mg[Cl^-] dm^{-3}), no FAC can be found. Two general mechanisms are responsible for this behavior:

(i) Formed FAC is converted to chloride by oxidants such as H_2O_2.
(ii) Formed FAC is oxidized to products such as chlorate and perchlorate in electrochemical reactions. Finally, only traces of chloride can be found in the treated water.

In long-term electrolysis, all prior existing Cl is finally distributed between the species FAC, ClO_3^-, and ClO_4^- [27]. Reaction rates are higher for BDD anodes as compared to MIO anodes. Intermediates are probable but not exactly known. Participation of radicals is also possible on MIO and Pt electrodes [28].

Considering electrode kinetics, the most probable first step is the oxidation of chloride to the chloride radical by electron transfer or by reaction with hydroxyl radicals:

$$Cl^- \rightarrow Cl + e^- \quad (13)$$

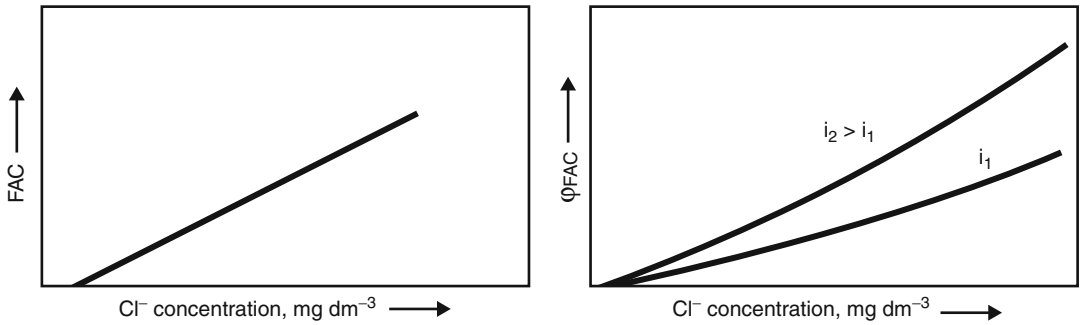

Disinfection of Water, Electrochemical, Fig. 5 Quasi-linear behavior of chlorine (FAC) production versus chloride concentration (*left*) and FAC current efficiencies versus chloride concentration at different current densities (*right*)

$$Cl^- + {}^{\cdot}OH \rightarrow Cl + OH^- \qquad (14)$$

Chlorine molecules formed from the chlorine radical quickly react with water and hydroxide ions to form hypochlorous acid and hypochlorite ions with a strong pH dependence of species distribution [4].

Chlorine Dioxide Generation from Chlorite

Chlorine dioxide is an effective disinfectant that reduces the formation of organic disinfection by-products. There are different chemical and electrochemical technologies for producing and adding ClO_2 onsite, initiating the reaction from chlorite or chlorate [5]. It is noteworthy here that even traces of chlorite added to a water stream may quickly react to form chlorine dioxide at low ppm levels [29]:

$$ClO_2{}^- \rightarrow ClO_2 + e^- \qquad (15)$$

When chloride ions are present during electrolysis, chlorine dioxide formation is accelerated [29], obviously as the result of the quick reaction with hypochlorous acid in the acidic electrode layer:

$$2HClO_2 + HClO \rightarrow 2ClO_2 + Cl^- + H_2O + H^+ \qquad (16)$$

Semi-inline technologies with chlorite additions are still under research.

Future Directions

Address Problems in Electrochemical Water Disinfection

By-Product Formation

Species produced by ECD must be classified as *disinfection products* (e.g., FAC), *disinfection by-products* (named as DBPs, e.g., chloramines and THMs) resulting from disinfectant reactions with organic matter or from inorganic reaction schemes (chlorate), and *electrolysis by-products* (e.g., nitrite and ammonium ions from cathodic processes or organic intermediates on BDD anodes). Ozone may be an electrolysis product or by-product depending on the target of electrolysis. Due to health risks, some of these by-products are regulated by legislation. Many by-products are not yet anchored in national or international rules. Overall, the subject has not yet been researched enough. Concerning reactions of FAC with organic matter, by-products similar to those observed in chlorination processes can be expected [30].

Electrochemical reaction behavior of organic compounds is difficult to assess. Research works sometimes show that intermediates may be formed that are more toxic than the initial system. The formation of chlorate [31], bromate on mixed oxide electrodes [32], peroxodisulfate, and H_2O_2 [19] is well known as well as the formation of DPDs such as THMs and AOX.

In studies of Bergmann and co-workers, the following by-products of inline drinking water electrolysis were identified for the first time: chlorate, perchlorate, bromate and perbromate on BDD, and other anodes; chlorine dioxide as a by-product in disturbed chloride electrolysis; nitrite, ammonia/ammonium as cathodic products on mixed oxide electrodes; and hydrogen peroxide on BDD anodes and MIO cathodes [8, 33–36]. Many results were confirmed by other researchers [37, 38]. Risks for halogenate and perhalogenate formation increase in the order of dosage of chlorine as Cl_2 – dosage as a hypochlorite solution – inline electrolysis of FAC species.

Electrochemical methods for ammonia and ammonium reduction were suggested by Kim et al., Kapalka et al., and others [39, 40]. Modification of reaction conditions and clarification of mechanisms are the subject of current research.

The state of legislation and control concerning electrochemical disinfection devices in environmentally oriented applications is not satisfactory. Only in the USA, first attempts for perchlorate restrictions in drinking water can be observed. In Germany, a first complex project on inline electrolysis was finished in 2010. Currently, the method is still outside legislation but tolerated. The project included cell producers, water authorities, and research groups.

Formation of Deposits on Electrodes and System Surfaces

Especially in cells without a separator between anode and cathode and in processes using natural water matrices, cathodes show a tendency to be coated with deposits. Due to the increased pH in the cathodic electrode layer, mainly calcareous and hydroxidic scaling with earth alkali ions is observed ($CaCO_3$, $Mg(OH)_2$, etc.). Several antiscaling methods have been suggested, such as periodic dissolution in acids, change of polarity, rotating brushes or cleaning vanes, ultrasonic treatment, and current pulsation. Many methods for scaling quantification were suggested (potential control, quartz mass balance, etc. [41, 42]). In practical application, cell voltage and cell current monitoring are the most widespread methods used. In some cases, deposition of iron hydroxide on water pipe walls was observed when electrolysis shifted the pH to a more basic pH region.

Gas Inside the System

If the chloride concentration is in the range of milligrams per liter, the primary electrochemical reaction is the splitting mechanism of water, with oxygen and hydrogen formation. Use of separators is the best way to keep hydrogen gas out; however, oxygen still remains in the system and should be allowed to escape in a sophistic way. Increased corrosion is sometimes reported as the result of changing water decomposition and pH during electrolysis.

References

1. Martinez-Huite CA, Brillas E (2008) Electrochemical alternatives for drinking water disinfection. Angew Chem 47:1998–2005
2. Matsunaga T, Namba Y, Nakajima T (1984) Electrochemical sterilization of microbial cells. Bioelectrochem Bioenerg 13:393–400
3. Bergmann H, Iourtchouk T, Schoeps K et al (2001) What is the so-called anodic oxidation and what can it do? GWF Wasser Abwasser 142: 856–869
4. White GC (1999) Handbook of chlorination and alternative disinfectants, 4th edn. Wiley, New York
5. Oloman C (1996) Electrochemical processing for the pulp and paper industry. The Electrochemical Consultancy, Romsey
6. Drogui P, Elmaleh S, Rumeau M et al (2001) Hydrogen peroxide production by water electrolysis: application to disinfection. J Appl Electrochem 31: 877–882
7. Qiang Z, Chang JH, Huang CP (2002) Electrochemical generation of hydrogen peroxide from dissolved oxygen in acidic solutions. Water Res 36:85–94
8. Bergmann MH (2009) Drinking water disinfection by inline electrolysis-product and inorganic by-product formation. In: Comninellis C, Chen G (eds) Electrochemistry for the environment. Springer, New York, pp 163–205
9. Kraft A, Stadelmann M, Blaschke M, Kreysig D et al (1999) Electrochemical water disinfection, part I: hypochlorite production from very dilute chloride solutions. J Appl Electrochem 29:861–868

10. Alkire RC, Kolb DM (eds) (2003) The electrochemistry of diamond, vol 8. Wiley-VCH, Weilheim
11. Kraft A, Wuensche M, Stadelmann M et al (2003) Electrochemical water disinfection. Recent Res Dev Electrochem (India) 6:27–55
12. Fujishima A, Einaga Y, Rao TN, Tryk DA (eds) (2005) Diamond electrochemistry. Elsevier, Amsterdam/Tokyo
13. Kraft A (2008) Electrochemical water disinfection: a short review. Platinum Met Rev 52: 177–185
14. Brillas E, Martinez-Huitle CA (eds) (2011) Synthetic diamond films: preparation, electrochemistry, characterization, and applications. Wiley, Hoboken
15. Mácová Z, Bouzek K, Híveš J et al (2009) Research progress in the electrochemical synthesis of ferrate (VI). Electrochim Acta 54:2673–2683
16. Comninellis C, Michaud S, Savall A et al (2002) Electrochemical preparation of peroxodisulfuric acid using boron doped diamond thin film electrodes. Electrochim Acta 48:431–436
17. Foller PC, Tobias CW (1982) The anodic evolution of ozone. J Electrochem Soc 129:1982
18. Da Silva LM, Santana MHP, Boodts JFC (2003) Electrochemistry and green chemical processes: electrochemical ozone production. Quim Nova 26:880–888
19. Marselli B, Garcia-Gomez J, Michaud PA et al (2003) Electrogeneration of hydroxyl radicals on boron doped diamond electrodes. J Electrochem Soc 150:D79–D83
20. Kraft A, Stadelmann M, Wünsche M et al (2006) Electrochemical ozone generation using diamond anodes and a solid polymer electrolyte. Electrochem Comm 8:883–886
21. Bergmann MEH (2006) On the applicability of DPD method for drinking water disinfection analysis. GWF Wasser Abwasser 147:780–786
22. Rosenberg B, van Camp L, Krigas T (1965) Inhibition of cell division in *Escherichia coli* by electrolysis products from a platinum electrode. Nature 205:698–699
23. Kerwick MI, Reedy SM, Chamberlain AHL et al (2005) Electrochemical disinfection, an environmentally acceptable method of drinking water disinfection? Electrochim Acta 50:5270–5277
24. Barashkov NN, Eiseinberg D, Eiseinberg S (2010) Electrochemical chlorine-free AC disinfection of water contaminated with *Salmonella typhimurium* bacteria. Russ J Electrochem 46:306–311
25. Li H, Zhu X, Ni J (2010) Inactivation of *Escherichia coli* in Na_2SO_4 electrolyte using boron doped diamond anode. Electrochim Acta 56:448–453
26. Reis A (1951) The anodic oxidation as an inactivator of pathogenic substances and processes. Klin Wschr 29:484–485
27. Bergmann MEH, Rollin J, Iourtchouk T (2009) The occurrence of perchlorate during drinking water electrolysis using BDD electrodes. Electrochim Acta 54:2102–2107
28. Jeong J, Kim C, Yoon J (2009) The effect of electrode material on the generation of oxidants and microbial inactivation in the electrochemical disinfection processes. Water Res 43:895–901
29. Bergmann H, Koparal AS (2005) Problems of chlorine dioxide formation during electrochemical disinfection. Electrochim Acta 50:5218–5228
30. Oh BS, Oh SG, Hwang YY et al (2010) Formation of hazardous inorganic by-products during electrolysis of seawater as disinfection process for desalination. STOTEN 408:5958–5965
31. Czarnetzki LR, Janssen LJJ (1992) Formation of hypochlorite, chlorate and oxygen during NaCl electrolysis from alkaline solutions at a RuO_2/TiO_2 anode. J Appl Electrochem 22:315–324
32. Cettou P, Robertson PM, Ibl N (1984) On the electrolysis of aqueous bromide solutions to bromate. Electrochim Acta 29:875–885
33. Bergmann MEH, Rollin J (2007) Product and by-product formation in disinfection electrolysis of drinking water using boron-doped diamond anodes. Catal Today 124:198–203
34. Bergmann MEH, Koparal AT, Koparal AS et al (2008) The influence of products and by-products obtained by drinking water electrolysis on microorganisms. Microchem J 89:98–107
35. Bergmann MEH, Iourtchouk T, Schmidt W et al (2011) Perchlorate formation in electrochemical water disinfection. Paperback Imprint Nova Science, New York
36. Bergmann MEH, Iourtchouk T, Rollin J (2011) The occurrence of bromate and perbromate on BDD anodes during electrolysis of aqueous systems containing bromide-first systematic studies. J Appl Electrochem 41:1109–1123
37. Polcaro AM, Vacca A, Mascia M et al (2008) Product and by-product formation in electrolysis of dilute chloride solutions. J Appl Electrochem 38:979–984
38. Sáez C, Cañizares P, Sánchez-Carretero A, Rodrigo MA (2010) Electrochemical synthesis of perbromate using conductive-diamond anodes. J Appl Electrochem 40:1715–1719
39. Kim KW, Kim YJ, Kim IT et al (2006) Electrochemical conversion characteristics of ammonia to nitrogen. Water Res 40:1431–1441
40. Kapałka A, Joss L, Anglada Á (2010) Direct and mediated electrochemical oxidation of ammonia on boron-doped diamond electrode. Electrochem Comm 12:1714–1717
41. Gabrielli C, Maurin G, Perrot H (2002) Investigation of electrochemical calcareous scaling – potentiostatic current- and mass-time transients. J Electroanal Chem 538(539):133–143
42. Kadyk T (2005) Comparative analysis of measuring techniques to investigate the scaling of the cathode in direct water disinfection electrolysis. Diploma thesis, Anhalt University, Köthen/Anh

DLVO Theory

Dominik Horinek
Institute of Physical and Theoretical Chemistry, University of Regensburg, Regensburg, Germany

DLVO Theory

DLVO theory [1–3] describes the stabilization of colloidal dispersions by an interplay of van der Waals and electrostatic forces (as opposed to steric repulsions of colloids by polymeric solubilizers). The theory was developed in the 1940s by Derjaguin and Landau [4] and by Verwey and Overbeek [5]. In DLVO theory, the two determining interactions for the stability of a colloidal system are the attractive van der Waals interactions between the colloidal particles and the repulsive electrostatic Coulomb interactions. When salt is added, the alteration of the electrostatic interactions affects the stability.

The strength of the van der Waals interactions is determined by the size and the shape of the colloidal particles and by the chemical composition of the system, which is described by the Hamaker constant A. Between two similar particles, the van der Waals forces are always attractive and A is a positive constant. For spherical particles of radius R at separation d, the van der Waals energy is given as

$$V(d) = -AR/12d.$$

This relation is valid until the particles are in contact, where a steep repulsion prevents steric overlap. For other shapes, the dependence on the separation d is different, but for all cases, a $1/d^n$ dependence is observed. The attractive van der Waals forces, which depend only weakly on the salt concentration, are strong at small separations and give the dominant energy contribution.

The second interaction that is relevant for the stability is of electrostatic nature: In the presence of inert salts (salts that are composed of ions that do not adsorb on the colloidal surface), an electrostatic double layer is formed around a charged colloidal particle. The simplest description, which holds for monovalent salts at low concentrations, is the Gouy-Chapman solution of the Poisson-Boltzmann equation, which yields that the resulting electrostatic potential decays exponentially with the distance from the colloid. How quick this decay is depends on the salt environment and is characterized by the screening length k^{-1}. According to the Gouy-Chapman model, the extent of the repulsion becomes shorter with increasing salt concentration: $\mathrm{k}^{-1} \sim \chi^{-1/2}$. During the coagulation process, two identical particles approach each other, and the electrostatic interaction between the two spherical particles, including their double layers, is

$$V(d) = RZ/2\ \mathrm{Exp}[-\mathrm{k}d]$$

In the following, we will consider particles with similar surface chemistry, for which Z is a positive constant that depends on the surface potential of the particles. For different shapes, rather similar expressions that depend on $\mathrm{Exp}[-\mathrm{k}d]$ are obtained. The electrostatic forces are therefore repulsive and act against coagulation. The sign and magnitude of the surface potential can be influenced by so-called potential-determining ions, which react with or bind to the surface. In many cases, colloidal particles have acidic or basic surface groups, and the surface potential control is achieved by changing the pH.

Two different electrostatic boundary conditions are frequently combined with DLVO theory: In the constant charge boundary condition, the surface charge does not depend on the particle separation, in contrast to the constant potential boundary condition, which accounts for changes in the surface charge of one particle that are induced by the potential of the other one. Under constant charge, the predicted repulsive force is an upper limit for the experimental force, while a lower estimate is given under constant potential conditions. Charge-regulation models are closer to the real situation, but they require additional input.

The DLVO approach to colloidal stability identifies the interactions between particles as the sum of the van der Waals energy and the screened Coulomb energy. Depending on their

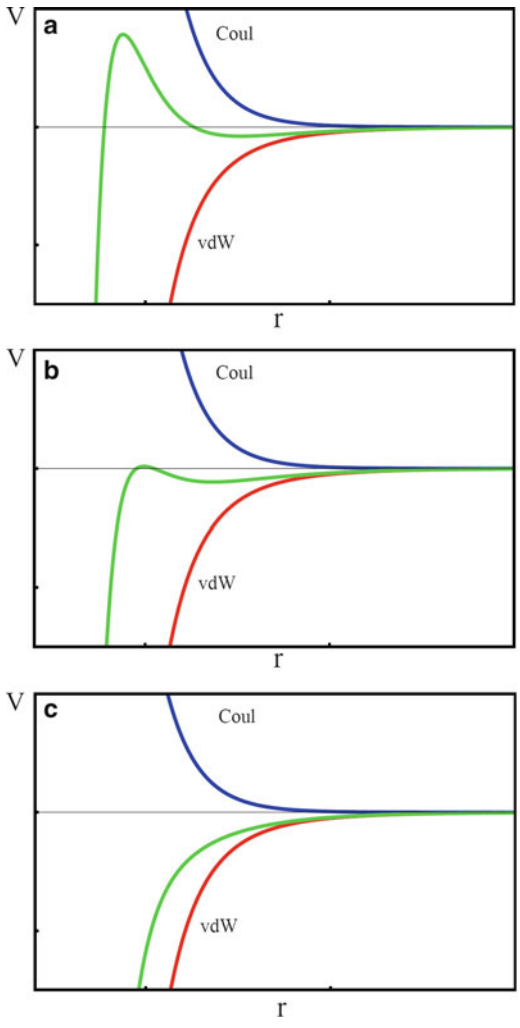

DLVO Theory, Fig. 1 Coulomb and vdW Energy between Colloidal Particles

relative strength, different behavior arises: For high surface potentials, there are two minima: a "primary" minimum at contact of the particles in the coagulated state, and a "secondary" minimum that describes flocculation, where a loose agglomerate of colloids is reversibly formed. Both minima are separated by an electrostatic barrier that prevents coagulation. This case is shown in Fig. 1a. For weaker surface potentials, this barrier gets smaller and eventually becomes zero. In this case, there is still a weak secondary minimum, but the colloidal dispersion is metastable, and rapid coagulation sets in. This case is shown in Fig. 1b. When the surface potential gets even smaller, the secondary minimum totally disappears. Particles always attract each other in this case, and coagulation from this unstable system will occur instantly. This case is shown in Fig. 1c.

In summary: High surface potentials stabilize colloidal systems. The addition of inert salt leads to stronger screening and destabilizes the system. The point at which rapid coagulation (case b) sets in is defined as the critical coagulation concentration (ccc). One key result of DLVO theory is the explanation of the Schultze-Hardy rule, which states that the ccc depends on the counterion valency z like $1/z^6$.

For the quantitative application of DLVO theory, it is important to notice that the origin, $d = 0$, of the van der Waals and Coulomb potential do not need to coincide. The screening layer starts at the outer Helmholtz plane (OHZ), which occurs at distances that are larger by a constant d than the origin of the van der Waals potential. This can drastically change the total potential: The primary minimum can be eliminated with values of d in the range of a few Ang. In this case, the system will be stable regardless of the extension of the screening layer.

At the times when DLVO theory was developed, the direct measurement of forces between colloidal particles and surfaces in solution was not possible, and the macroscopic observation of colloidal stability was the only experimental reference data. With increasing technological advancement, setups have been developed for the direct observation of such forces: The surface force apparatus (SFA) allows for the measurements of forces between surfaces in solution [6], and with an atomic force microscope (AFM), forces on a colloidal particle can be detected [7]. It is a major success that DLVO theory predicts forces that agree nicely with the measured forces for large particle separations (more than 3–10 nm), but at the same time, it is obvious that in the regime of short particle separations, not all effects are captured by DLVO. When the barrier for coagulation occurs at such low separations, the DLVO prediction for colloidal stability is not accurate (Fig. 2).

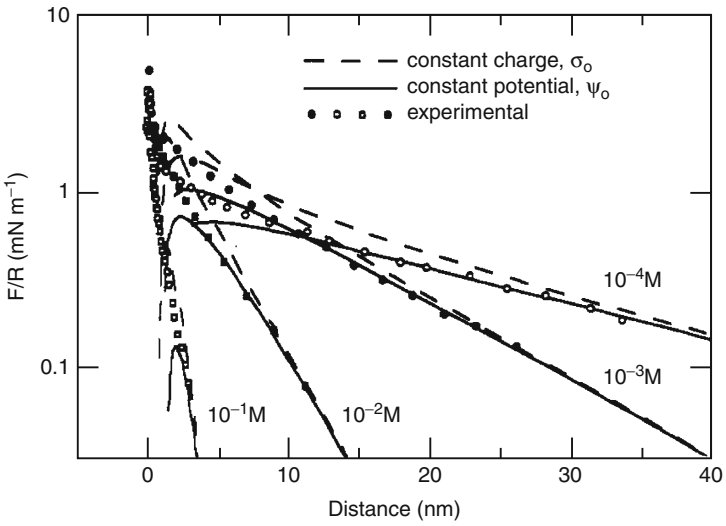

DLVO Theory, Fig. 2 Experimental Results

Despite its success, DLVO theory has various other limitations beside the failure at low particle separations. Intrinsically highly charged surfaces, where the ion's electrostatic interactions with the surface dominate, are often well described by DLVO theory. However, in the case of surfaces with weak intrinsic charge, non-electrostatic forces between ions and the surface become important. DLVO theory does not account for these ion-specific effects [8], which have their origin in ion-type-dependant interactions of the ions with the colloidal particles and with the surrounding solvent. Consequently, DLVO is not able to predict the stability of proteins [9] or of simple air bubbles in salt solutions [10], where ion-specific effects cannot be neglected. Especially ions that are attracted to the particle surfaces are enriched in the particle solvation shells and induce deviations from DLVO theory: For surfaces with hydrophobic character, large ions like I^- or SCN^- show such deviations, at the surface of hydrophilic colloidal particles binding between specific ions and specific functional surface groups is important, an important example is ion pairing at ionized carboxyl groups on a protein surface.

Finally, another limitation of DLVO theory is that ion-ion correlations, which are important for multivalent ions or at high salt concentrations, are also not included.

Future Directions

The main shortcoming of DLVO theory is that it treats the interactions between the ions and the colloidal particle as purely electrostatic. Ions close to the particle are also subject to ion-type specific, often solvent-mediated attractive forces. Their inclusion on the level of an extended Poisson-Boltzmann equation leads to a more complex scenario, in which the salt concentration also changes the effective surface charge of the colloid [9]. This can induce resolubilization at high salt concentrations when a potential barrier reappears due to overcharging. The inclusion of ion-colloid dispersion interactions into the Poisson-Boltzmann equation can also induce similar effects.

Cross-References

- ▶ Electrolytes, History
- ▶ Specific Ion Effects, Evidences
- ▶ Specific Ion Effects, Theory

References

1. Evans DF, Wennerström H (1999) The colloidal domain, 2nd edn. Wiley-VCH, New York
2. Hunter RJ (2000) Foundations of colloid science. Oxford University Press, New York

3. Israelachvili JN (2010) Intermolecular and surface forces, 3rd edn. Academic, Burlington
4. Derjaguin BV, Landau LD (1941) Theory of the stability of strongly charged lyophobic sols and of the adhesion of strongly charged particles in solution of electrolytes. Acta Physicochim URSS 14:633
5. Vervey EJW, Overbeek JTG (1948) Theory of stability of lyophobic colloids. Elsevier, Amsterdam
6. Israelachvili JN, Adams GE (1978) Measurements of forces between 2 mica surfaces in aqueous electrolyte solutions in the range 0–100 nm. J Chem Soc Faraday Trans I 74:975
7. Ducker WA, Senden TJ, Pashley RM (1992) Measurement of forces in liquids using a force microscope. Langmuir 8:1831
8. Boström M, Williams DRM, Ninham BW (2001) Specific ion effects: why DLVO theory fails for biological and colloidal systems. Phys Rev Lett 87:168103
9. Kunz W, Henle J, Ninham BW (2004) 'Zur Lehre von der Wirkung der Salze' (about the science of the effect of salts): Franz Hofmeister's historical papers. Curr Opin Coll Inter Sci 9:19
10. Craig VSJ, Ninham BW, Pashley RM (1993) Effects of electrolytes on bubble coalescence. Science 364:317
11. Schwierz N, Horinek D, Netz RR (2010) Reversed anionic Hofmeister series: the interplay of surface charge and surface polarity. Langmuir 26:7370

DNA/Electrode Interface, Detection of Damage to DNA Using DNA-Modified Electrodes

Jan Labuda[1] and Vlastimil Vyskocil[2]
[1]Institute of Analytical Chemistry, Faculty of Chemical and Food Technology, Slovak University of Technology, Bratislava, Slovakia
[2]UNESCO Laboratory of Environmental Electrochemistry, Faculty of Science, Department of Analytical Chemistry, Charles University in Prague, Prague, Czech Republic

Introduction

Deoxyribonucleic acid (DNA) itself and rather large scale of nucleic acids are utilized as biorecognition elements at DNA biosensors which represent often a type of DNA-modified electrodes with typical advantages of electrochemical sensors [1]. While electrodes covered by single-stranded DNA (ssDNA) are utilized as hybridization sensors (genosensors), electrodes with a layer of ssDNA or double-stranded DNA (dsDNA) can serve at the detection of damage to DNA. DNA damage is feature of normal body cells existence. However, as serious DNA damage can be induced by variety of physical or chemical agents occurring in the environment, generated in the organisms as by-products of metabolism or used as therapeutics, its detection is of great importance for human health and its protection. Damage to DNA generally represents an alteration in DNA chemical structure which include interruptions of the sugar–phosphate backbone (leading to strand breaks), release of the DNA bases due to hydrolysis of *N*-glycosidic bonds (resulting in abasic sites) and a variety of nucleobase lesions (resulting from reactions of DNA with genotoxic substances). Moreover, specific binding of a guest molecule to the double helix by intercalation, i.e., an insertion between the stacked base pairs, can cause a subtle damage like lengthening of the DNA helix, perturbation of the phosphate backbone and even untwisting of the helix [2].

Together with chromatographic, electrophoretic, and mass spectrometric methods of DNA damage detection [3, 4], electroanalytical techniques utilizing electrodes with immobilized DNA represent highly sensitive tools due to sensitivity of DNA response to its relatively small structural changes [5]. The electrochemical DNA-based biosensors have been used not only to detect but also to induce and control DNA damage at the electrode surface via electrochemical generation of the damaging (usually radical) species [2, 6].

Construction of DNA Biosensors

An electrode (transducer) material should be chosen with respect to the electrochemical process of interest and technique of DNA immobilization. Typically, mercury-based (mercury film, solid amalgams), carbon-based (glassy carbon (GCE),

carbon paste (CPE), graphite and pyrolytic graphite (PGE), graphite–epoxy composite) and some other (gold, platinum, indium tin oxide (ITO)) electrodes together with various thin- and thick-film electrodes like screen-printed carbon (SPCE) and gold electrodes are used in single or interdigitated (array) arrangement [7]. Typically, after a chemical or electrochemical pretreatment of the bare electrode, either thin DNA layer or thicker layers of DNA gel are formed as the electrode surface coverage. Techniques of the DNA immobilization vary depending on the kind of transducer and the biosensor application and play major role in the overall biosensor performance [8, 9]. Nanostructured interface between the bare electrode and DNA formed by various nanomaterials like gold nanoparticles and carbon nanomaterials represent an approach to enhancement of the biosensor response due to inherent electroactivity, effective electrode surface area, etc. [10, 11]. Nanometer-scale complex films of DNA, enzymes, polyions, and redox mediators were suggested for tests of genotoxic activity of various chemicals [12].

Methods of DNA Damage Detection

Voltammetric and chronopotentiometric detection modes are mostly used [20]. Together with them, electrochemical impedance spectroscopy (EIS) becomes to be popular at DNA-based biosensors [13]. According to electrochemically active species which responses are evaluated at the detection of damage to DNA, the experimental techniques can be classified as follows [1]:

(a) Label-free and often reagentless techniques which represent the work with no additional chemical reagents (indicators, redox mediators, enzyme substrates) needed to generate measured response
(b) Techniques which employ redox indicators either non-covalently bound to the DNA (groove binders, intercalators, anionic or cationic species interacting with DNA electrostatically) or present in the solution phase (e.g., hexacyanoferrate anions)
(c) Techniques which employ electrochemically active labels (enzymes, nanomaterials) covalently bound to DNA

Combination of these principles allows obtaining of more complex information on DNA changes [14].

The first group of techniques utilizes surface activity or redox activity of DNA itself [15]. The electrochemical activity is based on the presence of redox active sites at nucleobases and sugar residues. Adenine, cytosine and guanine possess reduction responses at mercury-based electrodes where the guanine residue yielded also an anodic signal due to electrooxidation of its reduction product. On the other hand, the common nucleobases undergo electrochemical oxidation at carbon and some other solid electrodes. As both the electrochemical reduction and oxidation of DNA bases are irreversible, measurements cannot be performed repeatedly. Initial increase in the anodic guanine response after short time incubation of the biosensor in prooxidative agents can indicate opening of the original dsDNA structure, while decrease in this response is an evidence for the deep DNA degradation [14]. Decrease of the anodic guanine peak height or area relative to that yielded by intact DNA was suggested as a measure representing damage to this nucleobase and proposed as a screening test for environmental toxicants present in water or wastewater samples [16]. Redox mediators such as rhodium or ruthenium complexes are sometimes used to shuttle electrons from guanine residues in distant parts of DNA chains to the electrode [17, 18]. Some of products of the DNA damage exhibit characteristic electrochemical signals (e.g., anodic oxidation of 8-oxoguanine (8-OG) [19] and 2,8-dihydroxyadenine [20]) which can be evaluated with better sensitivity than the change in original guanine response. An Os(III/II)-mediated electrochemical oxidation of 8-OG was reported [21]. The damaged DNA modified by "bulky" adducts with the nucleobases (e.g., mitomycin C and other drugs whose pharmacological effects involve DNA modification) is also able to give specific electrochemical response [22].

The second group of techniques employs electroactive compounds added to the measured

system and interacting with DNA non-covalently as its indicators (cationic indicators, intercalators and groove binders). They typically possess electrochemical response at a "safe" electrode potential and the response is high due to their accumulation at the immobilized DNA layer. Using the scheme of indicator accumulation – voltammetric measurement – chemical regeneration of the DNA layer (by removal/desorption of the accumulated indicator particles), the response of the indicator can be measured repeatedly [8]. Decrease in the intercalator or groove binder response indicates strand breaks and helix destruction. The redox indicators may be also used as diffusionally free species present in the solution phase. For instance, the hexacyanoferrate(III/II) anions, $[Fe(CN)_6]^{3-/4-}$, indicate the presence of DNA layer on the electrode surface on the basis of electrostatic repulsion between the indicator anion and negatively charged DNA backbone [23, 24].

Electroactive labels introduced into DNA also possess electrochemical signals at less extreme potentials than intrinsic DNA responses. An example is electroactive osmium tetraoxide with 2,2′-bipyridine bound to free 3′-ends of the ss regions created by a DNA repair enzyme exonuclease III, which responds to the extent of DNA damage [25]. The technique is capable of detection of one lesion per $\approx 10^5$ nucleotides in supercoiled plasmid DNA. DNA-hybridization biosensors were proposed for studies of DNA damage by common toxicants and pollutants where voltammetric transduction was achieved by coupling ferrocene moiety to streptavidin linked to biotinylated target DNA [26].

Detection of DNA Damage by Bioactivated Xenobiotics

DNA damage induced by environmental pollutants is a major endogenous toxicity pathway in biological system [27]. Most of organic pollutants may not directly cause DNA damage, but their metabolized products by enzyme reactions are genotoxic and may cause the DNA lesion [28]. Electrochemical DNA biosensors enabling detection of such DNA damage could serve as a basis for in vitro genotoxicity screening for new organic chemicals at an early stage in their commercial development. For example, styrene is one of the most widely used industrial chemicals and itself shows little genotoxicity [29]. However, after being metabolized by liver cytochrome P450 enzymes, its oxidized product styrene oxide can induce DNA damage by formation of DNA adducts [27, 29]; styrene oxide is classified as a probable human carcinogen (group 2A) [30].

Electrochemical genotoxicity biosensors based on enzyme–DNA films that detect relative DNA damage rates resulting from enzyme bioactivation of chemicals (e.g., styrene [31–33], epoxide [34], or arylamines [35]) and direct damage of DNA have been described [36]. A layer-by-layer technique was employed to immobilize DNA and enzymes on the sensor surfaces and film construction was verified by measuring frequency decrease using a quartz crystal microbalance. DNA damage was detected using catalytic square wave voltammetry with soluble $[Ru(bpy)_3]^{2+}$ (bpy = 2,2′-bipyridine), which catalyzes oxidation of guanine moieties [37]. Sensor response versus enzyme reaction time provided relative DNA damage rates that were related to indices of animal toxicity and were validated by directly measured rates of nucleobase adduct formation in DNA films using LC–MS/MS [38].

A bright future is expected for applications of enzyme–DNA films to toxicity biosensors and for the development of catalytic sensors for oxidative stress. The approach to sensor construction is achievable by room temperature solution processing and is amenable to automation, perhaps by using robotic solutions spotters. Electrode arrays could be developed to provide many tests simultaneously. For example, future sensor arrays could be configured to detect toxicity of metabolites generated by a range of human cytochromes P450 [36].

Future Directions

The DNA-modified electrodes already represent very effective and at the same time simple, fast,

cheap, miniaturized and mass-producible analytical devices for evaluation and maybe also classification of modes of genotoxic effects of individual compounds and complex food and environmental samples as well as for prescreening of new drugs and newly synthesized chemicals. Moreover, the evaluation of DNA protection (antioxidative) capacity of various natural and synthetic chemical substances together with tee and plant extracts is also possible using the detection of DNA damage by prooxidants [11, 39, 40]. Electrochemical signal formation and transduction remain to play a key role in both sensitivity and selectivity of these investigations with DNA-modified electrodes.

It can be anticipated that, in a near future, complex biorecognition layers will be suggested to detect potentially risk compounds and to improve further abilities of the biosensors to detect damage to DNA. The advanced level of medical and clinical diagnosis will be largely dependent on the successful development and implementation of new materials and technologies envisaging the fabrication of state-of-the-art biosensors [41]. The attractive properties of electrochemical devices are extremely promising for improving the efficiency of environmental screening, diagnostic testing, and therapy monitoring even more today with the construction of very large multiplexed arrays. Future DNA biosensors will require the development of new reliable devices or the improvement of the existing ones for use by nonspecialized personnel without compromising accuracy and reliability. Compact and portable devices will constitute another future area of multidisciplinary research on sensors [42].

Acknowledgements This work was supported by the Scientific Grant Agency VEGA of the Slovak Republic (Project 1/0182/11), by the Ministry of Education, Youth and Sports of the Czech Republic (Projects MSM 0021620857 and RP 14/63), and by Charles University in Prague (Project UNCE 2012/44).

Cross-References

► Biosensors, Electrochemical

References

1. Labuda J, Oliveira-Brett AM, Evtugyn G, Fojta M, Mascini M, Ozsoz M, Palchetti I, Palecek E, Wang J (2010) Electrochemical nucleic acid-based biosensors: concepts, terms, and methodology (IUPAC technical report). Pure Appl Chem 82:1161–1187
2. Fojta M (2005) Detecting DNA damage with electrodes. In: Palecek E, Scheller F, Wang J (eds) Electrochemistry of nucleic acids and proteins – towards electrochemical sensors for genomics and proteomics. Elsevier, Amsterdam
3. Pouget JP, Douki T, Richard MJ, Cadet J (2000) DNA damage induced in cells by gamma and UVA radiation as measured by HPLC/GC-MS and HPLC-EC and comet assay. Chem Res Toxicol 13:541–549
4. European Standards Committee on Oxidative DNA Damage (ESCODD) (2003) Measurement of DNA oxidation in human cells by chromatographic and enzymic methods. Free Radical Biol Med 34:1089–1099
5. Palecek E, Fojta M (2001) Detecting DNA hybridization and damage. Anal Chem 73:74A–83A
6. Vyskocil V, Labuda J, Barek J (2010) Voltammetric detection of damage to DNA caused by nitro derivatives of fluorene using an electrochemical DNA biosensor. Anal Bioanal Chem 397:233–241
7. Sassolas A, Leca-Bouvier BD, Blum LJ (2008) DNA biosensors and microarrays. Chem Rev 108: 109–139
8. Labuda J, Fojta M, Jelen F, Palecek E (2006) Electrochemical sensors with DNA recognition layer. In: Grimes CA, Dickey EC, Pishko MV (eds) Encyclopedia of sensors. American Scientific, Stevenson Ranch
9. Wang J (2005) Electrochemical nucleic acid biosensors. In: Palecek E, Scheller F, Wang J (eds) Electrochemistry of nucleic acids and proteins – towards electrochemical sensors for genomics and proteomics. Elsevier, Amsterdam
10. Ferancova A, Labuda J (2008) DNA biosensors based on nanostructured materials. In: Eftekhari A (ed) Nanostructured materials in electrochemistry. Wiley-VCH, Weinheim
11. Galandova J, Ziyatdinova G, Labuda J (2008) Disposable electrochemical biosensor with multiwalled carbon nanotubes–chitosan composite layer for the detection of deep DNA damage. Anal Sci 24: 711–716
12. Rusling JF (2005) Sensors for genotoxicity and oxidized DNA. In: Palecek E, Scheller F, Wang J (eds) Electrochemistry of nucleic acids and proteins – towards electrochemical sensors for genomics and proteomics. Elsevier, Amsterdam
13. Park JY, Park SM (2009) DNA hybridization sensors based on electrochemical impedance spectroscopy as a detection tool. Sensors 9:9513–9532
14. Ziyatdinova G, Labuda J (2011) Complex electrochemical and impedimetric evaluation of DNA

damage by using DNA biosensor based on a carbon screen-printed electrode. Anal Methods 3: 2777–2782
15. Palecek E, Jelen F (2005) Electrochemistry of nucleic acids. In: Palecek E, Scheller F, Wang J (eds) Electrochemistry of nucleic acids and proteins – towards electrochemical sensors for genomics and proteomics. Elsevier, Amsterdam
16. Mascini M, Palchetti I, Marrazza G (2001) DNA electrochemical biosensors. Fresenius J Anal Chem 369:15–22
17. Mugweru A, Rusling JF (2002) Square wave voltammetric detection of chemical DNA damage with catalytic poly(4-vinylpyridine)–Ru(bpy)$_2^{2+}$ films. Anal Chem 74:4044–4049
18. Popovich N, Thorp H (2002) New strategies for electrochemical nucleic acid detection. Interface 11:30–34
19. Oliveira-Brett AM, Piedade JAP, Serrano SHP (2000) Electrochemical oxidation of 8-oxoguanine. Electroanalysis 12:969–973
20. Oliveira SCB, Corduneanu O, Oliveira-Brett AM (2008) In situ evaluation of heavy metal-DNA interactions using an electrochemical DNA biosensor. Bioelectrochemistry 72:53–58
21. Holmberg RC, Tierney MT, Ropp PA, Berg EE, Grinstaff MW, Thorp HH (2003) Intramolecular electrocatalysis of 8-oxo-guanine oxidation: secondary structure control of electron transfer in osmium-labeled oligonucleotides. Inorg Chem 42:6379–6387
22. Tian L, Wei WZ, Mao Y (2004) Kinetic studies of the interaction between antitumor antibiotics and DNA using quartz crystal microbalance. Clin Biochem 37:120–127
23. Galandova J, Ovadekova R, Ferancova A, Labuda J (2009) Disposable DNA biosensor with the carbon nanotubes–polyethyleneimine interface at a screen-printed carbon electrode for tests of DNA layer damage by quinazolines. Anal Bioanal Chem 394:855–861
24. Labuda J, Ovadekova R, Galandova J (2009) DNA-based biosensor for the detection of strong damage to DNA by the quinazoline derivative as a potential anticancer agent. Microchim Acta 164:371–377
25. Havran L, Vacek J, Cahova K, Fojta M (2008) Sensitive voltammetric detection of DNA damage at carbon electrodes using DNA repair enzymes and an electroactive osmium marker. Anal Bioanal Chem 391:1751–1758
26. Nowicka AM, Kowalczyk A, Stojek Z, Hepel M (2010) Nanogravimetric and voltammetric DNA-hybridization biosensors for studies of DNA damage by common toxicants and pollutants. Biophys Chem 146:42–53
27. Scharer OD (2003) Chemistry and biology of DNA repair. Angew Chem Int Ed 42:2946–2974
28. Turesky RJ (2002) Heterocyclic aromatic amine metabolism, DNA adduct formation, mutagenesis, and carcinogenesis. Drug Metab Rev 34:625–650
29. Speit G, Henderson L (2005) Review of the in vivo genotoxicity tests performed with styrene. Mutat Res-Rev Mutat Res 589:67–79
30. Vodicka P, Koskinen M, Arand M, Oesch F, Hemminki K (2002) Spectrum of styrene-induced DNA adducts: the relationship to other biomarkers and prospects in human biomonitoring. Mutat Res-Rev Mutat Res 511:239–254
31. Zhou LP, Yang J, Estavillo C, Stuart JD, Schenkman JB, Rusling JF (2003) Toxicity screening by electrochemical detection of DNA damage by metabolites generated in situ in ultrathin DNA–enzyme films. J Am Chem Soc 125:1431–1436
32. Zhang Y, Hu NF (2007) Cyclic voltammetric detection of chemical DNA damage induced by styrene oxide in natural dsDNA layer-by-layer films using methylene blue as electroactive probe. Electrochem Commun 9:35–41
33. Zu Y, Hu NF (2009) Electrochemical detection of DNA damage induced by in situ generated styrene oxide through enzyme reactions. Electrochem Commun 11:2068–2070
34. Wang BQ, Rusling JF (2003) Voltammetric sensor for chemical toxicity using Ru(bpy)$_2$poly(4-vinylpyridine)$_{10}$Cl$^+$ as catalyst in ultrathin films. DNA damage from methylating agents and an enzyme-generated epoxide. Anal Chem 75:4229–4235
35. So M, Hvastkovs EG, Bajrami B, Schenkman JB, Rusling JF (2008) Electrochemical genotoxicity screening for arylamines bioactivated by N-acetyltransferase. Anal Chem 80:1192–1200
36. Rusling JF (2004) Sensors for toxicity of chemicals and oxidative stress based on electrochemical catalytic DNA oxidation. Biosens Bioelectron 20: 1022–1028
37. Thorp HH (1998) Cutting out the middleman: DNA biosensors based on electrochemical oxidation. Trends Biotechnol 16:117–121
38. So MJ, Hvastkovs EG, Schenkman JB, Rusling JF (2007) Electrochemiluminescent/voltammetric toxicity screening sensor using enzyme-generated DNA damage. Biosens Bioelectron 23:492–498
39. Ferancova A, Heilerova L, Korgova E, Silhar S, Stepanek I, Labuda J (2004) Anti/pro-oxidative properties of selected standard chemicals and tea extracts investigated by DNA-based electrochemical biosensor. Eur Food Res Technol 219:416–420
40. Ziyatdinova G, Galandova J, Labuda J (2008) Impedimetric nanostructured disposable DNA-based biosensors for the detection of deep DNA damage and effect of antioxidants. Int J Electrochem Sci 3: 223–235
41. Teles FRR, Fonseca LR (2008) Trends in DNA biosensors. Talanta 77:606–623
42. Cagnin S, Caraballo M, Guiducci C, Martini P, Ross M, SantaAna M, Danley D, West T, Lanfranchi G (2009) Overview of electrochemical DNA biosensors: new approaches to detect the expression of life. Sensors 9:3122–3148

DSP of Biomolecules

Matthias Franzreb[1] and Dirk Holtmann[2]
[1]Institute of Functional Interfaces, Karlsruhe Institute of Technology, Eggenstein-Leopoldshafen, Germany
[2]DECHEMA Research Institute of Biochemical Engineering, Frankfurt am Main, Germany

Introduction

Downstream processing of biomolecules means recovery and purification of the substances from natural sources such as animal or plant tissue or fermentation broth. It is an essential step in the manufacture of pharmaceuticals (e.g., of antibiotics, hormones, antibodies, and vaccines), natural fragrance and flavor compounds, amino and organic acids or enzymes. Often, 50–70 % of the total cost of a biotechnological process comes from downstream processing. Hence, it is important to develop the latter as an integral part of the overall process. Different downstream techniques based on electrochemical methods have been developed. The key advantages of electrochemical steps in downstream processes are inexpensive cell constructions and peripheral equipment, often no influence onto product stability, easy scale-up, high energy efficiency, and easy automation.

Electrokinetic Chromatography

Electrokinetic chromatography (EKC) is a separation technique based on the combination of electrophoresis and interactions of the analytes with additives which form a dispersed phase moving at a different velocity [1]. In order to achieve separation, either the analytes or the secondary phase should be charged. A special case of EKC is the micellar electrokinetic chromatography (MEKC), in which the secondary phase is a micellar dispersed phase in the capillary. As an example, the separation capillary is filled with an SDS micellar solution [2]. Under neutral or basic conditions, the solution migrates toward the cathode by the electroosmotic flow (EOF) when a high voltage is applied, while the micelle is forced toward the anode by electrophoresis. Normally, the EOF is stronger than the electrophoretic migration of the SDS micelle, and hence, the micelle migrates toward the cathode at a slower velocity than the aqueous phase. When a neutral analyte is injected into the micellar solution at the anodic end, it will be distributed between the micelle and the aqueous phase. An analyte that is not incorporated into the micelle at all migrates at the same velocity as the EOF toward the cathode, whereas an analyte that is totally incorporated into the micelle migrates at the lowest velocity or the same velocity as the micelle toward the cathode. As long as the analyte is electrically neutral, it migrates at a velocity between the two extremes or between the velocity of the EOF and that of the micelle. The analytes are detected in an increasing order of the distribution coefficients at the cathodic end. MEKC can be performed by adding an ionic micelle to the running solution without modifying the instrument. MEKC is a useful technique particularly for the separation of small molecules, both neutral and charged, and yields high-efficiency separation in a short time with minimum amounts of samples and reagents [3, 4]. Figure 1 shows a schematic representation of the separation principle of MEKC.

A further technique based on electrokinetic chromatography is the microemulsion electrokinetic chromatography (MEEKC). MEEKC is an electro-driven separation technique that offers the possibility of highly efficient separation of both charged and neutral analytes covering a wide range of water-soluble substances [5]. Microemulsions are solutions containing nanometer-size droplets of an immiscible liquid dispersed in an aqueous buffer. The droplets are coated with a surfactant to reduce the surface tension between the two liquid layers allowing an emulsion to form. The surface tension of the droplet is further lowered by addition of a short-chain alcohol, such as butanol, that stabilizes the system. A microemulsion containing ionic surfactant allows chromatographic

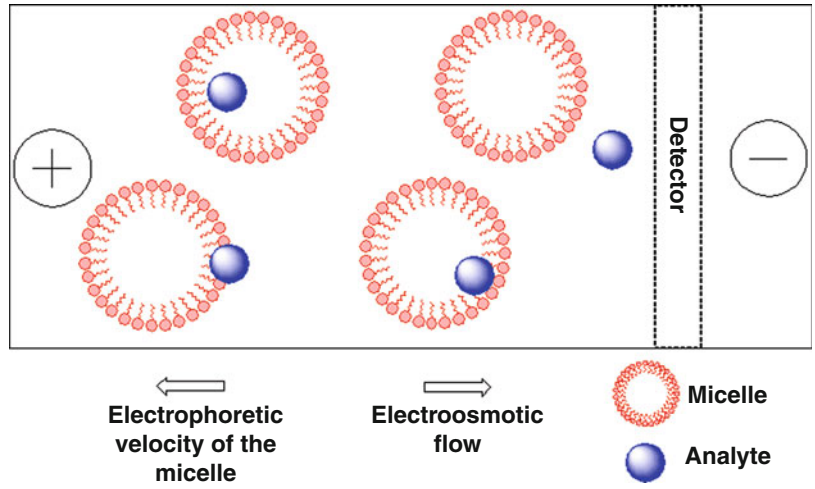

DSP of Biomolecules, Fig. 1 Schematic illustration of the micellar electrokinetic chromatography

separation to be obtained as analytes can partition between the charged oil droplets and the aqueous buffer phase. Water-insoluble compounds will favor inclusion into the oil droplets rather than into the buffer phase.

Capillary Electrophoresis and Capillary Electrochromatography

Capillary electrophoresis (CE) is an electro-driven separation technique. The main advantages are low reagent consumption, high efficiency, and selectivity with reasonably short analysis time [6]. In CE, the capillary is filled with a suitable buffer and after injecting analytes from the anode side, a relatively high voltage up to 30 kV is applied at its both ends. The positively or negatively charged analytes will move with different velocity and can be separated based on their electrophoretic mobility. Figure 2 shows a scheme of a CE experiment.

Capillary electrochromatography (CEC) is a hybrid technique utilizing the principles of electromigration techniques and chromatography [7]. The separation process is based on interactions of the analyte between the stationary and the mobile phases. In CEC, the flow of mobile phase is driven through the column by an electric field. The electroosmotic flow is generated by applying a high voltage across the column. Positive ions of the added electrolyte accumulate in the electrical double layer of particles of column packing, move toward the cathode, and drag the liquid mobile phase with them. As in capillary electrophoresis and micellar electrokinetic chromatography, small diameter columns with favorable surface area-to-volume ratio are employed to minimize thermal gradients from ohmic heating, which can have an adverse effect on band widths [8]. Table 1 shows a comparison of different electrochemically driven separation techniques.

Electrofiltration

Electrofiltration is a hybrid technology, combining pressure filtration and electrophoresis within a single device. In most cases, this combination is achieved by using a dead-end filtration system in which an electric field is applied parallel to the flow direction of the filtrate [9]. However, there also exist reports according to which a cross-flow filtration system is used. In the first case, higher concentration factors of the target molecules can be achieved [10], while the second case results in a continuous operation but also higher shear forces [11]. The idea behind electrofiltration is to impose an electrophoretic mobility onto charged biomolecules which points in the opposite direction of the filtration flow (see Fig. 3).

By this, the formation of a filtration cake can be retarded or even prevented and the filtration process can be greatly accelerated. For

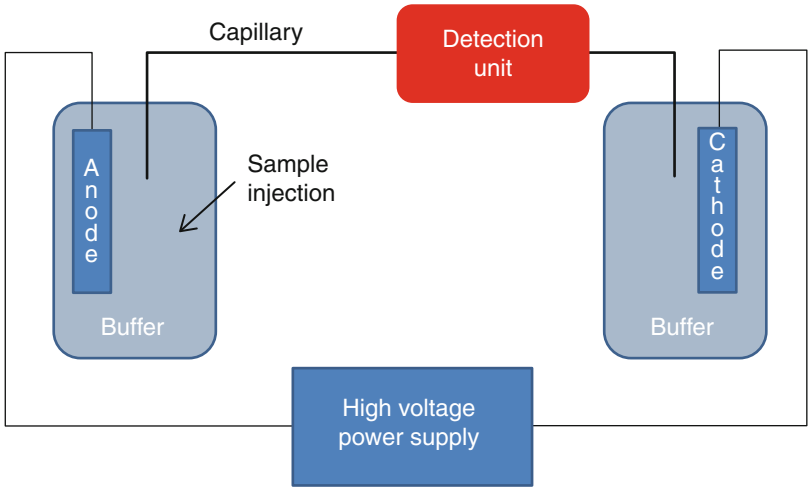

DSP of Biomolecules, Fig. 2 Scheme of a capillary electrophoresis. A CE instrument consists of a high-voltage power supply, a silica capillary with an internal diameter ranging from 20 to 200 µm, two buffer reservoirs, two electrodes connected to the power supply, and a detector. The capillary is filled with a buffer. The sample is injected from the anode side and both ends of the capillary and the electrodes are placed into buffer reservoirs; finally the voltage is applied across the capillary to start electrophoresis [6]

a theoretical description of electrofiltration of biomolecules, theories originally developed for colloidal inorganic particle suspensions can be adapted. In order to describe experimental data, the electroosmotic flow within the pores of the filtration membrane and, if present, in the filter cake has to be considered in addition in these theories [12]. Electrofiltration can be applied to charged biomolecules, especially to highly viscous, colloidal suspensions of biopolymers. The benefits of electrofiltration have been demonstrated for different polysaccharides, like poly(3-hydroxybutyrate), hyaluronic acid, chitosan and xanthan [13]. In the latter case, the filtration time is reduced from hours to minutes, making the filtration process economically feasible as compared to the usual precipitation step.

Electromembrane Extraction

The electromembrane extraction (EME) method extracts charged substances from a small sample volume through a thin membrane of organic solvent immobilized in the wall of a hollow fiber and into a solution inside the lumen of the hollow fiber. This extraction process is forced by an applied potential difference across the membrane, and this combination of well-known liquid–liquid extraction processes with electrokinetic migration yields a rapid and selective sample preparation method for ionic substances. The potential difference is utilized to extract charged analytes of interest from the sample across the organic membrane [14]. In EME using porous hollow fibers, target analytes are extracted as charged species from an aqueous sample, typically with a volume of 100–300 µl [15]. Figure 4 shows the scheme of an EME device.

Potential-Controlled Liquid Chromatography

Potential-controlled liquid chromatography (PC-LC) or electrochemically modulated liquid chromatography (EM-LC) is a further combination of electrochemical methods with liquid chromatography. The principle of PC-LC is related to ion exchange chromatography: The separation of molecules depends on their own electric charge and on the potential of the stationary chromatographic phase. The electrical

DSP of Biomolecules, Table 1 Comparison of capillary electrophoresis (*CE*), micellar electrokinetic chromatography (MEKC), capillary electrochromatography (*CEC*), potential-controlled liquid chromatography (*PC-LC*), and electrodialysis (*ED*) modified from [8]

	CE	MEKC	CEC	PC-LC	ED
(Main) separation principle	Different mobilities of ions in electric field	Partition between bulk solution and micelle moving in opposite direction to analyte	Partition between solid stationary phase and mobile phase	Different electrosorption of analytes	Selective transfer of ions through semi-permeable membranes
Stationary phase	None	None	Particles with bonded groups	Un-modified and modified conductive matrices	None
Sample type	Charged species	Neutrals	Neutral and charged species	Charged	Charged species

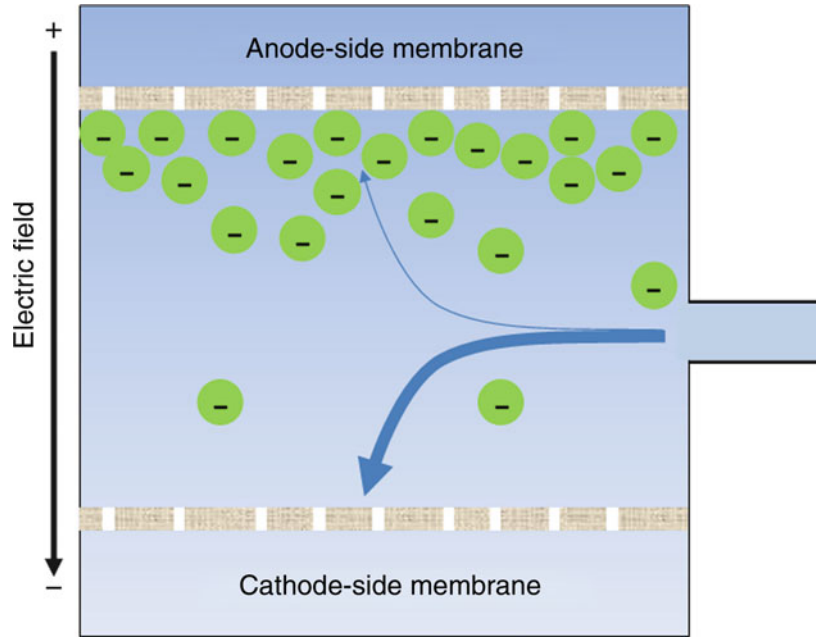

DSP of Biomolecules, Fig. 3 Electrofiltration of a negatively charged biopolymer. If the electric field is strong enough, the cathode-side membrane will be kept free of the biopolymer which will accumulate at the anode-side membrane, while the fluid flux will mainly pass through the cathode-side membrane. The figure shows a simplified principle without the ions of the electrolyte keeping electroneutrality and without flushing chambers of the electrodes

potential of this stationary phase can be easily controlled. In principle, a stationary phase can be used for either cation or anion exchange applications, depending on the selected electrode potential. In contrast to classical ion exchange chromatography, the electrical charge of the stationary chromatographic phase does not depend on immobilized charge carriers but on an adjustable abundance or a deficiency of electrons within the stationary phase itself. The principle of potential-controlled chromatography is illustrated in Fig. 5. Using an applied potential to a conductive packing (e.g., porous graphitic carbon), chromatographic resolution and retention are manipulated by altering the donor–acceptor interactions between the

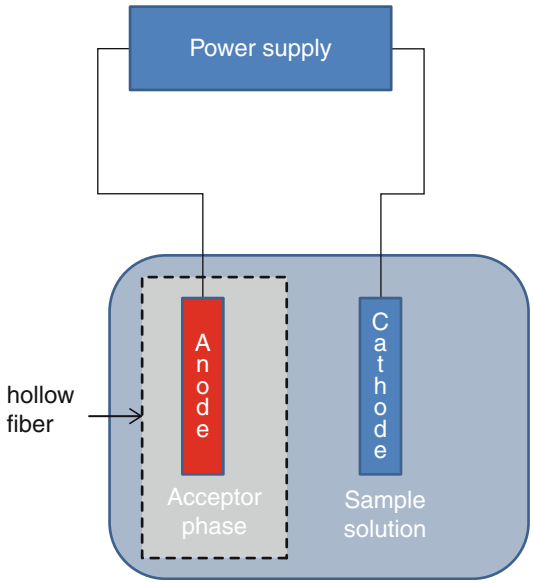

DSP of Biomolecules, Fig. 4 Scheme of electromembrane extraction (EME, adapted from [16]). Two electrodes are placed in the sample and the acceptor solution, respectively, and connected to a power supply. EME was found to be compatible with a wide range of biological matrices, e.g., whole blood and urine, preparing clean extracts in a short period of time with simple and inexpensive equipment

packing and analytes. In potential-controlled liquid chromatography, the conductive stationary phases like glassy carbon and porous graphitic carbon are packed into an HPLC column that is also configured to function as a three-electrode electrochemical cell. As such, the packing acts both as a chromatographic stationary phase and a high surface area working electrode. This dual function results in the unique ability to manipulate the surface charge density of the conductive packing through changes in applied potential, which, in turn, alters analyte retention. Stationary phases in PC-LC must possess several properties: High surface area, compositional and microstructural stability at the applied potentials, and high electrical conductivity [17–20].

Electrodialysis

An electrodialysis (ED) stack is composed of several flow chambers separated by ion exchange membranes and superimposed by an electric field. In most cases, an alternating arrangement

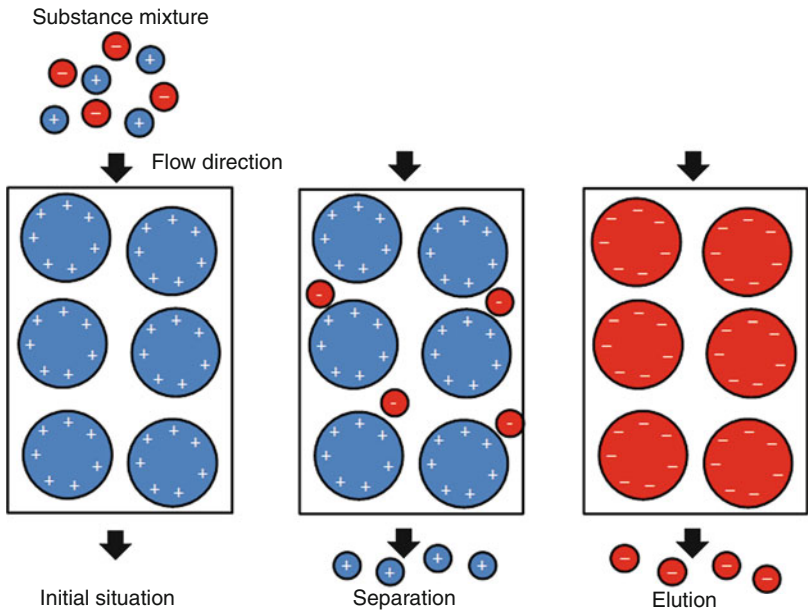

DSP of Biomolecules, Fig. 5 Simplified scheme of the separation of charged substances in potential-controlled liquid chromatography

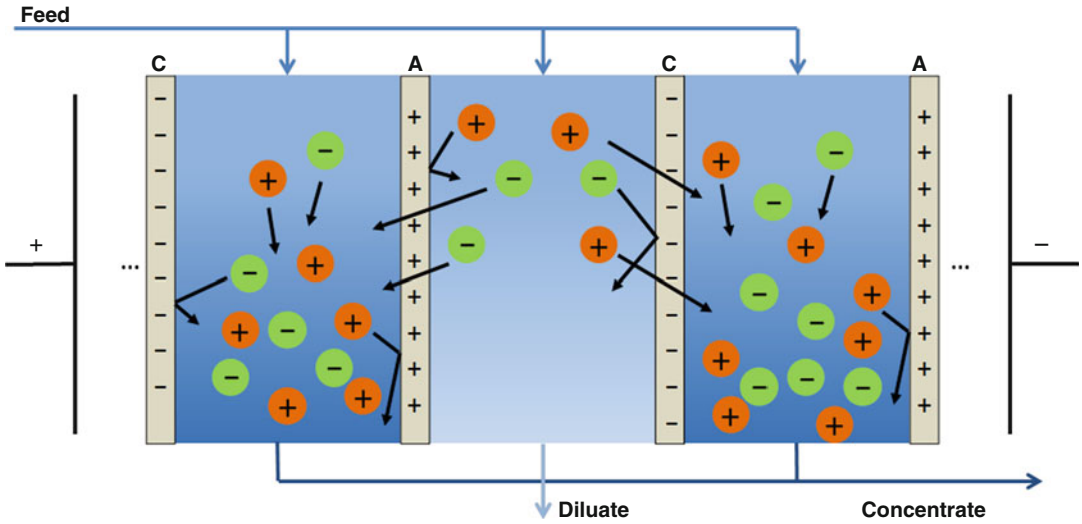

DSP of Biomolecules, Fig. 6 Working principle of electrodialysis. The illustration shows three cells of an electrodialysis stack and the respective trajectories of charged molecular species

of cation and anion exchange membranes is used. While a solution flows through the chamber, charged molecules are influenced by the electric field, resulting in a movement of anions toward the anode and cations toward the cathode. On their way, anions can penetrate anion exchange membranes but not cation exchange membranes and vice versa (see Fig. 6).

Given this arrangement, the charged species of the feed will deplete in one group of flow chambers and will concentrate in the adjacent chambers. Therefore, depending on which effluent is used as product stream, ED can be used for at least a partial desalting or a concentration of the charged species. The principle of ED is well known from the field of water technology. Here, the process is used for desalination of seawater as well as e.g., for recycling of rinsing water in wastewater treatment. However, for about two decades, the interest in ED as an efficient tool for downstream processing in biotechnology has constantly been increasing. Thinking about the application of ED, one has to be aware that conventional ion exchange membranes are practically non-porous and therefore molecules above approx. 500 Da are not able to penetrate the membrane irrespective of their charge [21]. Consequently, classical ED can be used for the separation of small biomolecules, like lactic acid from fermentation broth [22], but not for the fractionation of peptide or protein solutions. In order to extend the field of application, the ion exchange membranes in ED stacks can be replaced by nano- or ultrafiltration membranes [23, 24]resulting in a process often called EDUF (electrodialysis ultrafiltration) or electrophoretic separation.

Future Directions

The flexibility of separation processes based on electrochemical techniques, where the driving force can be easily controlled by an external power supply, makes these techniques more and more promising for application in biotechnology processes. Further improvements of the stationary phases, membranes and capillary systems are necessary to develop tailor-made processes for highly selective downstream processes. Furthermore, the understanding of protein adsorption at charged surfaces is important for a wide range of scientific disciplines including surface engineering, separation sciences, and pharmaceutical sciences [25]. Therefore, further investigations of the mechanism of the potential-dependent protein adsorption are essential for knowledge-based

processes. Besides further investigations in the laboratory, the development of reliable mathematical models to predict the interactions of the biomolecules with the charged electrochemical systems is important. In general, the development of electrochemical methods in downstream processing of biomolecules is an interdisciplinary approach to be used by (electro)-chemists, physicists, biotechnologists, and engineers.

Cross-References

- ▶ Electrophoresis
- ▶ Membrane Processes, Electrodialysis

References

1. Riekkola M-L, Jönsson JÅ, Smith RM (2004) Terminology for analytical capillary electromigration techniques. Pure Appl Chem 76(2):443–451
2. Otsuka K, Terabe S (2004) Chiral micellar electrokinetic chromatography. Methods in Molecular Biology 243:355-363
3. Terabe S (2009) Capillary separation: micellar electrokinetic chromatography. Ann Rev Anal Chem 2(1):99–120
4. Foley JP (1990) Optimization of micellar electrokinetic chromatography. Anal Chem 62(13):1302–1308
5. Mahuzier P-E et al (2003) An introduction to the theory and application of microemulsion electrokinetic chromatography. LC-GC Eur 16:22–29
6. Rizvi SAA, Do DP, Saleh AM (2011) Fundamentals of micellar electrokinetic chromatography (MEKC). Eur J Chem 2(2):276–281
7. Mikšík I, Sedláková P (2007) Capillary electrochromatography of proteins and peptides. J Sep Sci 30(11):1686–1703
8. Cikalo MG et al (1998) Capillary electrochromatography. Analyst 123:87R–102R
9. Iritani E, Mukai Y, Kiyotomo Y (2000) Effects of electric field on dynamic behaviors of dead-end inclined and downward ultrafiltration of protein solutions. J Membr Sci 164(1–2):51–57
10. Hofmann R, Posten C (2003) Improvement of dead-end filtration of biopolymers with pressure electrofiltration. Chem Eng Sci 58(17):3847–3858
11. Enevoldsen AD, Hansen EB, Jonsson G (2007) Electro-ultrafiltration of industrial enzyme solutions. J Membr Sci 299(1–2):28–37
12. Yukawa H et al (1976) Analysis of batch electrokinetic filtration. J Chem Eng Japan 9:396–401
13. Gözke G, Posten C (2010) Electrofiltration of biopolymers. Food Eng Rev 2(2):131–146
14. Gjelstad A, Pedersen-Bjergaard S (2011) Electromembrane extraction: a new technique for accelerating bioanalytical sample preparation. Bioanalysis 3(7):787–797
15. Petersen N et al (2010) On-chip electro membrane extraction. Microfluid Nanofluid 9(4):881–888
16. Petersen NJ et al (2011) Electromembrane extraction from biological fluids. Anal Sci 27(10):965
17. Muna GW et al (2008) Electrochemically modulated liquid chromatography using a boron-doped diamond particle stationary phase. J Chromatogr A 1210(2):154–159
18. Keller DW, Ponton LM, Porter MD (2005) Assessment of supporting electrolyte contributions in electrochemically modulated liquid chromatography. J Chromatogr A 1089(1–2):72–81
19. Knizia M et al (2003) Potential-controlled chromatography of short-chain carboxylic acids. Electroanalysis 15(1):49–54
20. Kocak F et al (2005) Potential-controlled chromatography for the separation of amino acids and peptides. J Appl Electrochemistry 35(12):1231–1237
21. Galier S, Roux-de Balmann H (2001) Study of the mass transfer phenomena involved in an electrophoretic membrane contactor. J Membr Sci 194(1):117–133
22. Boniardi N et al (1997) Lactic acid production by electrodialysis Part I: experimental tests. J Appl Electrochemistry 27(2):125–133
23. Horvath ZS et al (1994) Multifunctional apparatus for electrokinetic processing of proteins. Electrophoresis 15(1):968–971
24. Firdaous L et al (2009) Concentration and selective separation of bioactive peptides from an alfalfa white protein hydrolysate by electrodialysis with ultrafiltration membranes. J Membr Sci 329(1–2):60–67
25. Hartvig RA et al (2011) Protein adsorption at charged surfaces: the role of electrostatic interactions and interfacial charge regulation. Langmuir 27(6): 2634–2643

Dye-Sensitization

Laurence (Laurie) Peter
Department of Chemistry, University of Bath, Bath, UK

Definition

Photosensitization can be defined as a process in which light absorption by a photosensitizer molecule leads to a photophysical or photochemical change in a second molecule or system.

History

The scientific term *sensitization* referred originally to the process by which a photographic film or plate was made more sensitive to particular wavelengths of light. The history of dye-sensitization began in 1873 with the discovery by Hermann Wilhelm Vogel (1834–1898) that the sensitivity of silver halide photographic plates to green and red light was greatly enhanced by the presence of dyes in the photographic emulsion. Using a "cocktail" of different colored dyes, Vogel was able to achieve tone balance in black and white photographs [1]. It is now generally accepted that the photoexcited state of the dye injects electrons into the silver halide, leading to the formation of silver atoms. The oxidized dye can be regenerated by electron transfer from a "supersensitizer" such as hydroquinone or iodide.

At the end of the same century Oscar Raab reported the first observation of the phototoxic action of dyes, a discovery that led to the development of photodynamic therapy for treatment of tumors [2]. This therapy also relies on dye-sensitization. One of the mechanisms involved in the phototoxic effect is the creation of singlet oxygen by energy transfer to the (triplet) ground state of dioxygen from the triplet state of the photoexcited dye. Free radical formation by electron or hydrogen transfer reactions involving the triplet state can also occur. Dye-sensitization is also used more generally in photochemistry to generate reactive triplet states by energy transfer from a photoexcited dye to reactant molecules.

Dye-sensitization is also employed in electrostatic printing. This process, which is the basis of dry photocopying, involves electrostatic charging of small particles of a photoconductor such as zinc oxide dispersed in a resin binder. Illumination of the semiconductor discharges the photosensitive film so that it does not pick up the toner, and as a consequence only dark areas are printed. In 1962 RCA patented an invention by Harold Greig, who showed that the spectral sensitivity of the ZnO photoconductor could be enhanced in the visible region by addition of a wide range of organic dyes.

Photosensitization of (mostly single crystal) semiconductor electrodes was studied in a number of laboratories the 1960s [3]. Widespread interest in the process was sparked by the invention of the dye-sensitized solar cell, which was developed in the research group of Michel Grätzel at the Ecole Federal Polytechnique, Lausanne, Switzerland [4], and patented in 1992 [5]. The following 20 years have seen an exponential expansion of publications and patents dealing with dye-sensitized solar cells, and attempts are being made to commercialize the technology.

Dye-Sensitization of Semiconductors and Insulators

Dye-sensitization of semiconductors and insulators (including molecular crystals) generally involves photoexcitation of dye molecules adsorbed at the interface between the solid and an electrolyte solution. The photoexcited state of the dye may inject electrons or holes into the electrode or, if the emission spectrum overlaps with the absorption energy of optical transitions (e.g., from bulk or surface defect states) in the electrode, it may transfer its energy to the electrode, exciting electrons to higher energies [6]. The quantum efficiency of the first route can approach 100 %, whereas the second route generally leads to quenching of the excited state without significant photocurrent generation.

Depending on the positions of the highest occupied molecular orbital (HOMO) and lowest occupied molecular orbital (LUMO) of the dye, the photoexcited state may inject either electrons or holes into the conduction or valence band, respectively, of the solid [7] as shown in Fig. 1. (Note the broken arrows in Fig. 1 which show the direction in which *electrons* move).

Dye-sensitization of ZnO single-crystal electrodes was studied extensively in the late 1960s by Gerischer and Tributsch [8], Hauffe [9], and others. Illumination of ZnO electrodes coated with adsorbed monolayers of dyes such as rhodamine B, eosin, and methylene blue generates anodic current due to electron injection from the photoexcited dye. Around the same time,

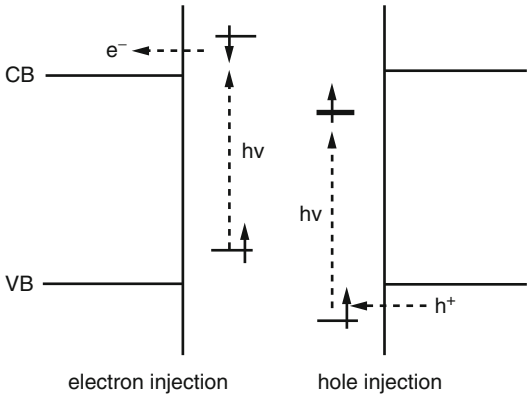

Dye-Sensitization, Fig. 1 Electron and hole injection from excited states of adsorbed dye molecules. Note that for electron injection, the LUMO level of the dye must lie above the conduction band. For hole injection, the HOMO level must lie below the valence band edge

injection of holes (i.e., extraction of valence band electrons) was observed for aromatic molecular crystals such as anthracene and perylene sensitized by similar dyes [10]. In both cases the external quantum efficiency is very low due to the very weak light absorption by the dye monolayer (typically <1 %). Figure 2 shows an example of the photocurrent excitation spectrum and the solution absorption spectrum for a mixture of three different cyanine dyes adsorbed on the (101) surface of a single crystal of the anatase from of TiO_2 [11].

Injection of electrons or holes from the illuminated layer of sensitizer dye leaves the dye in its oxidized or reduced state, respectively. As a consequence the dye layer usually degrades under illumination. In order to prevent this, a "supersensitizer" is added to the electrolyte. In the case of injection of electrons, the supersensitizer is an electron donor species such as iodide which regenerates the dye from its oxidized state. In the case of hole injection by the dye, an electron acceptor can be used as a supersensitizer. Provided that dye regeneration is faster than degradation reactions, the photosensitized system is stable.

This opens up the possibility of designing regenerative photoelectrochemical cells based on dye-sensitization. The sequence of reactions taking place in a regenerative cell is as follows (for the case of electron injection):

$D + hv \rightarrow D^*$ Photoexcitation of dye

$D^* \rightarrow D^+ + e^-$ (CB) Electron injection into conduction band

$D^+ + R \rightarrow D + O$ Regeneration of dye

$O + e^-$ (CE) $\rightarrow$ R Regeneration of R at the counter electrode (CE)

Dye-Sensitization of Mesoporous Wide-Band-Gap Oxides

As Fig. 2 shows, the external quantum efficiency or IPCE (incident photon to current conversion efficiency) for dye-sensitization of flat single-crystal surfaces is much less than 1 %. Attempts to enhance the IPCE by using thicker layers of dyes have not been successful because quenching occurs. In order to design an efficient solar cell based on the regenerative dye-sensitization scheme shown above, it is necessary to enhance the IPCE by at least two orders of magnitude. An obvious way around this problem is to increase the surface area of the semiconductor. In 1976, Tsubomura et al. [12] showed that a sintered ZnO pellet could be sensitized with rose Bengal to give much higher photocurrents. Their cell, which used an aqueous iodide/triiodide electrolyte to regenerate the dye, achieved a monochromatic power efficiency of 1.5 %. However no further progress was made until 1991, when O'Regan and Grätzel published a paper in Nature that demonstrated that sensitization of a mesoporous film of anatase by a ruthenium polypyridyl dye could be used as the basis for fabrication of dye-sensitized solar cells with solar conversion efficiencies of up to 7 % [4]. This remarkable breakthrough paved the way for the development of dye-sensitized solar cells with AM 1.5 efficiencies that have now exceeded 12 % [13]. One of the keys to the success of the DSC is the high internal surface area of the mesoporous anatase films used in the device. A 10-μm-thick mesoporous anatase layer formed by sintering particles with a size of 10–30 nm can have an internal surface that is more than 500 times greater than its geometric area.

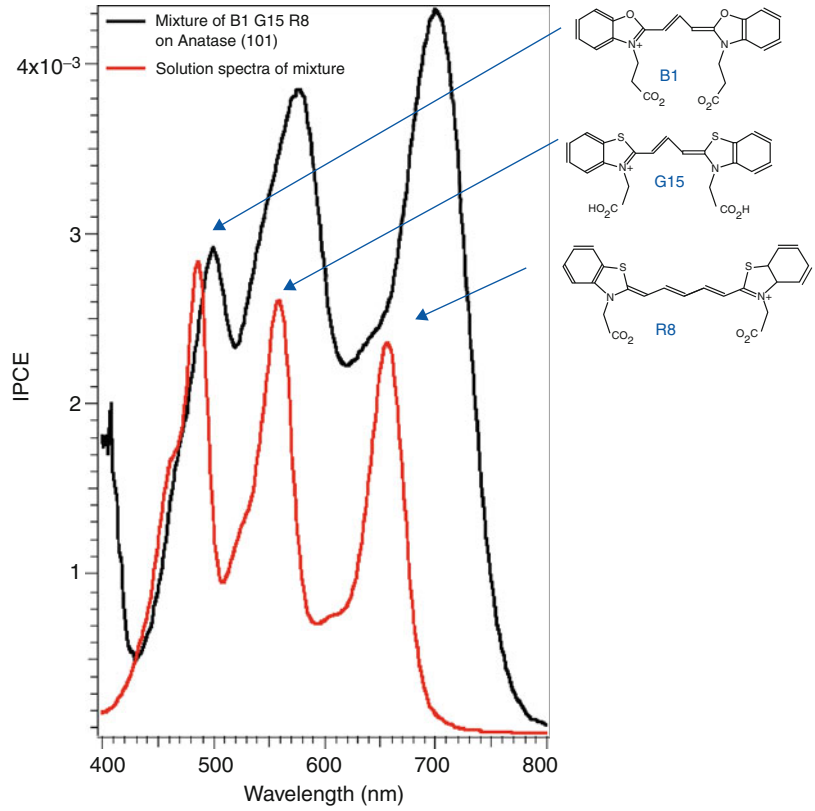

Dye-Sensitization, Fig. 2 Photocurrent spectrum for TiO_2 (101) anatase sensitized with a mixture of the three cyanine dyes shown on the right of the figure. The solution spectrum is shown for comparison. IPCE stands for incident photon to current efficiency, i.e., it is the external quantum efficiency (Reproduced with permission from Ref. [11])

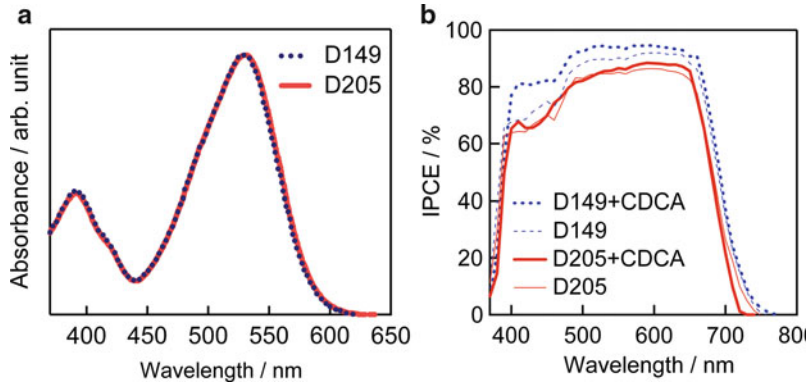

Dye-Sensitization, Fig. 3 IPCE spectra for two metal-free organic indoline dyes (Reproduced with permission from Ref. [15])

Considerable efforts have gone into the engineering of efficient panchromatic sensitizer dyes [14]. An enormous number of metal-ligand and metal-free dyes have been synthesized with the objective of improving the spectral response, which ideally should extend to around 900 nm for optimum performance under AM1.5 solar illumination. Figure 3 is an example of the very high IPCEs that are obtained with mesoporous anatase films and, in this case, the organic metal-free dye shown in Fig. 4 [15].

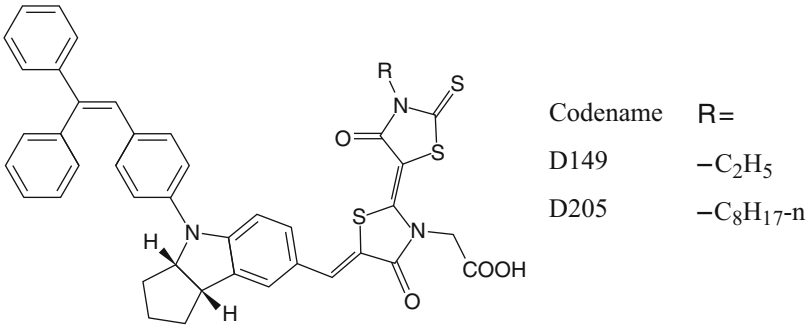

Dye-Sensitization, Fig. 4 Molecular structure of the indoline dyes D149 and D205 (Reproduced with permission from Ref. [15])

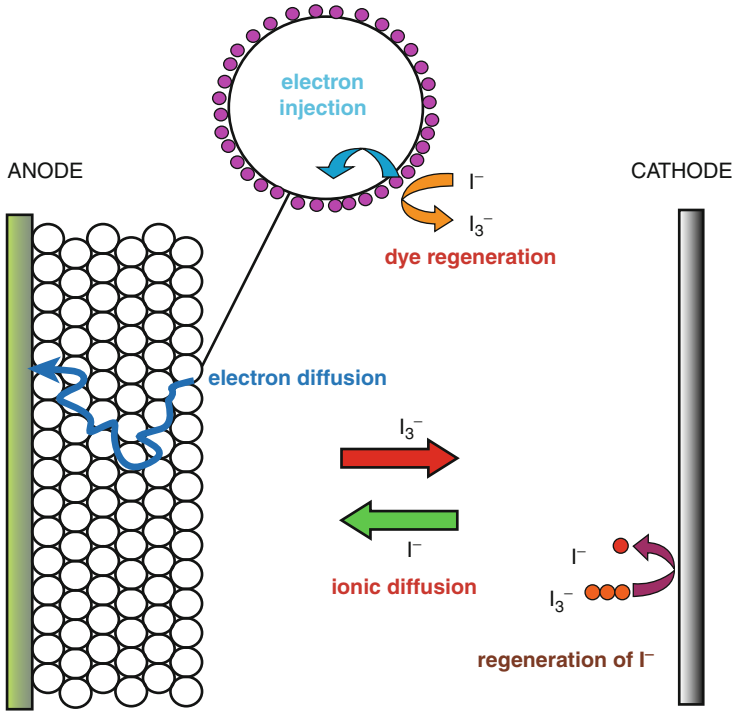

Dye-Sensitization, Fig. 5 Summary of the processes taking place in a DSC under illumination

The Dye-Sensitized Solar Cell or Grätzel Cell

The dye-sensitized solar cell (DSC), often called the Grätzel cell, is constructed as follows. A layer of titania paste consisting of anatase nanoparticles is spread onto a glass plate that is coated with a thin conducting layer of fluorine-doped SnO_2. The paste contains organic binders that are removed when the film is calcined in air (typically at 450–500 °C), leaving a mesoporous titania film (ca. 10 μm thick) with a porosity of around 50 %. The titania film is immersed in a dilute dye solution to impregnate it with dye. The counter electrode (cathode) consists of another sheet of conducting glass covered with a thin layer of platinum. The cell is assembled as a sandwich structure using a thin thermoplastic spacer, and the electrolyte is vacuum filled into the gap. The most widely used electrolyte is the I^-/I_3^- redox couple in organic solvents or ionic liquids. Several other redox systems have been used [16]; the most successful of these is a cobalt complex which outperforms the iodide electrolyte [13]. The processes taking place in the illuminated DSC are illustrated in Fig. 5.

The generic concept of the DSC has been adapted by replacing the dye with inorganic sensitizers costing of thin semiconductor layers or layers of quantum dots. The liquid electrolyte has been replaced by organic and inorganic hole conductors and the titania by other materials such as ZnO and SnO_2. The morphology of the oxide films has also been changed, with DSCs fabricated from a range of nanostructures including nanorods and nanotubes.

Kinetics of Electron Injection and Dye Regeneration

Transient optical and microwave absorbance measurements have established that electron injection can occur on a sub-picosecond time scale [17], competing effectively with other routes for deactivation of the excited state of the dye. Provided that geminate recombination does not occur (i.e., the injected electron transfers to the HOMO level of the dye), the injection efficiency can be high, approaching 100 % for the best ruthenium polypyridyl complexes. Regeneration of the dye from its oxidized state is much slower, taking place on a time scale of microseconds [18]. Nevertheless, regeneration is generally faster than back electron transfer from electrons present in the TiO_2, leading to high IPCE values. Competition between the rates of regeneration and decomposition of the oxidized state determines the turnover number for the dye. Since each dye molecule in the DSC absorbs around 1 photon per second, turnover numbers in excess of 10^8 are required for a 10-year lifetime.

Future Perspectives

Dye-sensitization is an example of a broader class of photophysical processes that involve charge transfer from an excited state. Other examples include sensitization of wide-band-gap semiconductors by quantum-confined nanoparticles (quantum dots) and by thin layers of semiconductors (extremely thin absorber layer – ETA cells). Charge transfer at the interface between donor and acceptor species in organic solar cells involves an analogous process in which mobile "excitons" dissociate at the interfaces to generate electrons and holes in the adjacent phases. These similarities are stimulating research into new types of solar cell that exploit the fundamental process of light-driven electron transfer. The challenge now is to move from the laboratory to commercial exploitation [19].

Cross-References

- ▶ Dye-sensitized Electrode, Photoanode
- ▶ Photoelectrochemistry, Fundamentals and Applications
- ▶ Photography, Silver Halides
- ▶ Quantum Dot Sensitization
- ▶ Semiconductor Electrode
- ▶ Semiconductor–Liquid Junction: From Fundamentals to Solar Fuel Generating Structures
- ▶ Solid State Dye-Sensitized Solar Cell

References

1. Vogel WH (2009) Die Photographie Farbiger Gegenstände in den Richtigen Tonverhältnissen. BiblioBazaar, Charleston
2. Szeimies R-M, Dräger J, Abels C, Landthaler M (2001) History of photodynamic therapy. In: Clazavera-Pinton P-G, Szeimies R-M, Ortel B (eds) Dermatology in photodynamic therapy and fluorescence diagnosis in dermatology. Elsevier, Amsterdam
3. Gerischer H, Tributsch H (1968) Electrochemistry of ZnO monocrystal spectral sensitivity. Ber Bunsenges Phys Chem 72:437–45
4. O'Regan B, Grätzel M (1991) A low-cost high-efficiency solar cell based on dye-sensitized colloidal TiO_2 films. Nature 353:737–740
5. Grätzel M, Liska P (1992) Photo-electrochemical cell and process of making same. US Patent 5084365
6. Memming R, Tributsch H (1971) Electrochemical investigations of spectral sensitization of gallium phosphide electrodes. J Phys Chem 75:562–570
7. Gerischer H, Michel-Beyerle ME, Rebentrost F, Tributsch H (1968) Sensitization of charge injection into semiconductors with large band gap. Electrochim Acta 13:1509–1515
8. Tributsch H, Gerischer H (1969) Electrochemical investigations on mechanism of sensitization and supersensitization of ZnO monocrystals. Ber Bunsenges Phys Chem 73:251

9. Hauffe K, Danzmann HJ, Pusch H, Range J, Volz H (1970) New experiments on the sensitization of zinc oxide by means of the electrochemical cell technique. J Electrochem Soc 117:993–999
10. Gerischer H, Willig F (1976) Reaction of excited dye molecules at electrodes. Top Curr Chem 61:31–84
11. Spitler MT, Parkinson BA (2009) Dye sensitization of single crystal semiconductor electrodes. Acc Chem Res 42:2017–2029
12. Tsubomura H, Matsamura M, Nomura Y, Amamiya T (1976) Dye-sensitized zinc oxide: aqueous electrolyte: platinum photocell. Nature 26:402–403
13. Yell A, Lee HW, Tsao HN (2012) Porphyrin-sensitized solar cells with cobalt(III/II)-based redox electrolyte exceed 12 percent efficiency. Science 334:629–634
14. Nazeeruddin K, Pechy P, Renouard T et al (2001) Engineering of efficient panchromatic sensitizers for nanocrystalline TiO_2-based solar cells. J Am Chem Soc 123:1613–1624
15. Ito S, Miur H, Uchida, et al. (2008) High-conversion efficiency organic dye-sensitized solar cells with a novel indoline dye. Chem Commun 5194–5196
16. Hamann TW, Ondersma JW (2011) Dye-sensitized solar cell redox shuttles. Energy Environ Sci 4:370–381
17. Huber R, Moser JE, Grätzel M et al (2002) Real-time observation of photoinduced adiabatic electron transfer in strongly coupled dye/semiconductor colloidal systems with a 6 fs time constant. J Phys Chem B 106:6494–6499
18. Pelet S, Moser JE, Grätzel M (2000) Cooperative effect of adsorbed cations and iodide on the interception of back electron transfer in the dye sensitization of nanocrystalline TiO_2. J Phys Chem B 104:1791–1795
19. Peter LM (2011) The Gratzel cell: where next? J Phys Chem Lett 2:1861–1867

Dye-Sensitized Electrode, Photoanode

Tsutomu Miyasaka
Graduate School of Engineering, Toin University of Yokohama, Yokohama, Kanagawa, Japan

Introduction

Study of dye-sensitized semiconductor electrodes has started in the late 1960s as an extension of photographic science where silver halide grains are photosensitive materials to be spectrally sensitized. Dye molecules adsorbed on the surface of silver halide crystals and photoexcited by absorption of visible light act as electron donors to silver halide and spectrally sensitize the formation of silver image. Gerischer and coworkers explored various semiconductors of metal oxides and inorganic compounds which can be sensitized with organic dyes in the structure of electrochemical cell [1, 2]. As the result of sensitization, n-type semiconductors such as ZnO, TiO_2, and CdS generate anodic photocurrents, and p-type semiconductors such as GaP generate cathodic photocurrents with their action spectra following the absorption spectra of the sensitizing dyes. The dye-sensitized photocurrent is generally larger in density and efficiency in the n-type sensitization than the p-type. In 1971, Tributsch and Calvin demonstrated photocurrent generation by a thin film of natural chlorophyll deposited on n-type semiconductor ZnO [3] to mimic spectral sensitivity of photosynthesis. This study was synchronized with the discovery by Fujishima and Honda (1972) of water photolysis on n-type semiconductor TiO_2 [4]. These studies established the field of photoelectrochemistry as a simple model of photosynthetic energy conversion. In the following years, the Langmuir-Blodgett method [5–7] has revealed that a single monolayer of adsorbed dye (sensitizer) only can contribute to photoexcited electron injection to n-type semiconductor electrode. This principle agreed with the theory of dye sensitization then established for silver halide photographic material [8]. Light absorption and energy conversion attained by a single dye layer, however, was too small to be applied to photovoltaic power generation. This application was later realized when the Grätzel group invented in 1991 a mesoporous semiconductor electrode with high surface area which enhances light absorption by adsorbed dye molecules [9]. Dye-sensitized cells constructed with mesoporous semiconductor photoelectrodes have achieved high efficiency in energy conversion and joined a class of utility-type solar cells.

Sensitization Mechanism

Semiconductor electrode in which electron is the dominant carrier for conductivity is classified as n-type, which has a Felmi level located close to

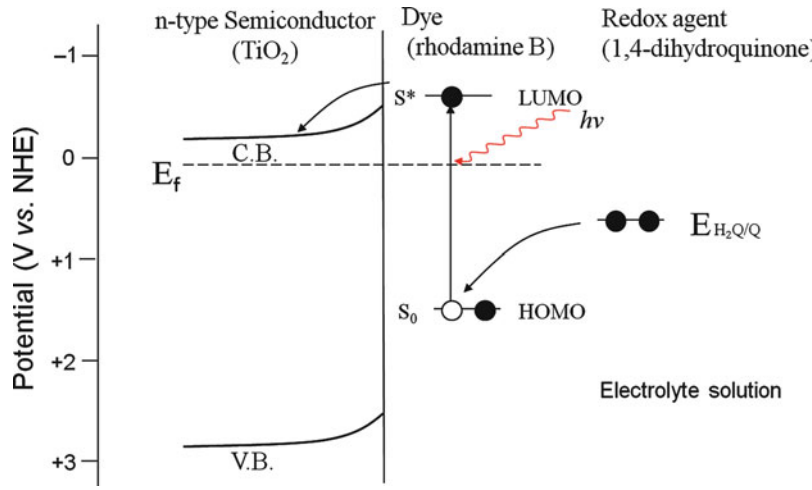

Dye-Sensitized Electrode, Photoanode, Fig. 1 Photoexcited electron transfer scheme for dye sensitization of n-type semiconductor electrode

the conduction band. Study of semiconductor electrodes in the early days has started by using single crystals of semiconductors such as TiO_2, ZnO, and CdS. In contact with an ionic electrolyte, surface potentials develop at the semiconductor surface through chemical equilibrium between metal oxide and ionic redox spices in electrolyte. With aqueous electrolytes, surface electrochemical potentials are pinned at oxide semiconductors as determined by the work function of the semiconductor and the electrolyte pH, the latter causing a potential shift according to the Nernst equation with a slope, –59 mV/pH. On polarization of the semiconductor electrode positively or negatively by means of a potentiostat, there occurs a potential bending (gradient) from the surface to the bulk of semiconductor.

Metal oxide semiconductors have their intrinsic sensitivity to light only in the ultraviolet and/or short wavelength regions due to their band gaps (e.g., 3.5 eV for TiO_2 and eV for ZnO). This limits utilization of incident photons to a low level for photovoltaic conversion. When the excited states of a dye molecule possess sufficiently long lifetimes and electrochemically more negative potentials than the conduction band edge potential, photoexcited electrons are injected to the conduction band leading to charge separation at the semiconductor-dye interface. Separated charges can however be recombined being influenced by the state of potential gradient. In the conditions of no potential gradient (flat-band condition) and cathodic polarization with a negative slope of potential, charge recombination takes place by back transfer of electrons to the dye. Anodic polarization that causes a positive potential slope favors unidirectional electron transfer from dye to the bulk of semiconductor. In a suitable condition of anodic polarization, i.e., external bias voltage, rectified photocurrent occurs as a result of dye sensitization. Action spectrum of the dye-sensitized photocurrent thus follows optical absorption spectrum of the dye adsorbed on the semiconductor surface, which covers some area of the visible light wavelength region, 400–800 nm.

The efficiency and density of the dye-sensitized photocurrent is a function of electrode potential applied by external bias (voltage). More positively regulated electrode potential enhances photocurrent by suppression of back electron transfers. More positive potential in effect enhances the potential barrier, i.e., a Schottky barrier, at the semiconductor surface in aspects of energy gap (eV) as well as in the thickness of space charge layer. This potential barrier is crucial to control the rectification of dye-sensitized photocurrent. Figure 1 shows the schematic diagram for dye-sensitized photocurrent generation on a TiO_2 single crystal electrode. Here, rhodamine B is presented as a sensitizer which strongly

absorbs light at around 550 nm. It is generally known that the sensitized photocurrent tends to saturate in the existence of a potential barrier (gradient) of more than 0.2 eV. Based on the carrier (donor) density of TiO_2 (10^{18} cm^{-3}), this polarization corresponds to formation of a space charge layer of a thickness of 50 nm. The maximum photovoltage of dye-sensitized electrode is obtained in the open-circuit condition of the cell in which the conduction band (CB) is filled with injected electrons. For a cell composed of a working photoelectrode and a counter electrode, open-circuit photovoltage is defined as the potential difference between the Felmi level of TiO_2 and the redox potential of electrolyte species that corresponds to the potential of counter electrode.

Dye-sensitized n-type semiconductors act as photoanodes which generate anodic photocurrents driven by generation of negative photovoltages. The quantum efficiency of sensitized photocurrent is influenced by several processes of energy dissipation which reduce the rectified photocurrent. Back electron transfers from electrode to the dye-oxidized state or to the electrolyte redox species are the main causes of photocurrent decrease. In addition, deactivation of the dye-excited state can occur before electron injection in case where the dye-excited state is not sufficiently high enough with respect to the CB level of semiconductor and/or its lifetime is too short. It is normally required that the excited state is positioned more than 0.1 eV higher than CB. Short lifetime of an excited dye can cause internal conversion to the ground state. This type of deactivation is caused by molecular aggregation of dyes as well as by energy transfer between dye molecules accompanied by photochemical quenching. The latter has been demonstrated by use of a monomolecular film of dye (chlorophyll) on SnO_2 electrode in which intermolecular distance is controlled by insertion of spacer molecules (lipids). Suppression of dissipative energy transfer and quenching largely improves the quantum efficiency of photocurrent [6]. This practice has led to the method of enhancing the performance of dye-sensitized solar cells by use of co-absorbents in dye adsorption.

Dye-Sensitized Mesoporous Photoanodes and Solar Cells

The theory of electron exchange reaction as well as experimental demonstration by means of Langmuir-Blodgett films teaches that the dye molecule in direct contact with the semiconductor surface only is capable of electron injection to electrode. Optical absorption by a single dye monolayer (1–3 % of incident light), however, is not sufficient to collect photons. Harvesting photons can be realized by using a mesoporous surface that gives 500 times or more large surface areas for dye loading per semiconductor thickness of 10 mm. Mesoporous semiconductor electrodes of TiO_2 and ZnO are prepared, e.g., by means of sintering (450–550 °C) of a TiO_2 particle-dispersed paste coated on a glass substrate or electrochemical deposition of ZnO from Zn^{2+}-containing aqueous electrolytes. A family of Ru bipyridyl complexes [10–14] has been widely employed as sensitizers on TiO_2 by taking the advantage of their broad absorption bands due to metal-ligand charge transfer as well as of their high stability to light. As a result of enhanced light scattering, action spectrum of the dye-sensitized photocurrent covers the visible region (400–900 nm) peaking at the green region (around 530 nm), giving a spectral sensitivity similar to those of amorphous silicon solar cells. With use of iodine/iodide redox couples in organic electrolytes (typically, acetonitrile), photocurrent density of 10–20 mA cm^{-2} in the short-circuit condition and open-circuit photovoltage of 0.6–0.8 V can be normally obtained under exposure to 1,000 W m^{-2} sun light; the output performance depends on the thickness and porosity of semiconductor and the composition of electrolyte. Figure 2 depicts the power generation scheme of the mesoporous solar cell. A unique characteristic of the mesoporous electrode is that the dyed (colored) electrode is optically semitransparent. This nature enables to construct a tandem photocell in which incident light is used twice by two superposed cells. After optimization for the cell structure, the power conversion efficiency of dye-sensitized solar cell has reached 11 % and more [15].

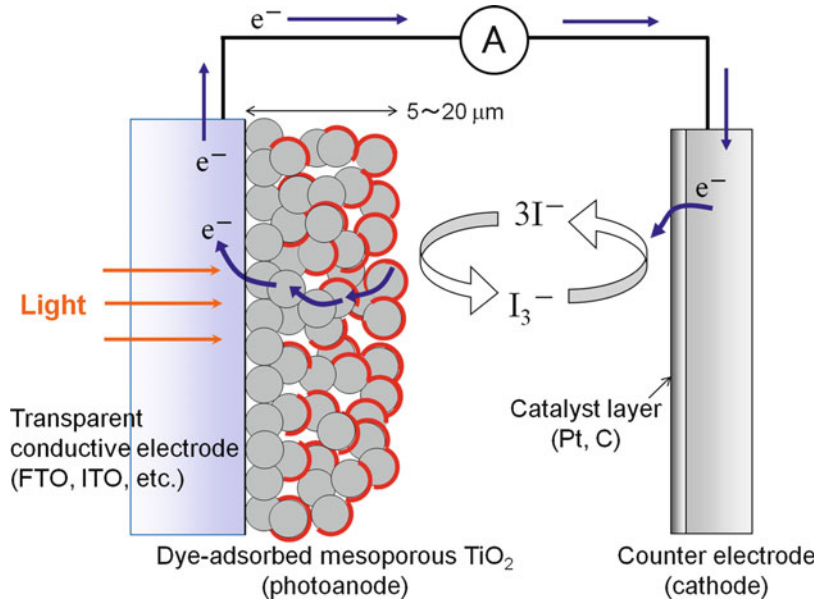

Dye-Sensitized Electrode, Photoanode, Fig. 2 Dye-sensitized solar cell based on mesoporous TiO_2 photoanode

Sensitizer plays a key role in expanding the spectral sensitivity, enhancing photon absorption, and determining the range of photovoltage. On TiO_2, Lowest unoccupied molecular orbital (LUMO) level of the excited state sensitizer should be normally higher than the conduction band by 0.15 eV or more. Sensitizers of lower LUMO levels tend to decrease not only the photocurrent density but also photovoltage. Among various kinds of dye sensitizers, indoline-type dyes [16–18], oxazole-type dyes [19], and porphyrin families [20, 21] possess high extinction coefficients and work as efficient sensitizers on TiO_2. Successful combination of sensitizer and redox agent allows further improvement of conversion efficiency. Use of metal porphyrins has achieved highest conversion efficiency, 12 %, when coupled with cobalt bipyridyl complexes as redox compounds which are capable of yielding high voltage around 1.0 V in combination with TiO_2 photoanode [21]. Various derivatives of Ru complex dyes have also been synthesized for improvement of extinction coefficient and chemical stability against degradation caused by photocatalytic reaction of TiO_2. Durability of dye-sensitized TiO_2 electrode has been examined under high temperature and continuous soaking to light. It is however generally found that exposure of the cell to ultraviolet (UV) light deteriorates the electrode performance. Lifetime of the cell under accelerated conditions can reach more than thousands of hours by applying UV filters [15, 22]. Inorganic nanocrystalline particle and quantum dots also work as spectral sensitizers. Their main advantage is addressed to the tunability of absorption wavelength (band gap) by changing the particle size as the quantum confinement effect. For examples, CdS [23], CdSe [24], and PbS [25] have been studied as quantum dot sensitizers to TiO_2. These inorganic sensitizers are intrinsically more stable against light soaking while their chemical stability against liquid electrolytes is subject of improvement. As an organic inorganic hybrid compound, an organo metal halide, $CH_3NH_3PbX_3$(X=Br, I) was found to act as high-efficiency photovoltaic material and light absorber on mesoporous metal oxide electrodes [26]. It forms a perovskite crystalline film on the surface of Al_2O_3 and TiO_2. A solid-state photovoltaic cell based on $CH_3NH_3PbI_2Cl$-coated Al_2O_3 yields 10.9% conversion efficiency [27]. Further high efficiencies, 12-15%, of the perovskite-based solar cell have been currently achieved with $CH_3NH_3PbI_3$-coated TiO_2 electrodes [28, 29]. This type of solid-state

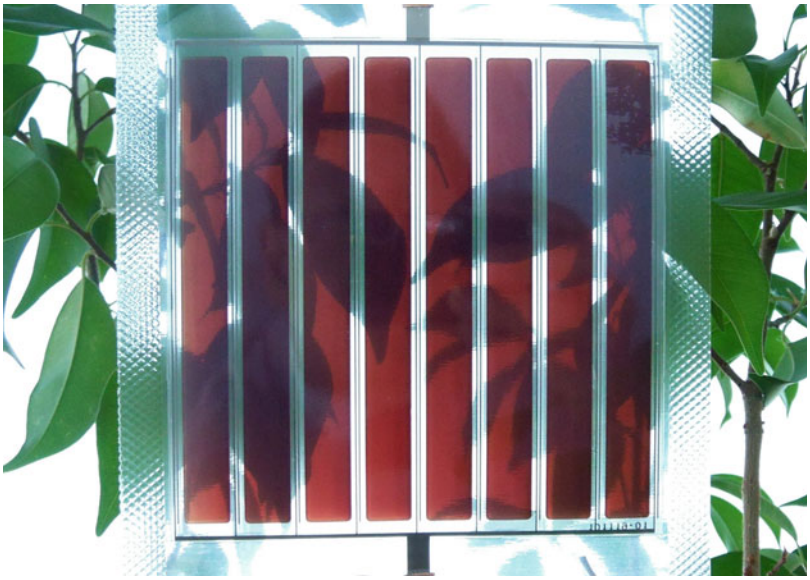

Dye-Sensitized Electrode, Photoanode, Fig. 3 Dye-sensitized solar cell of bifacial photovoltaic activity fabricated with thin plastic substrates

photovoltaic cell, however, is accepted as a new type, hybrid semiconductor solar cell rather than a family of dye-sensitized cell.

Future Perspectives

For industrial applications, a strong merit of dye-sensitized solar cell over the existing solid-state solar cells has been emphasized on account of its low-cost manufacturing processes without the high vacuum and nanoscale manipulation as required by the solid-state pn junction cells. Dye-sensitized photoelectrodes are fabricated not only on glass or metal substrates but also on plastic film substrates by applying low-temperature coating technologies for mesoporous TiO_2 and ZnO. Fabrication of lightweight plastic photoelectrodes has been subject of intense study and achieved conversion efficiencies of 5-6% for TiO_2 [30, 31]. Flexible solar cells and large-area modules have been designed with plastic electrodes to demonstrate them as low-cost printable solar cell for versatile applications including consumer's electronics. Figure 3 displays an example of the solar cell, which has a semitransparent body due to mesoporous electrodes and is capable of utilizing light on the both sides of the cell [32]. For future applications to energy industry, high sensitivity of dye-sensitized power generation to weak indoor light is especially advantageous for versatile applications to small power sources, which include power supply to computers and other IT equipment.

Cross-References

- Dye-Sensitization
- Dye-Sensitized Electrode, Photoanode
- Photoelectrochemistry, Fundamentals and Applications
- Solid State Dye-Sensitized Solar Cell

References

1. Tributsch H, Gerischer H (1969) The use of semiconductor electrodes in the study of photochemical reactions. Ber Bunsenges Phys Chem 73:850–854 and references therein
2. Memming R (2001) Semiconductor electrochemistry. Wiley-VCH, Weinheim
3. Tributsch H, Calvin M (1971) Electrochemistry of excited molecules: photoelectrochemical reaction of chlorophylls. Photochem Photobiol 14:95–112
4. Fujishima A, Honda K (1972) Electrochemical photolysis of water at a semiconductor electrode. Nature 238:37–38

5. Kuhn H, Möbius D, Bücher H (1972) Spectroscopy of monolayer assemblies. Physical Methods in Chemistry. In: A. Weissberger and B. W. Rossiter (eds.), Part IIIB Optical, Spectroscopic, and Radioactivity Methods. Wiley-Interscience, New York, 577–578
6. Miyasaka T, Watanabe T, Fujishima A, Honda K (1979) Highly efficient quantum conversion at chlorophyll a-lecithin mixed monolayer coated electrode. Nature 277:638–640
7. Miyasaka T, Watanabe T, Fujishima A, Honda K (1980) Photoelectrochemical study of chlorophyll-a multilayers on SnO_2 electrode. Photochem Photobiol 32:217–222
8. Tani T (1995) Photographic sensitivity: theory and mechanisms. Oxford University Press, New York
9. O'Regan B, Grätzel M (1991) A low-cost, high-efficiency solar cell based on dye-sensitized colloidal TiO_2 films. Nature 335:737–740
10. Nazeeruddin MK, Pechy P, Grätzel M (1997) Efficient panchromatic sensitization of nanocrystalline TiO_2 films by a black dye based on a trithiocyanato-ruthenium complex. J Chem Commun 18:1705–1706
11. Wang P, Zakeerruddin SM, Comte P, Charvet R, Humphry-Baker R, Grätzel M (2003) Enhance the performance of dye-sensitized solar cells by co-grafting amphiphilic sensitizer and hexadecylmalonic acid on TiO_2 nanocrystals. J Phys Chem B 107:14336–14341
12. Chen CY, Wu SJ, Wu CG, Chen JG, Ho KC (2006) A ruthenium complex with superhigh light-harvesting capacity for dye-sensitized solar cells. Angew Chem Int Ed 45:5822–5825
13. Jiang KJ, Masaki N, Xia JB, Noda S, Yanagida S (2006) A novel ruthenium sensitizer with a hydrophobic 2-thiophen-2-yl-vinyl-conjugated bipyridyl ligand for effective dye sensitized TiO_2 solar cells. Chem Comm 23:2460–2462
14. Wang P, Klein C, Humphry-Baker R, Zakeerruddin SM, Grätzel M (2005) A high molar extinction coefficient sensitizer for stable dye-sensitized solar cells. J Am Chem Soc 127:808–809
15. Chen CY, Wang M, Li JY, Pootrakulchote N, Alibabaei L, Ngoc-le C, Decoppet JD, Tsai JH, Grätzel C, Wu CG, Zakeeruddin SM, Grätzel M (2009) Highly efficient light-harvesting ruthenium sensitizer for thin-film dye-sensitized solar cells. ACS Nano 3:3103–3109
16. Horiuchi T, Miura H, Sumioka K, Uchida S (2004) High efficiency of dye-sensitized solar cells based on metal-free indoline dyes. J Am Chem Soc 126:12218–12219
17. Ito S, Zakeeruddin SM, Humphry-Baker R, Liska P, Charvet R, Comte P, Nazeeruddin MK, Péchy P, Takata M, Miura H, Uchida S, Grätzel M (2006) High-efficiency organic-dye- sensitized solar cells controlled by nanocrystalline-TiO_2 electrode thickness. Adv Mater 18:1202–1205
18. Kuang D, Uchida S, Humphry-Baker R, Zakeeruddin SM, Grätzel M (2008) Organic dye-sensitized ionic liquid based solar cells: remarkable enhancement in performance through molecular design of indoline sensitizers. Angew Chem Int Ed 47:1923–1927
19. Zhang XH, Wang ZS, Cui Y, Koumura N, Furube A, Hara K (2009) Organic sensitizers based on hexylthiophene-functionalized indolo[3,2-b]carbazole for efficient dye-sensitized solar cells. J Phys Chem C 113:13409–13415
20. Ikegami M, Ozeki M, Kijitori Y, Miyasaka T (2008) Chlorin-sensitized high-efficiency photovoltaic cells that mimic spectral response of photosynthesis. Electrochem 76:140–143
21. Yella A, Lee HW, Tsao HN, Yi C, Chandiran AK, Nazeeruddin MK, Diau EWG, Yeh CY, Zakeeruddin SM, Grätzel M (2011) Porphyrin-sensitized solar cells with cobalt (II/III)–based redox electrolyte exceed 12 percent efficiency. Science 334:629–634
22. Yu Q, Zhou D, Shi Y, Si X, Wang Y, Wang P (2010) Stable and efficient dye-sensitized solar cells: photophysical and electrical characterizations. Energy Environ Sci 3:1722–1725
23. Chang CH, Lee YL (2007) Chemical bath deposition of CdS quantum dots onto mesoscopic TiO_2 films for application in quantum-dot-sensitized solar cells. Appl Phys Lett 91:053503–1–053503–3
24. Diguna LJ, Shen Q, Kobayashi J, Toyoda T (2007) High efficiency of CdSe quantum-dot-sensitized TiO_2 inverse opal solar cells. Appl Phys Lett 91:023116–1–023116–3
25. Plass R, Pelet S, Krueger J, Grätzel M, Bach U (2002) Quantum dot sensitization of organic–inorganic hybrid solar cells. J Phys Chem B 106:7578–7580
26. Kojima A, Teshima K, Shirai Y, Miyasaka T (2009) Organometal halide perovskites as visible-light sensitizers for photovoltaic cells. J Am Chem Soc 131:6050–6051
27. Lee MM, Teuscher J, Miyasaka T, Murakami TN, Snaith HJ (2012) Efficient hybrid solar cells based on meso-superstructured organometal halide perovskites. Science 338:643–647
28. Noh JH, Im SH, Heo JH, Mandal TN, Seok SI (2013) Chemical management for colorful, efficient, and stable inorganic−organic hybrid nanostructured solar cells. Nano Lett 13:1764–1769
29. Grätzel M (2013) Perovskite nano-pigments and new molecularly engineered porphyrin light harvesters for mesoscopic solar cells. Hybrid and Organic Photovoltaics Conference (HOPV13), Sevilla, Spain, 7 May 2013
30. Miyasaka T, Ikegami M, Kijitori Y (2007) Photovoltaic performance of plastic dyesensitized electrodes prepared by low-temperature binder-free coating of mesoscopic titania. J Electrochem Soc 154:A455–A461
31. Lee KM, Wu SJ, Chen CY, Wu CG, Ikegami M, Miyoshi K, Miyasaka T, Ho KC (2009) Efficient and stable plastic dye-sensitized solar cells based on a high light-harvesting ruthenium sensitizer. J Mater Chem 19:5009–5015
32. Miyasaka T (2011) Toward printable sensitized mesoscopic solar cells: Light-harvesting management with Thin TiO_2 films. J Phys Chem Lett 2:262–269

Dynamic Methods in Solid-State Electrochemistry

Ulrich Guth
Kurt-Schwabe-Institut für Mess- und Sensortechnik e.V. Meinsberg, Waldheim, Germany
FB Chemie und Lebensmittelchemie, Technische Universität Dresden, Dresden, Germany

Definition

Although the most of the methods using solid electrolytes cells are those in which the measured values are time independent (stationary), there are also techniques in which the excitation signal (sensor response) is time dependent (in-stationary). According to the values that are changed, it can be distinguished between controlled potential techniques (voltammetric techniques) and controlled current techniques (coulostatic techniques) [1]. The excitation function can be changed with time periodically (impedance) or according to a special time regime (voltammetry). In solid-state electrochemistry linear sweep mainly voltammetric and impedimetric techniques are applied. Current as a function of a controlled electrode potential and time is recorded as a so-called voltammogram.

Voltammetric Techniques

Mostly the voltage is changed linearly with constant sweep rate (dU/dt) or as cyclic voltammetry where the current response of the electrode potential is measured in increasing direction up to the turning point and decreasing to the starting potential [2]. When an electrochemical active component is present, an anodic current peak can be detected. In the reverse scan a corresponding cathodic peak may be observed. The peak potential is typical for the electrode reaction and the peak current depends on the scan rate, the number of electrons, and the diffusion coefficient of the active species. Symmetric bell-shaped oxidation–reduction peaks are obtained for reversible reactions so for the oxygen reduction and the oxidation of O^{2-} ions are approximately reversible reactions [3]. Also differential techniques like differential pulse voltammetry (DPV) and square wave voltammetry (SQV) are in use to enlarge the response signal.

Linear sweep voltammograms are suited to investigate the electrode activity [4]. As an example the polarization behavior of metal electrodes is shown in Fig. 1 [5]. For the catodic O_2 reduction, the following row is obtained using the charge transfer resistance calculated by means of the current density (i) vs. voltage (U) curves: $R_{ct}(Pt) < R_{ct}(PtAu) < R_{ct}(PtAuRh)$. Regarding to the O_2-reduction, the PtAuRh/YSZ-electrode is ideally polarizable because the current density j is nearly zero in the range $0\ V > U > -0.22\ V$. In contrast to that a remarkable cathodic currents due to the NO reduction can be detected in this potential range shown in the differential change of j-U-curves.

Alternating Current Measurements (Impedance)

Up to now mostly the electrochemical impedance spectroscopy (▶ *EIS*) was used to investigate the electrochemical cell regarding the electrolyte and the electrochemical transfer reaction. If the relaxation times ($RC = \left[\frac{UIt}{IU}\right] = [t]$ has the dimension time) for single processes are different, then their separation is possible. Otherwise an overlap of semicircles can be observed. The separation may be achieved by changing of temperature because the temperature dependence for single processes is mostly different.

The Ohm's Law for alternating current can be expressed as a vector equation:

$$\vec{U} = \vec{Z} \cdot \vec{I} \tag{1}$$

For sinusoidal voltage and current are valid:

$$U(t) = U_{\max} e^{j\omega t} \tag{2}$$

$$I(t) = I_{\max} e^{j(\omega t - \varphi)} \tag{3}$$

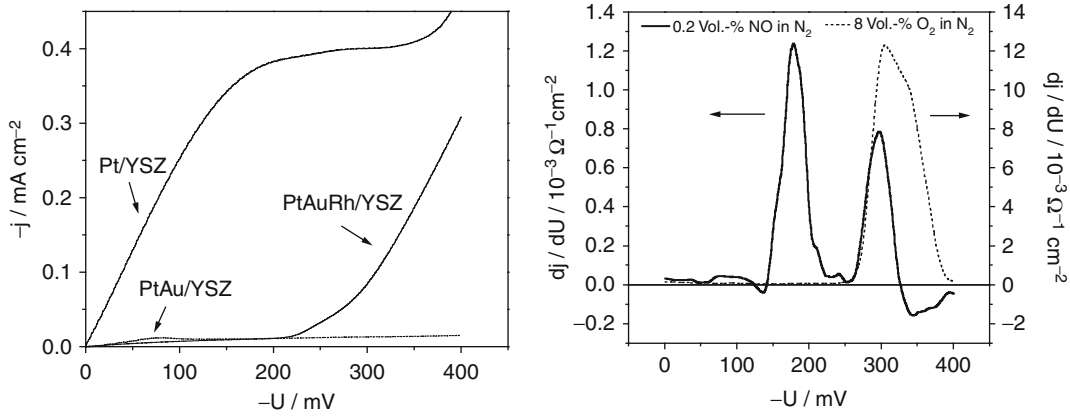

Dynamic Methods in Solid-State Electrochemistry, Fig. 1 Voltammetric investigation on different electrode materials in N_2, 1 vol.-% O_2 (*left*), dj/dU-U-curves of a PtAuRh/YSZ-electrode at 550 °C in 8 vol.-% O_2 in N_2 und 0.2 Vol.-% NO in N_2 (*right*)

where ω is angular frequency, and φ is the phase shift between voltage and current due to the capacitive effect. With the Euler's formula

$$e^{j\omega t} = \cos \omega t + j \sin \omega t \text{ and } j^2 = -1 \quad (4)$$

the impedance can be written as a complex number $\vec{Z} = a + bj$

$$\vec{Z} = |Z| \cos \varphi + j|Z| \sin \varphi \quad (5)$$

$|Z|$, $|Z| \cos \varphi$, and $|Z| \sin \varphi$ are the modulus (norm), real part, and imaginary part of the impedance $\vec{Z}$, respectively.

In Nyquist plots (imaginary part vs. real part of the impedance) for each separated physical process, a semicircle is obtained. Mostly, the imaginary part is plotted as an ordinate in positive direction because the inductivities do not play an important role in solid electrolyte cells. Ideally, the middle point of the semicircle is located on the real axis. This equates an *RC* combination. In reality, due to the inhomogeneity of the electrode, depressed semicircles are obtained with middle points below the real axis. The intercepts with the real axis and maxima are related to a resistance and capacitor. The complex impedance diagram is not unambiguous. It is useful to interpret this by means of an equivalent circuit in terms of values of physical processes [6]. In Fig. 2 the Nyquist diagram for a simple R(RC) combination is shown. For a solid electrolyte cell, this circuit gives an easy interpretation: R_1 is attributed to the solid electrolyte resistance and the circle with the maximum of the imaginary part $\omega_{(extr.\ Im(Z))} = 1/(R_2C)$ corresponds to the electrode impedance. The total resistance (second intercept) equates the dc cell resistance. Variations of the cell geometry (diameter and thickness), the cell temperature, and the gas partial pressure are proper means to verify physically the equivalent circuit. The resistance of solid electrolytes is proportional to the thickness (l) and reverse proportional to the electrode area (A), whereas the polarization resistance depends only on the electrode area (A). Furthermore results of dc techniques like steady-state current voltage measurements may help to support the model.

In Bode diagrams phase angle (phase shift between current and voltage) and the modulus of the impedance or its logarithm are plotted vs. log frequency (really spectroscopic plots). For the circuit given in Fig. 2, R_1 (high frequency) and $R_1 + R_2$ (low frequencies) are plateaus parallel to the frequency axis in modulus versus log frequency plot. In between the curve is bent in an s-shape manner. The inflection point of the curve corresponds to the minimum in the phase angle versus log frequency curve at the angular frequency $\omega_{(extr.\ \varphi)}$ ($\omega = 2\pi\upsilon$) where υ is the

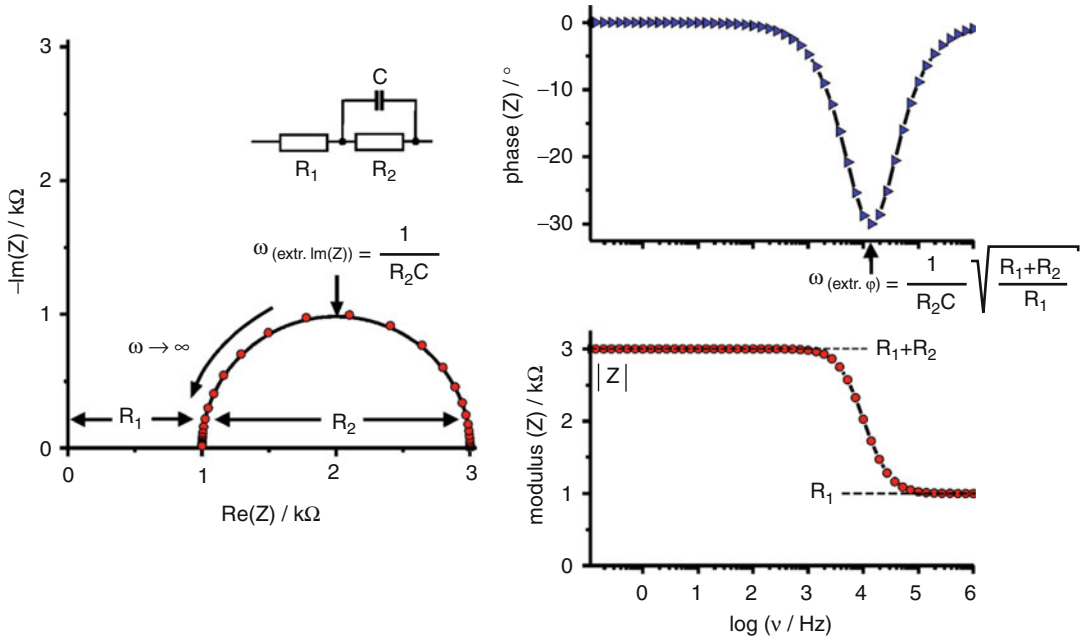

Dynamic Methods in Solid-State Electrochemistry, Fig. 2 Impedance plot for a simple $R_1(R_2C)$ combination, Nyquist diagram (*left*), Bode diagram (*right*)

frequency of the alternating voltage. At the phase angle minimum

$$\omega_{(\text{extr}.\varphi)} = \frac{1}{R_2 C}\sqrt{\frac{R_1 + R_2}{R_1}} \qquad (6)$$

is obtained.

For detailed investigations of electrodes, more complex equivalent circuits are necessary which are described in the literature [7, 8]. In solid-state electrochemistry mostly Nyquist impedance plots are used, which are suited to:

- Separate the bulk resistance and the grain boundary resistance in solid electrolytes
- Separate the solid electrolyte resistance from the electrode impedance
- Separate charge transfer process from transport phenomena
- Determine the rate limiting step of the electrochemical process

First, who introduced the alternating current measurements and used Nyquist plots in the solid-state electrochemistry, was Bauerle [9]. As earlier as 1967, Hartung and Möbius described

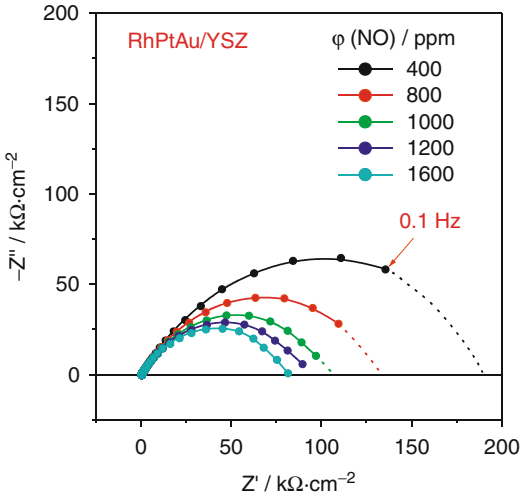

Dynamic Methods in Solid-State Electrochemistry, Fig. 3 Nyquist plots of a solid electrolyte electrode, NO, O_2, RhPtAu/YSZ at various NO concentrations [12]

polarization effect on Pt/zirconia electrodes by means of impedance measurements [10]. Now this technique is used for both the development of sensors [11] and as a sensor principle demonstrated in Fig. 3 [12]. The impedance of the solid

electrolyte gas electrode, RhPtAu/YSZ, depends on both the concentrations of oxygen and nitric oxide. At (nearly fixed) O_2 only the NO sensitivity has an influence on the diameter of the semicircle. It is not necessary to measure the whole frequency range. Measurements at only a few selected frequencies are sufficient to extrapolate mathematically a semicircle and to determine the intercepts for $\omega \rightarrow 0$. Such sensors are also denoted as impedimetric (impedance) sensors or impedancemetric sensors [13].

Cross-References

- ▶ Controlled Flow Methods for Electrochemical Measurements
- ▶ Cyclic Voltammetry
- ▶ Electrochemical Impedance Spectroscopy (EIS) Applications to Sensors and Diagnostics
- ▶ Voltammetry of Adsorbed Proteins

References

1. Scholz F (2012) Dynamic techniques. In: Bard A, Inzelt G, Scholz F (eds) Electrochemical dictionary, 2nd edn. Springer, Heidelberg, pp 238–239
2. Marken F (2012) Cyclic voltammetry. In: Bard A, Inzelt G, Scholz F (eds) Electrochemical dictionary, 2nd edn. Springer, Heidelberg, pp 183–185
3. Shoemaker EL, Vogt MC, Dudek FJ (1996) Cyclic voltammetry applied to an oxygen-ion-conducting solid electrolyte as an active electro-catalytic gas sensor. Solid State Ion 92:285–292
4. Kenjo T, Yamakoshi Y, Wada K (1993) An estimation of the electrode-electrolyte contact area by linear sweep voltammetry in Pt/ZrO_2 oxygen electrodes. J Electrochem Soc 140:2151–2157
5. Schmidt-Zhang P, Zhang W, Gerlach F, Ahlborn K, Guth U (2006) Electrochemical investigations on Pt-alloy/YSZ electrodes for amperometric gas sensors (in German). Abh Sächs Akad Wiss Leipzig Math-naturw Klasse 63:121–126
6. Rickert H (1982) Electrochemistry of solids. Springer, Berlin/New York/Heidelberg
7. Barsoukov E, Macdonald JR (2005) Impedance spectroscopy theory, experiment, and application, 2nd edn. Wiley, Hoboken
8. Orazem WE, Tribollet B (2008) Electrochemical impedance spectroscopy. Wiley, Hoboken
9. Bauerle JE (1969) Study of solid electrolyte polarization by a complex admittance method. J Phys Chem 30:2657–2670
10. Hartung R, Möbius HH (1967) About alternating current polarization in platinum electrodes on oxygen ion conducting solid electrolyte (in German). Z Chem (Leipzig) 7:325
11. Matsui N (1981) Complex-impedance analysis for the development of zirconia oxygen sensors. Solid State Ion 3–4:525–529
12. Guth U, Zosel J (2004) Electrochemical solid electrolyte gas sensors – hydrocarbon and NO_x analysis in exhaust gases. Ionics 10:366–377
13. Nakatou M, Miura N (2006) Detection of propene by using new-type impedancemetric zirconia-based sensor attached with oxide sensing-electrode. Sens Actuator 120:57–62

Dynamics of Mobile Ions in Materials with Disordered Structures - the Case of Silver Iodide and the Two Universalities

Klaus Funke
Institute of Physical Chemistry, University of Muenster, Muenster, Germany

Introduction

In solid electrolytes that exhibit the key property of structural disorder, three types of nonvibrational motion of the mobile ions may be discerned. These are:

1. A "liquid-like" motion, as for instance in alpha silver iodide
2. A correlated hopping motion, which leads to macroscopic transport
3. A correlated localized motion, which creates the Nearly Constant Loss effect

By comparison, the situation is much simpler in ionic crystals with comparatively low degrees of disorder, in which the mobile point defects may be regarded as "random walkers." An example of such a material is crystalline silver bromide at 200 °C [1].

The Case of Alpha Silver Iodide

In marked contrast to silver bromide, silver iodide in its high-temperature alpha phase,

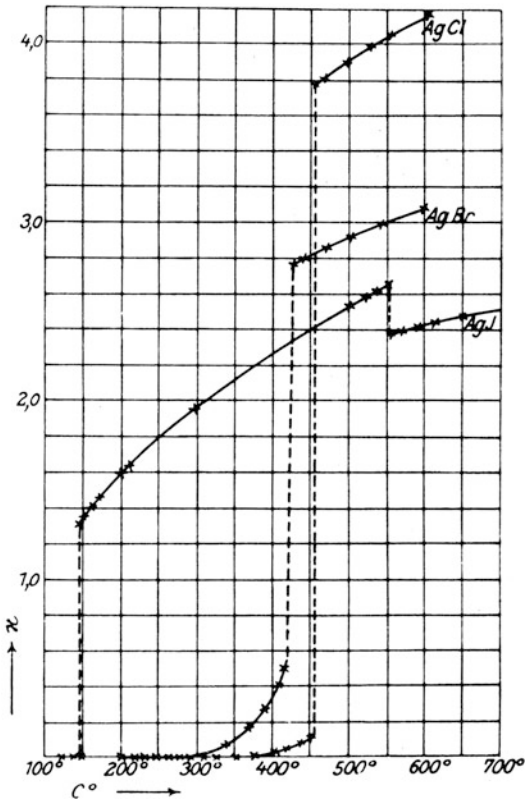

Dynamics of Mobile Ions in Materials with Disordered Structures - the Case of Silver Iodide and the Two Universalities, Fig. 1 Ionic conductivity of the silver halides, original plot of Tubandt and Lorenz [2]

α-AgI, is *structurally* disordered, see below. It is indeed the archetypal fast ion conductor. The unexpected properties of α-AgI were discovered by C. Tubandt and E. Lorenz in 1914 [2], on the occasion of their measurements of the electric conductivities of the silver halides, AgCl, AgBr, and AgI. Their original plot is reproduced in Fig. 1.

From the figure it is seen that the highly conducting α-phase of AgI is stable between 147 °C and 555 °C. At the β to α phase transition, the conductivity increases by more than three orders of magnitude up to 1.3 Ω^{-1} cm^{-1}. Within the α-phase, it increases only by a factor of two and then drops upon melting. From their measurements of transference numbers and from interdiffusion experiments, Tubandt and his coworkers concluded that the charge was carried by the cations [3]. Note that the extraordinarily high value of the ionic conductivity in α-AgI is comparable to the best conducting liquid electrolytes.

Since Tubandt's times, the silver ions in α-AgI have, therefore, been regarded as moving in a "liquid-like" fashion within the crystallographic framework provided by the anions. A first structural analysis of α-AgI was presented by L.W. Strock in 1934 and 1936 [4], who assigned a body-centered cubic (bcc) structure to the iodide sublattice, while considering as many as 42 possible positions for the two silver ions in the bcc unit cell.

In 1977, a contour map of the probability density of the silver ions in α-AgI, $\rho(\underline{r})$, was constructed on the basis of single-crystal neutron-diffraction data [5], showing flat maxima of $\rho(\underline{r})$ at the tetrahedral voids and flat minima at the octahedral positions. It may thus be concluded that the periodic potential barriers provided by the anions for the translational diffusion of the cations are only of the order of the thermal energy, which corroborates the view of a liquid-like motion.

Three years later, quasielastic neutron-scattering spectra taken on single-crystalline α-AgI were reproduced (including their anisotropy) by a model that approximated the actual liquid-like motion of the silver ions by a spatial convolution of two processes [6]. One of them was a fast diffusive motion in a local cage of about 0.1 nm radius, while the other was a random hopping via tetrahedral positions.

Remarkably, the ionic conductivity of α-AgI displays no frequency dependence up to at least 40 GHz [7]. This implies that the mobile silver ions move so fast that any memory of individual movements is erased after a time which is the inverse of $2\pi \cdot 40$ GHz, i.e., after 4 ps.

The Two Universalities

In contrast to α-AgI, structurally disordered ionic materials usually exhibit strongly frequency-dependent ionic conductivities. Examples

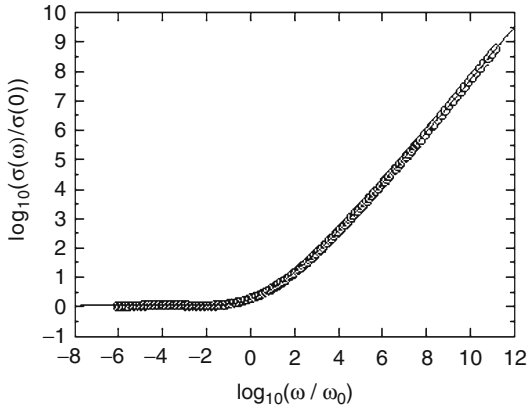

Dynamics of Mobile Ions in Materials with Disordered Structures - the Case of Silver Iodide and the Two Universalities, Fig. 2 First universality: This scaled representation [8] of experimental and model conductivities (*circles* and *solid line*, respectively, with data from 0.45 LiBr · 0.56 Li_2O · B_2O_3 glass) is characteristic of many disordered ion conductors which largely differ in their structures and compositions. Its slope increases continuously, slowly tending towards unity

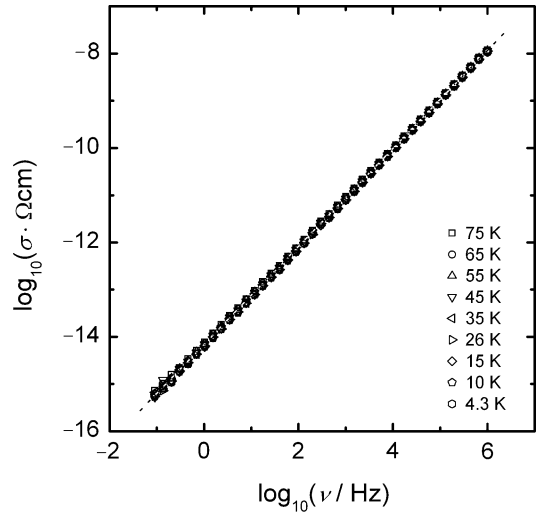

Dynamics of Mobile Ions in Materials with Disordered Structures - the Case of Silver Iodide and the Two Universalities, Fig. 3 Second universality (Nearly Constant Loss): low-temperature conductivity isotherms displaying a linear frequency dependence and essentially no temperature dependence (Data from 0.3 Na_2O · 0.7 B_2O_3 glass [11])

include crystalline, glassy, and polymeric electrolytes [8, 9] and even molten salts [9] and ionic liquids [10]. While these materials greatly differ in phase, structure, and composition, their broadband conductivity spectra are characterized by an unexpected degree of similarity. In particular, two surprising "universalities" have been detected, see Figs. 2 and 3.

The "first universality" is a fingerprint of activated hopping along interconnected sites, while the "second universality" reflects non-activated, localized movements of interacting ions. The former is observed at sufficiently high temperatures, while the other is seen at low ones, e.g., in the cryogenic temperature regime.

In disordered solid electrolytes, conductivity spectra taken at different temperatures typically show a gradual transition from one universality to the other, as seen in the example of Fig. 4.

Notably, the transition is much easier to locate on the temperature scale, when iso-frequency conductivity data are plotted versus inverse temperature, see Fig. 5 and the text further below. The crossover points marked in the two figures are identical.

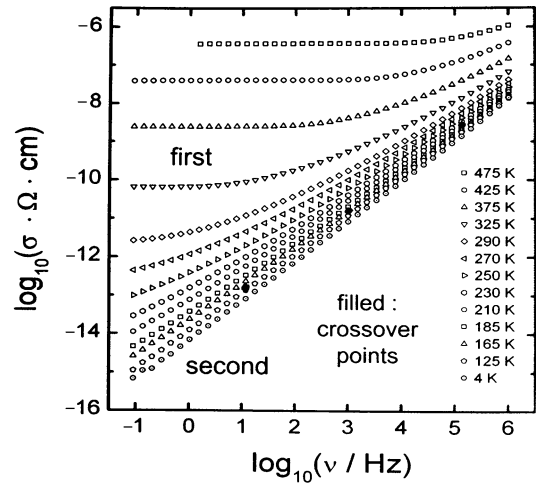

Dynamics of Mobile Ions in Materials with Disordered Structures - the Case of Silver Iodide and the Two Universalities, Fig. 4 The two universalities, here demonstrated on the basis of experimental frequency-dependent conductivities of 0.3 Na_2O · 0.7 B_2O_3 glass taken at different temperatures [12]. The three *darkened points* show the crossover between "ordinary" correlated hopping (first universality) and strictly localized ionic motion (second universality), cf. Fig. 5.

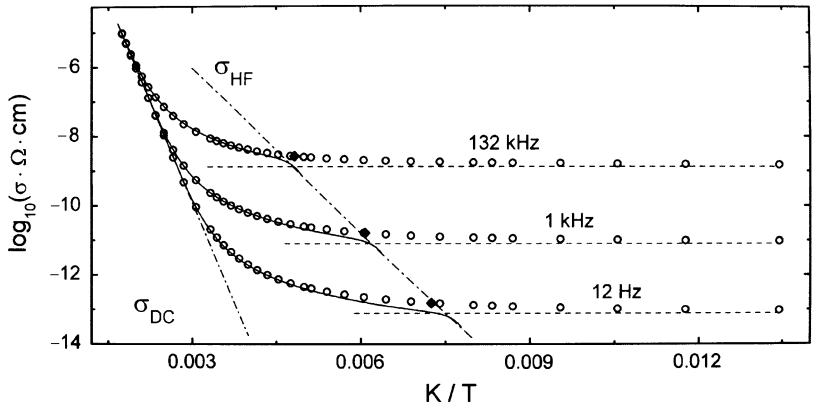

Dynamics of Mobile Ions in Materials with Disordered Structures - the Case of Silver Iodide and the Two Universalities, Fig. 5 Iso-frequency representation of log σ versus $1/T$ for 0.3 $Na_2O \cdot 0.7B_2O_3$ glass. The dash-dotted lines indicate the Arrhenius temperature dependence of the DC conductivity, σ_{DC}, and the high-frequency conductivity, σ_{HF}. The filled diamonds represent the crossover from the first to the second universality. For details, see main text and Ref. [12]

First Universality

For any fast ion conductor featuring an activated hopping of ions, a scaled master curve like the one of Fig. 2 can be constructed by suitably shifting its conductivity isotherms in a log-log plot of conductivity times temperature, $\sigma \cdot T$, versus frequency, ν. If the conduction mechanism does not change with temperature, the isotherms are found to collapse when shifted along a straight line with a slope of one. This (most frequent) case of "time-temperature superposition" [13–15] is called "Summerfield scaling" [16]. The underlying reason is obvious. The macroscopic coefficient of self-diffusion, which is proportional to DC conductivity times temperature, $\sigma_{DC} \cdot T$, varies at the same rate as the frequencies that characterize the motion of the mobile ions. The first universality now states that virtually identical master curves are obtained for a multitude of ionic materials including crystals, glasses, polymers, and ionic liquids, cf. Fig. 2.

This was first noted by A.K. Jonscher in 1975 [17, 18]. Based on his observations, he introduced his famous power-law description, $\sigma(\nu) - \sigma_{DC} \propto \nu^p$, with a constant exponent p. He also coined the terms *Universal Dielectric Response* and *Universal Dynamic Response*, often abbreviated as UDR. In the meantime, however, it has become apparent that the simple power-law approach is at variance with both experiment and theory, see, e.g., Ref. [19].

Shortly after Jonscher's findings, K.L. Ngai formulated his *Coupling Concept* [20, 21], which emphasized the importance of ion-ion interactions without violating linear response theory [22]. However, the *Coupling Concept* also features the unrealistic power-law increase of $\sigma(\nu)$, before a high-frequency plateau, σ_{HF}, is eventually attained.

In their Monte Carlo studies, A. Bunde et al. considered the effects of structural disorder and long-range Coulomb interactions systematically [23, 24]. In particular, they reproduced the frequent occurrence of correlated forward-backward hopping sequences, which are the main cause of the first-universality phenomenon. Disorder and interactions were also taken into account in the *Counterion Model* developed by W. Dieterich et al., who derived realistic spectra, $\sigma(\nu)$, from their numerical simulations [25].

In the *Random Barrier/Random Energy Models*, the non-random ion dynamics have been modeled in a formal fashion by considering individual mobile ions in random potential landscapes that are static in time [26, 27], again yielding realistic shapes of $\sigma(\nu)$.

The alternative viewpoint was to assume that the site potentials of the ions were not static, but varied in time, thus reflecting their changing momentary arrangements and interactions. This view led to the so-called Jump Relaxation Models, which are based on simple rate equations for the ion dynamics [8, 9, 28]. The solid lines included in Fig. 2 and Fig. 5 have been derived from the most recent model version, called the *MIGRATION concept* [29].

Second Universality

In 1991, A.S. Nowick and his coworkers discovered a new, "second" universality, which is ubiquitous in disordered ionic materials ("present in every plastic bag") but becomes visible only at sufficiently low temperatures and/or high frequencies [30]. The phenomenon is also called *Nearly Constant Loss* (NCL) effect, since the dielectric loss function, $\varepsilon'' \propto \sigma/\nu$, appears to be virtually independent of both frequency and temperature, cf. Fig. 3.

There is a broad consensus that the second universality reflects cooperative localized movements of a large number of ions. In ionic crystals, the effect is seen to develop from ordinary Debye relaxation as the number density of locally mobile ionic defects is drastically increased [31].

In early interpretations, static distributions of asymmetric double-well potentials (ADWP) were assumed to exist for the locally mobile ions, providing a wide range of relaxation times. This model, which was based on ideas of Pollak and Pike [32], has often been used to fit experimental data [33, 34].

The decisive step forward was made when W. Dieterich and his coworkers treated the locally mobile ions as reorienting electric dipoles, with Coulomb interactions between them [35, 36]. In their Monte Carlo simulations, they considered collections of such interacting dipoles, which were randomly distributed in space, and studied their localized reorientational movements. The resulting conductivity spectra show the following features. As frequency is increased, the slope of $\log\sigma$ versus $\log\nu$ first changes from two to one and later from one to zero. The linear NCL regime thus lies between two crossover points. The frequency range spanned by the NCL is found to increase as the ratio of Coulomb energy by thermal energy increases, that is, with increasing number density and with decreasing temperature.

Very similar results have also been obtained from a suitably modified version of the *MIGRATION concept* [9, 37], see also Ref. [8]. According to this treatment, the Coulomb interactions seem to provide rapid see-saw-type variations of the local potentials that are experienced by the individual ions, resulting in their collective localized movements [11, 37].

Cross-References

- ▶ Conductivity of Electrolytes
- ▶ Defect Chemistry in Solid State Ionic Materials
- ▶ Defects in Solids
- ▶ Dynamic Methods in Solid-State Electrochemistry
- ▶ Electrolytes, Classification
- ▶ Electrolytes, History
- ▶ Ion Mobilities
- ▶ Ionic Mobility and Diffusivity

References

1. Funke K, Lauxtermann T, Wilmer D, Bennington SM (1995) Creation and recombination of Frenkel defects in AgBr. Z Naturforsch A 50:509
2. Tubandt C, Lorenz E (1914) Molekularzustand und elektrisches Leitvermögen kristallisierter Salze. Z Physik Chem 87(513):543
3. Tubandt C (1932) Leitfähigkeit und Überführungszahlen in festen Elektrolyten. In: Wien W, Harms F (eds) Handbuch der Experimentalphysik XII, part 1. Akadem Verlagsges, Leipzig
4. Strock LW (1934) Kristallstruktur des Hochtemperatur-Jodsilbers α-AgJ. Z physik Chem B 25 (1934) 411 and B 31 (1936) 132
5. Cava RJ, Reidinger F, Wuensch BJ (1977) Single-crystal neutron-diffraction study of AgI between 23° and 300° C. Solid State Comm 24:411

6. Funke K, Höch A, Lechner RE (1980) Quasielastic neutron scattering from a single crystal of alpha silver iodide. J de Physique 41:C6–17
7. Funke K, Roemer H, Schwarz D, Unruh H-G, Luther G (1983) On the microwave conductivity of alpha silver iodide, part II: complex conductivity by measurement of the complex transmission factor. Solid State Ion 11:254
8. Funke K, Banhatti RD, Brückner S, Cramer C, Krieger C, Mandanici A, Martiny C, Ross I (2002) Ionic motion in materials with disordered structures – conductivity spectra and the concept of mismatch and relaxation. Phys Chem Chem Phys 4:3155
9. Funke K, Banhatti RD (2006) Ionic motion in materials with disordered structures. Solid State Ion 177:1551
10. Šantić A, Wrobel W, Mutke M, Banhatti RD, Funke K (2009) Frequency-dependent fluidity and conductivity of an ionic liquid. Phys Chem Chem Phys 11:5930
11. Laughman DM, Banhatti RD, Funke K (2010) New nearly constant loss feature detected in glass at low temperature. Phys Chem Chem Phys 12: 14102
12. Banhatti RD, Laughman D, Badr L, Funke K (2011) Nearly constant loss effect in sodium borate and silver meta-borate glasses: new insights. Solid State Ion 192:70
13. Taylor HE (1956) The dielectric relaxation spectrum of glass. Trans Faraday Soc 52:873
14. Isard JO (1970) Dielectric dispersion in amorphous conductors. J Non-Cryst Solids 4:357
15. Kahnt H (1991) Ionic transport in oxide glasses and frequency dependence of conductivity. Ber Bunsenges Phys Chem 95:1021
16. Summerfield S (1985) Universal low-frequency behaviour in the a.c. hopping conductivity of disordered systems. Philos Mag B 52:9
17. Jonscher AK (1975) The interpretation of non-ideal dielectric admittance and impedance diagrams. Phys Status Solidi A 32:665
18. Jonscher AK (1977) The 'universal' dielectric response. Nature 267:673
19. Funke K, Banhatti RD (2008) Translational and localized ionic motion in materials with disordered structures. Solid State Sci 10:790
20. Ngai KL (1979) Universality of low-frequency fluctuation, dissipation and relaxation properties of condensed matter, parts I and II. Comments Solid State Phys 9 (1979) 127 and 9 (1980) 141
21. Ngai KL (2003) The dynamics of ions in glasses: importance of ion-ion interactions. J Non-Cryst Solids 323:120
22. Kubo R (1957) Linear response theory of irreversible processes. J Phys Soc Jpn 12:570
23. Meyer M, Maass P, Bunde A (1993) Spin-lattice relaxation: non-Bloembergen-Purcell-Pound behavior by structural disorder and Coulomb interactions. Phys Rev Lett 71:573
24. Maass P, Meyer M, Bunde A (1995) Nonstandard relaxation behavior in ionically conducting materials. Phys Rev B 51:8164
25. Knödler D, Pendzig P, Dieterich W (1996) Ion dynamics in structurally disordered materials: effects of random Coulombic traps. Solid State Ionics 86–88:29
26. Dyre JC (1988) The random free-energy barrier model for ac conduction in disordered solids. J Appl Phys 64:2456
27. Schrøder TB, Dyre JC (2002) Computer simulations of the random barrier model. Phys Chem Chem Phys 4:3173
28. Funke K (1993) Review: Jump relaxation in solid electrolytes. Prog Solid State Chem 22:111
29. Banhatti RD, Funke K (2004) Dielectric function and localized diffusion in fast-ion conducting glasses. Solid State Ion 175:661
30. Lee W-K, Liu JF, Nowick AS (1991) Limiting behavior of ac conductivity in ionically conducting crystals and glasses: A new universality. Phys Rev Lett 67:1559
31. Nowick AS, Lim BS (2001) Electrical relaxations: simple versus complex ionic systems. Phys Rev B 63:184115
32. Pollak M, Pike GE (1972) ac conductivity of glasses. Phys Rev Lett 28:1449
33. Jain H, Krishnaswami S (1998) Composition dependence of frequency power law of ionic conductivity of glasses. Solid State Ion 105:129
34. Jain H (1999) 'Jellyfish' atom movement in inorganic glasses. Met Mater Process 11:317
35. Rinn B, Dieterich W, Maass M (1998) Stochastic modeling of ion dynamics in complex systems: dipolar effects. Philos Mag B 77:1283
36. Höhr T, Pendzig P, Dieterich W, Maass P (2002) Dynamics of disordered dipolar systems. Phys Chem Chem Phys 4:3168
37. Laughman DM, Banhatti RD, Funke K (2009) Nearly constant loss effects in borate glasses. Phys Chem Chem Phys 11:3158